Modeling Hydraulic Resistance of Floodplain Vegetation

Promotion committee:

prof. dr. F. Eising	Universiteit Twente, chairman/secretary
prof. dr. S.J.M.H. Hulscher	Universiteit Twente, promotor
dr.ir. D.C.M. Augustijn	Universiteit Twente, assistant-promotor
prof. dr. ir. H.J. De Vriend	Technische Universiteit Delft
prof. dr. ir. B.J. Geurts	Universiteit Twente
dr. H. Middelkoop	Universiteit Utrecht
prof. dr. V. Nikora	University of Aberdeen
dr. ir. J.S. Ribberink	Universiteit Twente
ir. E.H. Van Velzen	Rijksinstituut voor Integraal Zoetwaterbeheer en Afvalwaterbehandeling (RIZA)

This research is supported by:

The Technology Foundation STW, applied science division of NWO and the technology programme of the Ministry of Economic Affairs, the Netherlands.

Bundesanstallt für Gewässerkunde (Federal Institute of Hydrology), Koblenz, Germany.

HKV Consultants, Lelystad, the Netherlands.

ISBN 978-90-365-2553-4
Cover: *Net echt (464 kb)*
Copyright © 2007 by Fredrik Huthoff, Enschede, the Netherlands
Typeset in LaTeX
Printed by Dratex, Lelystad, The Netherlands

Modeling Hydraulic Resistance of Floodplain Vegetation

PROEFSCHRIFT

ter verkrijging van

de graad van doctor aan de Universiteit Twente,

op gezag van de rector magnificus,

prof.dr. W.H.M. Zijm,

volgens besluit van het College voor Promoties

in het openbaar te verdedigen

op vrijdag 5 oktober 2007 om 15.00 uur

door

Fredrik Huthoff

geboren op 29 maart 1974

te Bremen, Duitsland

Dit proefschrift is goedgekeurd door:

prof. dr. S.J.M.H. Hulscher	promotor
dr. ir. D.C.M. Augustijn	assistent-promotor

Contents

Preface **1**

Summary **3**

Samenvatting **5**

Zusammenfassung **9**

1 Introduction **13**
1.1 River flows, floods and the importance of hydrodynamic modeling 13
1.2 Hydrodynamic modeling - the challenge of flow resistance 13
1.3 Hydraulic resistance in floodplain flows 14
1.4 Modeling hydraulic resistance of floodplain vegetation 17
1.4.1 Objective 18
1.4.2 Research questions 18
1.4.3 Used data 18
1.4.4 Thesis outline 19

2 Modeling turbulent flow and vegetation resistance in rivers **21**
2.1 Introduction 21
2.2 Turbulent flows and Hydraulic Resistance 22
2.2.1 A short history in turbulence 22
2.2.2 Kolmogorov's phenomenological theory of turbulence . . . 24
2.2.3 Hydraulic resistance 25
2.3 Computations of turbulent flows in presence of vegetation 29
2.3.1 Solving the Navier-Stokes equation 30
2.3.2 Solving the Reynolds-averaged Navier-Stokes equation . . 31
2.3.3 Using spatially-averaged flow descriptions 32
2.4 Appropriate flow detail for river-reach models 33
2.5 A generally applicable vegetation resistance description? 36
2.6 Conclusions 37

3 Velocity profile method for submerged cylindrical vegetation **39**
3.1 Introduction: vegetation as cylinders? 40
3.2 Analytical velocity profile 41
3.2.1 Flow in the surface layer 41
3.2.2 Flow in the resistance layer 42

3.3 Calibration of the analytical velocity profile 46
3.4 Depth-averaged flow velocity based on vertical velocity profile . . 49
3.4.1 Depth-averaged velocity in the surface layer 49
3.4.2 Depth-averaged velocity in the resistance layer 51
3.4.3 Overall depth-averaged flow velocity 52
3.5 Discussion: complete slip and turbulence models 52
3.6 Conclusions 54

4 A bulk flow model including vegetation resistance 57
4.1 Introduction 57
4.2 The two-layer approach 59
4.3 The resistance layer 61
4.3.1 Emergent vegetation 61
4.3.2 Submerged vegetation 61
4.4 The Surface Layer 63
4.4.1 Shear stress in the surface layer 63
4.4.2 Turbulent energy and Kolmogorov scaling 64
4.4.3 Similarity considerations 65
4.5 Comparison to data from flume experiments 67
4.5.1 The flume experiments 67
4.5.2 Average velocities in the two flow layers 68
4.5.3 A two-layer scaling model for the entire flow depth 70
4.6 Discussion 71
4.6.1 Length scales in the surface layer 71
4.6.2 Hydraulic resistance of natural vegetation 73
4.7 Conclusions 75
4.8 Appendix: Explanation for the turbulent length scale 75

5 Evaluation of bulk flow model in vegetated waterways 77
5.1 Introduction: Hydraulic resistance due to vegetation in natural waterways 77
5.2 Fixed-point measurements in a Green River 79
5.2.1 The study location 79
5.2.2 Methodology & Results 80
5.2.3 Comparison to model predictions 83
5.2.4 Discussion 85
5.3 Vessel-borne flow measurements in the Dutch Upper Rhine . . . 87
5.3.1 The study location 87
5.3.2 Methodology & Results 88
5.3.3 Comparison to model predictions 95
5.3.4 Discussion 97
5.4 Conclusions 99
5.5 Assuming a constant water surface slope 100

6 Applicability of vegetation resistance in river flow models 103
6.1 Performance of vegetation resistance methods 103
6.1.1 Models of hydraulic resistance of vegetation 103
6.1.2 Comparison of vegetation resistance methods to laboratory data 104
6.2 Simplified descriptions of turbulent flows affected by vegetation . 106
6.2.1 Velocity and turbulence profiles 107
6.2.2 Turbulent energy spectra 109
6.3 Discussion 112
6.4 Conclusions 114

7 Interacting Divided Channel Method 117
7.1 Introduction 117
7.2 Interacting Divided Channel Method 119
7.2.1 Model equations for two-stage channel 119
7.2.2 Derivation of the interface stress 120
7.2.3 Analytical solution for two-stage channel 122
7.3 Comparison to laboratory data 122
7.3.1 Overview of experiments 122
7.3.2 Results 123
7.4 Discussion 127
7.5 Conclusions 128
7.6 Generalization of IDCM to arbitrary compound channels 129

8 Discussion 131
8.1 Simulation of natural floodplain vegetation in river flow models . 131
8.2 Calibrating river-reach models on resistance parameters 132
8.3 Limitations of the Interacting Divided Channel Method 133
8.4 The use of simplified flow models 133
8.5 Flood prevention: where to go next? 134

9 Conclusions & recommendations 137
9.1 Answers to research questions 137
9.2 Achievements 140
9.3 Recommendations 141

Bibliography 142

Notation 157

List of publications 161

About the author 163

Preface

In 2002 the Bundesanstallt fur Gewässerkunde (BfG, Koblenz, Germany) initiated the research project *Planungsmanagement für Auen* (i.e. *managing floodplains*), with the objective to gain insight into the interplay between plant ecology and riverine hydraulics. When I entered the project in August 2003, the research focus shifted towards understanding the hydraulic effects caused by vegetation. The topic of hydraulic resistance of vegetation had also been of interest to HKV Consultants (Lelystad, the Netherlands), who had conducted laboratory and theoretical investigations in preceding years. Throughout the course of the current work, HKV Consultants staid involved in an advisory role.

The chosen focus of hydraulic resistance of vegetation also fitted the objective of the STW project *Rough Water: Roughness modelling for managing natural shallow water systems*, for which Suzanne Hulscher received a VICI grant in 2003. Therefore, as the BfG project came to an end in December 2005, the current work became part of *Rough Water*. Within this project, several research paths were defined aiming at advancing river management methodologies associated with flow response to natural surroundings: Andries Paarlberg focusses on the dynamics of hydraulic resistance caused by river dunes during floods, Rolien van der Mark on the effects of irregularities in bed surface characteristics, Arjan Tuijnder on bed forms and morphological development in rivers, Mindert de Vries on the influence of biological processes on bed roughness and morphology, first Daniëlle Noordam and later Jord Warmink on the impact of uncertainties in river management decisions, and Saskia Hommes on the actual applicability of new river management techniques. All these researches are still ongoing, the current work on hydraulic resistance of vegetation being the first PhD-project to be completed within the *Rough Water* framework.

Towards completion of this thesis I am grateful to many people. Those who gave me the opportunity in the first place: Suzanne Hulscher, Denie Augustijn, Kees Vermeer, Hans Hartong and Matthijs Kok. Thanks for the support, the freedom and the necessary pushes in the right direction at the right time. Having five bosses is not as scary as it sounds. At the Bundesanstallt für Gewässerkunde, thanks to Volker Hüsing for the warm reception in Koblenz and for your involvement in the project's user group. Many thanks also to STW and the other members of the user group for their help and their critical remarks: Jan Rik van der Berg, Hans Middelkoop, Anne Wijbenga, Emiel van Velzen, Marijke Visser, Huib de Vriend and Martin Baptist. The discussions with and suggestions by Francisco Fontanele Araujo, Detlef Lohse, Wim Uijttewaal, Astrid Blom and

Vladimir Nikora were also greatly appreciated.

Two working places give many colleagues. Thank you all for the good times at HKV and the Water Management Department at the University of Twente. Some I wish to mention separately (the others get a free drink). At HKV: Anne Wijbenga for all-round support throughout the PhD process, Job Udo for showing me the HKV-way and introducing me to the world of hydraulic calculations, Hermjan Barneveld and Paul Termes for questioning the results, Bertus de Graaff for asking, Tiemen Bakker, Ellen van Zelm and Melanie van 't Riet for their patience. In Twente: you're a funny bunch Daniëlle Noordam, Saskia Hommes, Xiaohua Dong, Anne Wesselink, Rolien van der Mark, Arjan Tuijnder, 'N.T.' Giang, Tatiana Filatova and Judith Janssen! To two role models in the department, Jebbe van der Werf and Pieter Roos, you taught me more than you think (and I don't mean football). And if I *really* don't know what to do anymore (copy machines, printers, organizing stuff, computers) there are still Joke Meijer-Lentelink, Anke Wigger-Groothuijs, Brigitte Leurink, the guys from IT-support and René Buijsrogge.

Pieter van Oel and Andries Paarlberg were on this journey together with me. Thanks for sharing the ups and downs, and backing me up all the way to the end.

For good times and teaching effectiveness, thank you Aafke. Also, thanks to the homies in Amsterdam, Enschede, Leiden and The Hague. Enschede became home thanks to the Gersties: Rolf Bouwman, Martine Budding, Christoph '04' Hötzel, Joost Bos and, of course, Daniëlle Sikma.

And then, they don't want it but deserve it most, thanks to my parents Bärbel and Dieter for their unlimited support and trust (and German translations), to my brothers Hendrik and Malte for having a different look on things, *always*.

Blanca$^{\heartsuit}$, it wasn't me, *you* the best.

Fredrik Huthoff.

Oegstgeest, 14 August 2007.

Summary

In this thesis, methods are investigated that describe the impact of vegetation on a flow field, and their potential for application in river-reach hydraulic computational models. This field of research is of great importance to river flood studies, as vegetation-covered floodplains commonly become part of the river flow section during high-discharge conditions. In this respect, the obstruction of vegetation to flow needs to be taken into account if trying to predict overall flow behavior. To describe the impact of vegetation on a river-reach scale, obstructing vegetation should be incorporated in terms of easily measurable input parameters and require only minimal additional computational effort. In the current work, such a method is proposed.

Modeling the impact of vegetation in river flows

Towards the objective of finding a suitable method to describe the hydraulic effect of vegetation in river-reach settings, first, physical laws of turbulent flows are reviewed and possible ways to capture the impact by obstructing vegetation (Chapter 2). It appears that simple wall-roughness approaches do not suffice to describe the hydraulic response due to vegetation. Alternatively, flow through vegetation is best treated separately from flow over vegetation, effectively yielding a two-layer model that captures the most important flow processes in and above the vegetation.

An analytic method based on such a two-layer approach is reexamined on its detailed model characteristics (Chapter 3). Even though the method performs well when compared to idealized laboratory conditions, some characteristics of the method are poorly understood or unrealistic. In particular, the treatment of momentum losses due to dominant turbulent mixing patterns remains ambiguous. Furthermore, a complete-slip wall-boundary condition is required to yield accurate results. This model-property contradicts well-known empirical results. Despite these shortcomings, the model produces accurate outcomes, which suggests that flow in presence of vegetation does not need to be described in full detail to still give a realistic representation of the large-scale flow properties.

Bulk descriptions of turbulent flows

The finding that small-scale turbulence motions do not necessarily need to be explicitly described to still give accurate representation of overall flow behavior, motivates a new approach to describe the hydraulic resistance caused by vegetation (Chapter 4). In the newly proposed method, the average velocity of the

overall flow field above the vegetation is directly linked to small-scale turbulent motions in between the vegetation, which are assumed to be responsible for most momentum losses (using *Kolmogorov scaling*). Consequently, a simple analytic flow model of the average flow velocity is derived, which only describes the *bulk behavior* of the flow as affected by overall vegetation properties. Detailed turbulent measurements around obstructing cylinders (i.e. *idealized vegetation*) are analyzed (Chapter 6), in order to check the validity of assumptions made in the Kolmogorov scaling technique. It seems justified to use Kolmogorov scaling whenever the small-scale flow patterns, associated with dominant momentum losses in the flow field, are much smaller than the characteristic size of the flow domain (i.e. the depth of flow above the vegetation).

As with the earlier investigated vegetation resistance method (in Chapter 3), the newly proposed model is based on a two-layer approach, it depends on readily measurable (averaged) vegetation characteristics and yields good agreement with flow measurements collected in the laboratory, where vegetation is represented by homogeneously distributed cylinders. Furthermore, the method is based on physical principles yet remains mathematically simple. Therefore, in principle, the method is suitable for application on river-reach scales. In Chapter 5 flow measurements from two full-scale grassed channels are compared to model predictions. Even though it appears difficult to isolate the effect of vegetation on the flow field, model predictions seem promising.

Inspired by the successful bulk flow model for flow over (idealized) vegetation, a similar bulk flow model is proposed for another important process that is also responsible for hydraulic resistance in rivers: lateral momentum exchange in compound channels (Chapter 7). The proposed method, again, remains mathematically simple while it gives accurate predictions of the large-scale effect on flow velocities. The method seems particularly suitable to account for the impact of lateral momentum exchange in one-dimensional river flow models.

Conclusions

Simple wall-roughness approaches do not suffice to describe the hydraulic response due to vegetation. Alternatively, flow *through* vegetation is best treated separately from flow *over* vegetation, effectively yielding a two-layer model that captures the most important flow processes in each layer. Among the considered two-layer flow models in this thesis, a new simple bulk flow model is presented that describes flow over idealized vegetation accurately, is based on physical principles and requires only little computational effort. Derivation of the method is based on idealized vegetation characteristics, although comparison with data involving natural vegetation (in flume and field) yielded promising results. General application to real situations requires further research on how to describe natural vegetation in overall (averaged) properties.

The predictive capability of two newly proposed bulk flow models in this thesis demonstrate that in certain situations large-scale turbulent flows can be adequately described using rough scaling assumptions. In hydraulic engineering, advances in computational abilities are thus not the only way forward.

Samenvatting

In dit proefschrift worden methodes ontwikkeld en getoetst voor de beschrijving van de invloed van vegetatie op een stromingsveld. We kijken met name naar de geschiktheid van dergelijke methodes voor toepassing in grootschalige riviermodellen. Dit soort methodes zijn van groot belang voor overstromingsstudies, omdat bij situaties met hoge rivierafvoeren begroeide uiterwaarden vaak onderdeel worden van het rivierstromingsveld. Er moet dus rekening worden gehouden met de stromingsweerstand ten gevolge van aanwezige begroeiing, zodat het gehele stromingsveld goed beschreven wordt. Om de invloed van vegetatie te kunnen beschrijven op de schaal van een riviertraject is het wenselijk om vegetatieweerstand uit te drukken in meetbare grootheden (planteigenschappen) zonder dat daarbij de computerrekenlast veel groter wordt. In het voorliggende werk wordt hiervoor een methode voorgesteld.

Modelleren van de invloed van vegetatie op rivierstromen

Om een geschikte vegetatieweerstandsmethode voor stromingsmodellering in rivieren te ontwikkelen, worden eerst de algemene fysische eigenschappen van turbulente stromingen onderzocht (Hoofdstuk 2). Het blijkt dat eenvoudige wandruwheidsbeschrijvingen niet volstaan om de invloed van vegetatie op een stromingsveld goed weer te geven. In plaats daarvan kan de stroming in aanwezigheid van vegetatie het beste worden beschreven middels een twee-lagen model, waarbij de stroming boven en tussen de vegetatie apart worden behandeld. Op deze manier wordt op de meest eenvoudige wijze rekening gehouden met de belangrijkste stromingsprocessen.

De impliciete aannames van een analytische methode gebaseerd op een dergelijke twee-lagen aanpak worden in dit proefschrift onderzocht (Hoofdstuk 3). Ondanks dat de methode een goede weergave geeft van de stroming in aanwezigheid van geïdealiseerde vegetatie (starre staven), zijn enkele eigenschappen van de methode slecht begrepen of onrealistisch. Een zwak punt is de manier waarop met turbulente stroming rekening wordt gehouden. Daarbij komt dat de bodemwrijving moet worden verwaarloosd om nauwkeurige resultaten te krijgen. Deze modeleigenschap is in tegenspraak met welbekende stromingseigenschappen. Ondanks de genoemde zwakke punten, geeft de methode toch nauwkeurige stromingsvoorspellingen. Dit suggereert dat het niet strikt noodzakelijk is om de detaileigenschappen van turbulente stromingen volledig te beschrijven, om toch grootschalige stromingseigenschappen realistisch weer te geven.

Bulkbeschrijvingen van turbulente stroming

Het inzicht dat kleinschalige turbulente wervels niet noodzakelijkerwijs beschreven dienen te worden voor een goede weergave van het gemiddelde stromingsveld, is de motivatie voor een nieuwe vegetatieweerstandmethode beschreven in dit proefschrift (Hoofdstuk 4). In de nieuwe methode wordt het diepte-gemiddelde stromingsveld direct gerelateerd aan algemene eigenschappen van turbulente wervels, waarvan wordt aangenomen dat deze verantwoordelijk zijn voor de meeste stromings-energieverliezen (hierbij wordt gebruik gemaakt van zogenaamde *Kolmogorov schaling*). Als gevolg van deze aanname is een eenvoudig analytisch stromingsmodel afgeleid dat alleen het gemiddelde *bulkgedrag* van stroming weergeeft, zoals beïnvloedt door aanwezige vegetatie. Ook gedetailleerde metingen van turbulente stromingen langs starre staven (*geïdealiseerde vegetatie*) zijn onderzocht (Hoofdstuk 6), om de aannames die ten grondslag liggen aan de gebruikte Kolmogorov-schaling te toetsen. Het lijkt verantwoord om de schalingsmethodiek te hanteren indien kleinschalige wervels, die grotendeels verantwoordelijk zijn voor stromings-energieverliezen, aanzienlijk kleiner zijn dan de karakteristieke lengteschaal van het stromingsdomein, zoals bijvoorbeeld de diepte van de stromingslaag boven de vegetatie.

Net als in de eerder onderzochte vegetatieweerstandsmethode (Hoofdstuk 3), is de nieuw voorgestelde methode gebaseerd op een twee-lagen beschrijving. De beschrijving is afhankelijk van meetbare planteigenschappen en komt goed overeen met laboratoriummetingen van stroming over geidealiseerde vegetatie. Bovendien is de nieuwe methode eenvoudig en gebaseerd op fysische principes. De nieuwe methode is daarmee geschikt voor toepassing in stromingsmodellen op de schaal van een riviertraject. In Hoofdstuk 5 worden meetgegevens van stromingen in natuurlijk begroeide uiterwaarden vergeleken met modelvoorspellingen. Het blijkt moeilijk om in de metingen de invloed van vegetatieweerstand te isoleren, maar toch zijn de modelvoorspellingen veelbelovend.

Geïnspireerd door de succesvolle uitkomsten van het vereenvoudigde vegetatieweerstandsmodel, is op vergelijkbare manier een model ontwikkeld voor een ander belangrijk proces dat stromingsweerstand veroorzaakt: laterale impulsoverdracht tussen de stroming in de hoofdgeul en uiterwaarden (Hoofdstuk 7). De voorgestelde methode is wederom eenvoudig en geeft nauwkeurige voorspellingen van het gemiddelde effect van impulsoverdracht. Deze methode lijkt met name geschikt voor integratie in ééndimensionale riviermodellen.

Conclusies

Eenvoudige wandruwheidsbeschrijvingen zijn niet geschikt voor de weergave van de invloed van vegetatie op een stromingsveld. In plaats daarvan is het beter om de stroming tussen en boven vegetatie apart te beschrijven. Op deze manier worden in een twee-lagen stromingsmodel alleen de meest relevante processen weergegeven. In dit proefschrift is een dergelijk twee-lagen model ontwikkeld, waarbij detaileigenschappen van de turbulente stroming niet expliciet worden beschreven. Deze eenvoudige bulkbeschrijving van de stroming

in aanwezigheid van vegetatie is gebaseerd op fysische principes en geeft een nauwkeurige weergave van het gemiddelde stromingsveld. De afleiding van de methode is gebaseerd op geïdealiseerde vegetatie-eigenschappen, maar geeft ook in situaties met natuurlijke vegetatie veelbelovende resultaten. Voor verdere algemene toepassing van deze methode wordt aanbevolen om te onderzoeken hoe eigenschappen van natuurlijke vegetatie het best gevangen kunnen worden in algemene plantkarakteristieken.

De voorspellende kwaliteit van twee nieuwe bulkstromingsmodellen laat zien dat in specifieke situaties de grootschalige uitwerking van turbulente stroming goed weergegeven kan worden met gemiddelde schalingsaannames. Vooruitgang in waterloopkunde is dus niet alleen via geavanceerde numerieke modellen en grotere rekenkracht te bereiken.

Zusammenfassung

In dieser Studie werden Methoden untersucht, die den Einfluss von Vegetation auf Strömungsfelder beschreiben. Insbesondere wurde untersucht in wieweit die Methoden möglicherweise für Flussmodelle anwendbar sind. Die Untersuchung auf diesem Gebiet ist von großer Wichtigkeit für Überflutungsstudien, weil bei hohen Wasserständen das bewachsene Vorland oft einen Teil des Flussströmungsquerschnittes ausmacht. Man muss also den durch Vegetation verursachten Strömungswiderstand mitberücksichtigen will man das gesamte Strömungsverhalten abschätzen. Um den Einfluss der Vegetation auf das Flussströmungsgebiet zu beschreiben, muss der Vegetationswiderstand in messbaren Einheiten ausgedrückt werden, und nur geringen zusätzlichen Aufwand bei Computerberechnungen erfordern. In der vorliegenden Arbeit wird eine solche Methode vorgestellt.

Modellierung des Einflusses der Vegetation auf die Flussströmung

Mit dem Ziel eine angemessene Methode fr den Vegationswiderstandseffekt in flussnahen Gebieten zu finden, sind erst allgemein physische Eigenschaften von turbulenten Strömungen untersucht worden (Kapitel 2). Es scheint dass einfache Wandrauheitsbeschreibungen nicht ausreichen um den Vegetationseinfluss in einem Strömungsfeld dar zu stellen. Stattdessen kann die Strömung durch Vegetation am besten anhand eines Zweischichtenmodelles beschrieben werden, wobei die Strömungen über und durch die Vegetation separat behandelt werden. Dadurch werden auf einfache Weise die wichtigsten Strömungseigenschaften berücksichtigt.

Eine auf der Zweischichtenmodelle basierende analytische Methode wird in dieser Studie auf ihre speziellen Modelleigenschaften untersucht (Kapitel 3). Obgleich die Methode unter idealisierten Laborbedingungen (steife Zylinder) gute Ergebnisse erzielt, sind einige Eigenschaften der Methode kaum zu verstehen oder unrealistisch. Insbesondere die Behandlung der Widerstandsverluste durch die turbulenten Strömungsveränderungen bleibt unklar. Hinzu kommt dass Wandgleit-Grenzbedingungen vollständig ausgeschaltet werden um genaue Resultate zu erzielen. Ungeachtet dieser Vernachlässigungen liefert das Model genaue Ergebnisse. Daraus lässt sich schließen, dass es nicht unbedingt notwendig ist alle Detaileigenschaften turbulenter Strömungen genau zu beschreiben und dennoch dass die Gesammtströmung realistisch wiedergegeben wird.

Vereinfachte Gesamtbeschreibung turbulenter Strömungen

Die Erkenntnis, dass kleine Turbulenzbewegungen nicht notwendigerweise im Detail beschrieben werden müssen um genaue Gesamtströmungseigenschaften wiederzugeben, sind Motivation in dieser Arbeit den Strömungswiderstand, der durch die Vegetation verursacht wird, auf neuer Weise zu beschreiben (Kapitel 4). In der neuen Methode wird die Durchschnittsgeschwindigkeit des gesamten Strömungsfeldes direkt verbunden mit den allgemeinen Eigenschaften turbulenter Wirbel von denen angenommen wird, dass sie für den größten Teil des Strömungsenergieverlustes verantwortlich sind (hier kommt die *Kolmogorov Skalierung* in Anwendung). Als Konsequenz aus dieser Annahme ist ein einfaches analytisches Strömungsmodell für die Durchschnittsgeschwindigkeit abgeleitet, das nur das Gesamtverhalten der Strömung unter dem Einfluss der allgemeinen Vegetationseigenschaften beschreibt. Detaillierte Turbulenzmessungen in der Nähe von Zylindern (idealisierte Vegetation) wurden analisiert (Kapitel 6) um die Gültigkeit, die mit der Kolmogorov Skalierungstechnik vorrausgesetzt wurde, zu prüfen. Es scheint vertretbar die Kolmogorov Skalierung anzuwenden, wenn die kleinen Wirbel, die zum größten Teil für Strömungsverluste verantwortlich sind, viel kleiner sind als die charakteristischen Abmessungen des Strömungsbereiches (z.B. die Strömungstiefe über der Vegetation).

Wie in eher untersuchten Vegetations-Widerstandmethoden (in Kapitel 3), basiert das neu vorgeschlagene Modell auf einer Zweischichten-Beschreibung. Die Beschreibung ist abhängig von der messbaren (durchschnittlichen) Eigenschaft des Bewuchses und gibt gute Übereinstimmungen mit Strömungsmessungen aus Laboruntersuchungen, bei denen die Vegetation als gleichmässig verteilte Zylinder representiert wird. Außerdem basiert die neue Methode auf physikalischen Prinzipien und ist mathematisch einfach. Die neue Methode ist deshalb geeignet für die Anwendung in Strömungsmodellen von Flussströmungsgebieten. In Kapitel 5 wurden Messungen aus natürlich bewachsenen Strömungsgebieten verglichen mit Schätzungen aus Modellberechnungen. Es scheint schwierig bei den Messungen den Einfluss des Vegetationswiderstandes auf die Strömung zu isolieren, dennoch erscheinen die Modellvorausschätzungen vielversprechend.

Ermutigt durch die erfolgreichen Ergebnisse aus dem allgemeinen Vegetationswiderstandmodell, ist auch eine andere vereinfachte Gesammtbeschreibung eines wichtigen Vorganges entwickelt, der auch für die Verursachung von Strömungswiderstnden in Flüssen verantwortlich ist: laterale Impulsübertragung zwischen Strömungen in der Hauptgerinne und im Vorland (Kapitel 7). Die vorgeschlagene Methode ist ebenfalls einfach und gibt genaue Vorausschätzungen der Gesamteinwirkung von Impulsübertragung. Diese Methode scheint besonders geeignet, den Einfluss von lateralen Impulsübertragungen in eindimensionale Flussströmungsmodellen zu berücksichtigen.

Schlussfolgerungen

Einfache Wandrauheitsbeschreibungen sind nicht geeignet für die Beschreibung von Strömungseinflssen durch Vegetation. Stattdessen ist es besser Strömung durch Vegetation unabhängig von Strömung ber Vegetation zu behandeln. Auf diese Weise werden in einem Zweischichten-Strömungsmodell nur die wichtigsten Vorgänge in jeder Schicht berücksichtigt. Bei den hier berücksichtigten Zweischichten-Modellen ist auch ein neues einfaches Gesammt-Strömungsmodell vorgestellt. Dieses Modell, das die Gesammt-Strömung ber idealisierte Vegetation genau beschreibt, basiert auf physikalischen Prinzipien und erfordert nur geringen mathematischen Aufwand. Die Ableitung dieser Methode basiert auf idealisierten Vegetationseigenschaften, sie gibt jedoch auch in Situationen mit natürlicher Vegetation vielversprechende Ergebnisse. Zur Anwendung dieser Methode bei natürlichen Situationen sind weitere Untersuchungen erfordert um herauszufinden wie natürliche Vegetation in allgemeinen (Durchschnitts-) Eigenschaften beschrieben werden kann.

Die vorhersagende Qualität zweier neuer Gesamtströmungsmodelle zeigt, dass in bestimmten Situationen die Auswirkung kleiner Turbulenzbewegungen anhand von Durchschnitts-Skalierungsannahmen gut beschrieben werden kann. Technologische Fortschritte im hydraulischen Ingenieurswesen sind also nicht nur durch hochentwickelte numerische Modelle und größere Rechenkapazität zu erreichen.

Chapter 1

Introduction

1.1 River flows, floods and the importance of hydrodynamic modeling

Rivers are sometimes referred to as the "arteries of the world" (e.g. Van Lohuizen 2003); they are vital carriers of water and nutrients, they may be used as sources of energy, and may provide important transport routes. Therefore, surroundings of rivers have since long also been popular settling areas. As a result, rivers may also pose a threat to activities that take place in its immediate vicinity: at extreme discharge conditions floods may occur that could damage nearby infrastructure and also cause casualties. At a global scale, the economic damage due to river flooding amounts to tens of billions US$ each year, and between 1985 and 2003 approximately 300,000 people have lost their life as a result of river floods (Douben and Ratnayake 2006).

To reduce flood risk, hydrodynamic models of river flow may aid in achieving better protection measures against floods. The hydraulic response of a river system can be investigated for potential discharge magnitudes, thereby providing insight in flood-critical regions in the river basin. Also, with the use of hydrodynamic models different safety measures can be evaluated on their flood protection efficiency (see, for example, Van Vuren et al. 2005 and Huthoff and Stijnen 2005). For this purpose, it is essential that flow behavior and the hydraulic impact of the surrounding flow domain is well-understood and realistically represented.

1.2 Hydrodynamic modeling - the challenge of flow resistance

The fundamental laws that describe flow behavior have been established nearly 200 years ago, and remained undisputed ever since (e.g. L'vov and Procaccia 1997). However, because of the complex nature of these laws, simplifications remain necessary to describe the dynamics of fluid flows in complex large-scale settings as in rivers. Such simplifications may limit the general validity of the flow model, and hence, the reliable range of application.

Of particular importance in river flow modeling is to understand the determining factors of *hydraulic resistance* or, in other words, to understand how topographical boundaries of the flow domain and their surface characteristics

Figure 1.1: A flooded floodplain alongside the River IJssel in the Netherlands (Feb. 3rd 1995). Picture by Henri Cormont, Rijkswaterstaat (`www.BeeldbankVenW.nl`).

affect internal flow mixing patterns. Mixing patterns feed on kinetic energy from the mean streamwise flow field, thereby decreasing the overall flow velocity and causing higher water levels at a certain discharge. In this respect, De Vriend (2006) points out that river flow modeling still lacks generally applicable descriptions of the dynamic resistance of river beds and of flow resistance of vegetated floodplains or valleys. Another important process responsible for flow resistance which remains difficult to quantify in river reach models, is the lateral mixing that occurs if the high velocity flow in the main channel interacts with slower flow on the floodplain (Pasche and Rouvé 1985, Helmiö 2002, 2004). Better understanding of these processes is important because the sensitivity of river-reach flow models to hydraulic resistance parameters can be quite large (e.g. Casas et al. 2006). In addition, Wheater (2002) emphasizes the need for hydraulic parameterization in flood models that can be assimilated with available ground measurements or remote sensing data. In effect, widely applicable methods to describe hydraulic resistance are required, for which the model parameters are readily measurable.

1.3 Hydraulic resistance in floodplain flows

In particular, the issue of hydraulic resistance of floodplains has in recent years become increasingly important in river engineering. The prospect of climate change in combination with several floods and threatening situations in the past decades has changed the vision of river engineers and authorities. The general attitude in many countries is now to restore natural river systems, instead of increasing dike heights to meet protection standards, and look for alterna-

tive ways to enlarge the discharge capacity of rivers (e.g. Silva et al. 2001, Willi 2006). Floodplain lowering, dike shifting, the installation of side channels, and removal of hydraulic obstacles in floodplains are some of the measures considered. A consequence of this trend in river management is the opportunity for nature development and restoration of the ecological corridor function of floodplains (e.g. Muhar et al. 1995, Duel et al. 2001).

In contrast, nature development in floodplains may pose potential flood threat because of the resulting hydraulic resistance of the vegetation in the floodplain: increased vegetation abundance leads to a decrease in flow velocity and a rise of water levels. Various studies have shown that the presence of vegetation may have an important impact on water levels, easily causing a water level rise of 10 cm or more locally (e.g. Huthoff and Augustijn 2004, Wang and Wang 2007). Even seasonal variation of vegetation characteristics may significantly impact hydraulic resistance in a river reach (Fisher 1995, De Doncker et al. 2006). By Dutch law, any increase in design water levels due to changes in the floodplain must be compensated (Pluimakers and van Rijswick 2003). Understanding of flow resistance due to vegetation is therefore of great importance in river-engineering studies. In addition to acquiring more accurate flood-safety levels, a sound understanding of vegetation resistance may also aid the development of nature rehabilitation schemes, if local safety standards have to be taken into account.

Due to the importance of vegetation resistance in rivers, many studies have been devoted to this topic over the last decades. As a result, several vegetation-resistance methodologies have been proposed (see Table 1.1 for a selection of methods). Not all these methods are equally suitable for integration in river-reach flow models. Unsuitable models are either too complex for large-scale implementation, require difficult to measure input parameters, or have limited ranges of applicability.

The most detailed vegetation resistance models in Table 1.1 are to be incorporated in hydrodynamic models that resolve the flow field in three spatial dimensions (e.g. '3D', as the methods proposed by López and García 2001, Uittenbogaard 2003 and Choi and Kang 2006). These methods are based on a volume-averaged drag descriptions in the flow layer that is penetrated by the vegetation, and on detailed turbulent energy transport models. The range of applicability of these models within a river flow setting is in principle unlimited, as long as a plant-specific drag coefficient is available. Nevertheless, such detailed vegetation resistance models incorporated in a 3D river reach model require accurate boundary conditions and also yield large computation times. In practice, numerical modeling of flows in three dimensions is therefore usually restricted to relatively small flow domains (e.g. Ge and Sotiropoulos 2005, Jia et al. 2005), instead of full river-reach scales.

Alternatively, river reach studies are based on 2D models, describing the depth-averaged flow field, or based on cross-sectionally averaged 1D models, which only explicitly describe flow interaction in streamwise direction (e.g. Horritt and Bates 2002). A hybrid form of these approaches has also become increasingly popular, so-called 1D-2D models, combining advantages of com-

Table 1.1: A selection of vegetation resistance methods.

Reference	Main characteristics	Applicability
US Soil Conservation Service (1954)	Empirical relation for roughness coefficient ('n-UR method')	Plant specific, limited range of channel slopes
Kouwen et al. (1969)	Adjusted boundary layer profile, empirical roughness height	Submerged short vegetation (grass)
Kouwen and Unny (1973)	Dimensional analysis, regression analysis	Specific types of submerged flexible vegetation
Petryk and Bosmajian (1975)	Physically based drag description of vegetation layer	Emergent vegetation
Kaiser (1984)	Physically based drag description of vegetation layer	Emergent vegetation
Klopstra et al. (1997)	Physically based two-layer model combining drag and adjusted boundary layer	Turbulent flow with submerged or emergent vegetation
Freeman et al. (2000)	Dimensional analysis, regression analysis	Specific types of submerged flexible vegetation
Fischenich (2000)	Combination of drag term with turbulent velocity profile over vegetation (regression analysis)	Specific types of submerged flexible vegetation
López and García (2001)	Drag description in between vegetation, turbulent transport model	3D flow models
Stephan and Gutknecht (2002)	Adjusted boundary layer profile, empirical roughness height	Submerged flexible vegetation
Van Velzen et al. (2003)	Simplified form of method proposed by Klopstra et al. (1997)	Turbulent flow with submerged or emergent vegetation
Uittenbogaard (2003)	Drag description in between vegetation, turbulent transport model	3D flow models
Järvelä (2004)	Physically based drag description, including effects of leaves and side branching	Emergent bushes or trees
Choi and Kang (2006)	Drag description in between vegetation, turbulent transport model	3D flow models
Baptist et al. (2007)	Dimensionally correct data-driven model	Turbulent flow with submerged or emergent vegetation

putational efficiency with explicitly modeling dominant physical processes (e.g. Stelling and Verwey 2005, Tayefi et al. 2007). All these spatially-averaged models require corresponding spatially-averaged hydraulic resistance parameters, describing the effective flow response in the represented spatial domain.

Early attempts to describe the impact of vegetation on the depth-averaged flow velocity were based on the assumption that an equivalent bed roughness can be attributed to vegetation, as was known to be a successful method for flow over rough surfaces (e.g. Chow 1959). However, limitations of this approach were immediately evident as the equivalent vegetation bed roughness appeared to be flow-dependent (e.g. US Soil Conservation Service 1954). Consequently, so-called 'n-UR' relations were established that describe a hydraulic resistance parameter (Manning's coefficient 'n') in terms of flow properties (flow velocity 'U' and hydraulic radius 'R'). A clear disadvantage of such relations is that the dependencies between flow properties and effective hydraulic resistance have to be investigated for a wide range of flow conditions and vegetation types. Wilson and Horritt (2002) point out that these relations have limited ranges of applicability as even for one vegetation type no unique n-UR relationship can be established. Furthermore, because underlying physical processes are not well understood, transportation or extrapolation to new situations is difficult and unreliable.

In a more detailed approach, the vertical velocity profile of flow over vegetation is investigated, using measurable vegetation characteristics to typify the shape of the velocity profile. In case of emergent vegetation, these methods appeared to be quite successful (e.g. Petryk and Bosmajian 1975, Kaiser 1984, Järvelä 2004), while for submerged vegetation poorly understood closure parameters remained required (e.g. Kouwen et al. 1969, Klopstra et al. 1997, Stephan and Gutknecht 2002, Van Velzen et al. 2003). Thus, again, lack of understanding of some model components limits the confidence in general application of these methods.

1.4 Modeling hydraulic resistance of floodplain vegetation

Ideally, including the effect of obstructing vegetation in a river flow model is done in terms of easily measurable vegetation characteristics and, most importantly, accurately describes the relation between discharge and hydraulic response (i.e. resulting water level) for a wide range of flow conditions and vegetation types. Among existing vegetation resistance methods the most widely applicable methods (i.e. detailed numerical models including turbulence equations) are not suitable at river-reach scales. On the other hand, more simplified methods often lack understanding based on fundamental physical principles, thus limiting the reliable range of applicability and the potential for extension to complex vegetation configurations. The current work aims at improving the incorporation of hydraulic impacts of vegetation in river flow models.

1.4.1 Objective

To develop a model of hydraulic resistance of vegetation for river management purposes that is able to describe the hydraulic response for a wide range of vegetation types and flow conditions, allows for incorporation in river-reach flow models and requires input data that can be measured in the field.

1.4.2 Research questions

In accordance with the objective stated above, the following research questions (Q) are identified:

Q1: How can vegetation effects be included in flow models, and which methods are suitable at river-reach scales?

Q2: Focussing on ease of application and reliability, among existing methods, what is potentially the most generally applicable method to describe vegetation in river-reach models?

Q3: What are limitations of this method and can these be solved?

Q4: In floodplain flows, is it possible to describe the overall flow field in a physically sound way, without explicitly describing detailed flow processes?

Q5: How does the method perform in full-scale vegetated waterway settings?

1.4.3 Used data

To represent the hydraulic impact of vegetation in a river flow model it is necessary to describe vegetation in terms of readily measurable parameters, such as geometrical dimensions, leaf cover density and flexibility. In principle, these parameters can be quantified for particular conditions, but this may become complicated if a large area needs to be sampled, and if a large degree of spatial variability is present in the field. In Straatsma (2007) methodologies are proposed to obtain vegetation characteristics in the field, and also methods to obtain complementary hydraulic data for river-reach model calibration. In contrast, the current work focusses on how to *represent* vegetation resistance reliably, preferably based on physical principles. To understand the importance of particular vegetation characteristics in a flow field, it is essential that these characteristics and the flow conditions are accurately measured, much more accurate than possible in natural vegetated waterways. Therefore, in the current work, laboratory data is used to evaluate the validity of steps taken in the model-development procedure.

The used laboratory data is adopted from flow studies with rigid cylinders and natural reed, as performed at the *De Voorst* WL|Delft Hydraulics facility in 1997 and 1998 (Meijer and van Velzen 1998, Meijer 1998a, 1998b). The flume was 100 m long, 3 m wide and vegetation was placed over a length of 22 m. Figure 1.2 shows a picture of the flume set-up, including rigid cylinders to represent vegetation. The three components of the velocity field were measured

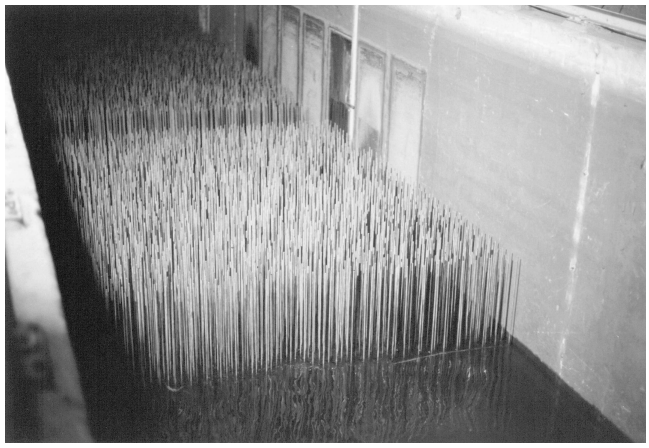

Figure 1.2: In 1997 and 1998 flume experiments were conducted by HKV Consultants at the *De Voorst* WL|Delft Hydraulics facility (Meijer and van Velzen 1998, Meijer 1998a, 1998b). Several configurations of different water levels, cylinder heights, cylinder surface densities and natural reed were used.

with an Acoustic Doppler Velocimeter (ADV) at different depths with a sampling frequency of 25 Hz (during ∼100 s). Results from the flow measurements are also reported in Oberez (2001) and Baptist (2005).

1.4.4 Thesis outline

Chapter 2: This Chapter gives an overview of theory of turbulent flows, in particular related to wall-bounded flows and applicability in river engineering. The objective of this chapter is to provide an answer to **Q1** and to identify methods that may serve as a reliable basis for achieving a generally applicable vegetation resistance method (**Q2**).

Chapter 3: This Chapter focusses on the vegetation resistance method proposed by Klopstra et al. (1997), which appears to be a promising method with respect to the objective of this thesis, and is currently also used for river engineering purposes in the Netherlands. Relating to **Q3**, an in-depth study of its properties is performed to identify shortcomings and inconsistencies of the method.

Chapter 4: Motivated by the results from Chapter 3, in Chapter 4 an alternative description of depth-averaged flow over (idealized) vegetation is presented (**Q3**). A bulk force balance, energy considerations of turbulent flow and scaling assumptions are used to estimate the overall spatially-averaged flow velocity over vegetation. The bulk flow model is also compared to laboratory data (**Q4**).

Chapter 5: Because of the appealing characteristics of the new method from Chapter 4, i.e. its mathematical simplicity and its accurate description

of flow resistance of idealized vegetation, in Chapter 5 the method is compared to flow measurements that were collected in natural waterways (**Q5**). Two particular field cases are used for this purpose; in the first case flow conditions were measured in a geometrically simple grassed channel, and in the second case flow in a more complex floodplain environment is analyzed.

Chapter 6: Reflecting again on **Q2**, in Chapter 6 a synthesis of investigated vegetation resistance models is given, and detailed characteristics of the two methods are compared. Two other resistance models are also included in a comparison-study with data from a wide range of laboratory flow experiments. Relating to all resistance methods, advantages and disadvantages for practical application are discussed. Also, suggestions are made for future experiments that may provide required input data for the proposed resistance methods, and experiments are proposed that could discard methodologies.

Chapter 7: The successful scaling technique of turbulent flows as demonstrated in Chapter 4 is also used in Chapter 7, to derive a new bulk flow method that includes the effect of lateral momentum transfer in overbank flows. Again, **Q4** is addressed.

Chapter 8: In this Chapter, consequences for river flood forecasting and opportunities for other fields of applications are discussed.

Chapter 9: Finally, answers are given to the research questions **Q1** - **Q5**, supplemented with recommendations for practical application and future research.

Chapter 2

Modeling turbulent flow and vegetation resistance in rivers

In this chapter an overview is given of characteristics of turbulent flows and ways to describe vegetation resistance in flow models. By comparing available methods, it is identified which methodologies appear most promising towards achieving a generally applicable method to describe vegetation resistance in river-reach flow models. Based on the practical capabilities of gathering required input parameters, it is concluded that flow through vegetation is best described using a spatially-averaged empirical drag coefficient. For flow over vegetation, several methods seem suitable, such as methods based on transport of turbulent energy or adjusted boundary layer profiles. Whether these methods have similarly wide ranges of applicability requires further investigations, in which general dependencies of respective model parameters are determined.

2.1 Introduction

River flows are driven by gravity. To understand what processes are slowing down the flow, and how those processes can be quantified, is much more difficult. Already in 1797 Venturi realized that resistance to flow in rivers is largely due to disorderly mixing processes, or *turbulent eddies* (translation by Darrigol 2005):

> *"One of the principal and most frequent causes of retardation in a river is produced by the eddies incessantly formed in the dilations of the bed, the cavities of the bottom, the inequalities of the banks, the bends or windings of its course, the criss-crossing currents, and the streams that intersect with different velocities."*

Describing flow resistance in rivers thus requires understanding of turbulent flows, which may be affected by various characteristics of the flow domain. A cause of flow resistance that Venturi did not explicitly mention is the presence of obstructing vegetation. Turbulent flow patterns created in the wake of the vegetation stems (e.g. Nepf 1999) feed on kinetic energy in the mean streamwise flow field, which effectively slows down the flow. Due to the complex nature of vegetation resistance, a general methodology suitable for integrated modeling is still lacking (Brookes et al. 2000). This issue is of great importance to river-reach flood modeling as the hydraulic resistance of vegetation can play a

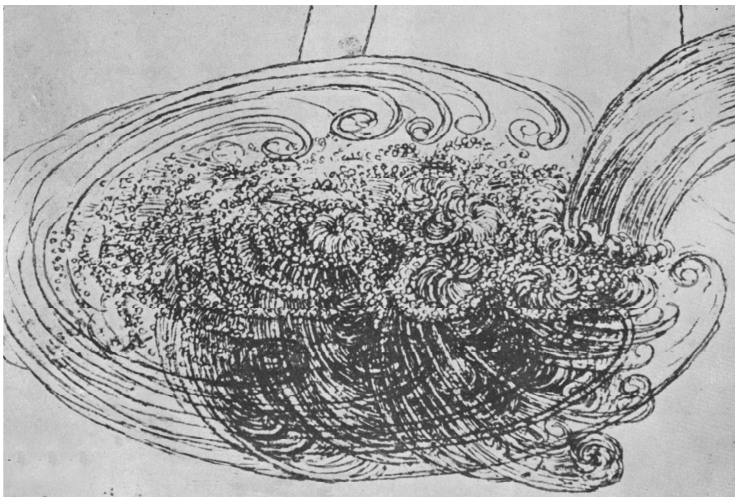

Figure 2.1: A drawing of turbulent flow by Leonardo da Vinci (1510).

major role in the hydrodynamics of rivers with extensive natural floodplains (e.g. Huthoff and Augustijn 2004).

Towards the objective of finding a generally applicable methodology for describing vegetation resistance, in this Chapter an overview is given of characteristics of turbulent flows, how these may be modeled, and how to include effects due to obstructing vegetation. In relation to modeling river-reach flows, it is argued which approaches are most appealing and opportunities for a generally applicable treatment of vegetation resistance are discussed.

2.2 Turbulent flows and Hydraulic Resistance

2.2.1 A short history in turbulence

Early attempts to understand turbulence were made by da Vinci (early 1500's), who made detailed sketches of turbulent eddies (Figure 2.1). More than a century later, a deterministic description of fluid flows was given by Euler, who in 1752 derived the fluid flow equivalent of Newton's second law of motion (e.g. Truesdell 1953, Darrigol 2005):

$$\frac{\partial \mathbf{u}}{\partial t} + (\mathbf{u} \cdot \nabla)\mathbf{u} = -\frac{1}{\rho}\nabla p + \frac{F}{\rho}, \tag{2.1}$$

where the flow velocity $\mathbf{u}$ is driven by an external force F, or a pressure p that is exerted on the fluid (which has density ρ). However, the description of fluid flows as given by Euler was still incomplete, as it failed to explain how an object immersed into flow experiences drag (*d'Alembert's paradox*, e.g. Stewartson 1981). A next step forward in the physical understanding of flows was made by Navier (1820's), who believed that flow resistance was caused by friction

between flow layers, owing to 'molecular adhesion' (Darrigol 2005). Drag on a solid was thus due to the fluid 'sticking' to the surface. Based on his own earlier work on elasticity of solid objects, Navier expanded Euler's equation, adding a contribution due to molecular forces. Several others also derived this equation: Cauchy in 1823, Poisson in 1829, Saint-Venant in 1837 and Stokes in 1845 (Darrigol 2005), which is now known as the *Navier-Stokes* equation (e.g. Pope 2000)

$$\frac{\partial \mathbf{u}}{\partial t} + (\mathbf{u} \cdot \nabla)\mathbf{u} = -\frac{1}{\rho}\nabla p + \frac{F}{\rho} + \nu \Delta \mathbf{u}, \tag{2.2}$$

where the kinematic viscosity ν accounts for forces at the molecular level. Today, it is still believed that all details of fluid flow can be described by the Navier-Stokes equation in combination with appropriate boundary conditions. However, general solutions have never been found*.

In 1871 Saint-Venant simplified the Navier-Stokes equation for flows in open channels, by treating the flow velocity as a spatially averaged value (e.g. Mujumdar 2001). To account for the effects of small-scale flow processes that are no longer explicitly described, an additional term is introduced to the flow equation: the *hydraulic resistance*. Consequently, the 1D shallow water equation for slowly varying flow becomes (e.g. Chow 1959)

$$\frac{\partial U}{\partial t} + U\frac{\partial U}{\partial x} = -g\frac{\partial h}{\partial x} + gi - gS, \tag{2.3}$$

where U is the cross-sectionally averaged flow velocity in the x-direction, which is oriented along the inclination of the channel bed i, g is the gravitational acceleration, h the flow depth and, to reflect hydraulic resistance, S the newly introduced *friction slope*. Alternatively, Boussinesq interpreted hydraulic resistance as a large-scale effective viscosity (the *Boussinesq hypothesis*). While simplifying the Navier-Stokes equation, Saint-Venant and Boussinesq introduced new conceptual parameters which values could only be determined empirically.

In the late 19th century, a major breakthrough in understanding turbulent flow came with the work of Osborne Reynolds (e.g. Jackson and Launder 2007). Reynolds realized that the Navier-Stokes equation contains the description of turbulence, and proposed to isolate characteristics of turbulence by treating velocity fluctuations separate from the mean flow velocity†. The resulting Reynolds Averaged Navier-Stokes (RANS) equations are (e.g. Rodi 1980, Pope 2000)

$$\frac{\partial u_\mathrm{i}}{\partial t} + u_\mathrm{j}\frac{\partial u_\mathrm{i}}{\partial x_\mathrm{j}} = -\frac{1}{\rho}\frac{\partial p}{\partial x_\mathrm{i}} + \frac{F_\mathrm{i}}{\rho} + \frac{\partial}{\partial x_\mathrm{j}}\left(\nu\frac{\partial u_\mathrm{i}}{\partial x_\mathrm{j}} - \overline{u_\mathrm{i}' u_\mathrm{j}'}\right), \tag{2.4}$$

*The Clay Mathematics Institute of Cambridge, Massachusetts (CMI) has named seven Millennium Prize Problems, among which the identification or proof of existence of a general solution to the Navier-Stokes equation (see `www.claymath.org/millennium/`).

†Interestingly, already in 1510 Da Vinci suggested separate treatment of mean flow and superimposed turbulent fluctuations (Lumley 1992, translation by U. Piomelli): *"Observe the motion of the surface of the water, which resembles that of hair, which has two motions, of which one is caused by the weight of the hair, the other by the direction of the curls; thus the water has eddying motions, one part of which is due to the principal current, the other to the random and reverse motion."*

where u_i is the time-averaged velocity component in direction i = x, y or z. Likewise, x_i is the spatial coordinate for any of the three directions. In the *Reynolds averaging approach*, u_i is averaged over a time-scale that is large compared to the time-scale of turbulent motion, but small compared to the time-scale of the mean flow. As a result of Reynolds-averaging, a term with correlations between turbulent velocity fluctuations appears ($\overline{u_\mathrm{i}' u_\mathrm{j}'}$, where the overbar denotes time-averaging), which accounts for energy losses to the mean flow field due to turbulent mixing patterns. The behavior of these so-called *Reynolds stresses* is unknown and has to be modeled separately.

Also, from several experiments with flow in pipes Reynolds observed that for a range of flow velocities, pipe diameters (d) and fluid viscosities, the fluid went from a steady, predictable motion to a disorderly, chaotic state. This transitions occurs at roughly the same value of the dimensionless parameter

$$\mathrm{Re} = \frac{Ud}{\nu}, \tag{2.5}$$

It is now understood that the *Reynolds number* Re reflects the relative importance of inertial forces in contrast to viscous forces. Therefore, Re also reflects whether molecular viscosity or internal mixing patterns (and thus the Reynolds stresses) are mainly responsible for hydraulic resistance.

2.2.2 Kolmogorov's phenomenological theory of turbulence

An alternative description of turbulent flows is proposed by Kolmogorov (1941). Based on the view that turbulent eddies are generated at the largest spatial scale of the flow domain, and are subsequently broken up into smaller eddies until viscosity limits the smallest motions, the so-called phenomenological theory of turbulence is established. In this theory, a fundamental quantity is the energy flux ε, which reflects the rate of energy transfer between eddies at different spatial scales. Three ranges are defined referring to spatial scales in the flow field: (i) the *energy containing range*, (ii) the *inertial subrange* and (iii) the *dissipation range*. In the energy containing range, characterized by the largest eddies which contain most energy, eddies are anisotropic because they are driven by geometrical scales. From the largest eddies, energy is transferred to smaller-scale eddies in the inertial subrange, which are no longer affected by geometrical scales. Finally, in the dissipation range, energy of the smallest eddies is dissipated to heat by viscosity.

Closely related to the definitions of the three scale ranges, three hypotheses form the basis of Kolmogorov's theory (after Pope 2000):

Hypothesis of local isotropy: At sufficiently high Reynolds number, the turbulent motions in the inertial range are statistically isotropic.

First similarity hypothesis: In turbulent flow at sufficiently high Reynolds number, the statistics of motions in the dissipation range have a universal form uniquely determined by the viscosity ν and ε.

Second similarity hypothesis: In turbulent flow at sufficiently high Reynolds number, the statistics of motions in the inertial subrange have a universal form uniquely determined by ε, independent of the viscosity ν.

Based on the hypothesis of local isotropy and the second similarity hypothesis an energy spectrum for the inertial subrange is derived (reflecting the energy contained in motions with certain length-scales)

$$E(k_w) = C_\kappa \varepsilon^{2/3} k_w^{-5/3}, \tag{2.6}$$

where $k_w = 2\pi/\ell$ is the wave number of eddies with size ℓ, and C_κ a universal constant ($C_\kappa \simeq 0.5$, e.g. Nezu 2005). The prediction of the -5/3 power exponent in the energy spectrum is one of the most important results from Kolmogorov's theory, which has been confirmed many times in different types of turbulent flows (e.g. Phillips 1991 in oceanic flows, Zocchi et al. 1994 in helium gas). Furthermore, based on the first similarity hypothesis, Kolmogorov (1941) used dimensional analysis to derive characteristic micro scales for the dissipation range

$$\eta_\kappa = \left(\frac{\nu^3}{\varepsilon}\right)^{1/4}, \tag{2.7}$$

$$\tau_\kappa = \left(\frac{\nu}{\varepsilon}\right)^{1/2}, \tag{2.8}$$

where η_κ is the spatial scale where viscous forces become responsible for energy dissipation and τ_κ the corresponding time scale. These scales are important for calculating turbulent flows, as they describe where turbulent mixing ceases to be responsible for energy transfer. The input of energy into turbulent eddies is estimated based on the kinetic energy of the mean flow (which scales with U^2) that is transferred to smaller-scale motions on the time-scale T

$$\varepsilon \simeq \frac{U^2}{T}. \tag{2.9}$$

Next, the time-scale T, or the *turnover time*, is associated with largest eddy motions and estimated by assuming that the largest eddies have a characteristic velocity that scales with U and are bounded by a characteristic length-scale of the flow domain L. Therefore, T scales with L/U, which yields for the turbulent energy input

$$\varepsilon \simeq \frac{U^3}{L}. \tag{2.10}$$

2.2.3 Hydraulic resistance

In hydraulic studies of river flows, where one of the main concerns is the prediction of the overall (large-scale) water movement, the bulk flow approach proposed by Saint-Venant has remained popular (Werner and Lambert 2007). Comparing equation (2.3) with equation (2.4) shows that in the Saint-Venant equation all effects due to Reynolds stresses, viscosity and local pressure differences are absorbed into the hydraulic resistance. In order to apply the bulk

flow approach to a wide range of situations, the challenge becomes to describe hydraulic resistance in terms of readily measurable quantities, such as the flow velocity and geometrical boundaries. Based on dimensional analysis, hydraulic resistance may be defined as

$$gS = f\frac{U^2}{R}, \tag{2.11}$$

where R is the *hydraulic radius* and f the dimensionless hydraulic resistance coefficient. The hydraulic radius is defined as the ratio between the flow cross-section area A and the perimeter P where fluid is in contact with the solid boundaries (the *wetted perimeter*).

$$R = \frac{A}{P} \tag{2.12}$$

For flow in a circular pipe, the hydraulic radius reduces to the radius of the pipe, and for flow in a wide open channel to the flow depth.

In turbulent flows, the viscous term in the RANS equation is much smaller than the Reynolds stresses. Therefore, describing hydraulic resistance in turbulent flows requires estimations of Reynolds stresses and pressure differences. For two particular types of flows the characteristics of Reynolds stresses and pressure differences have been extensively studied: flow over a solid surface, and flow past an obstructing object.

Shear flows over a solid surface

Understanding of shear flows largely relies on the work of Prandtl, commonly referred to as Boundary Layer Theory (e.g. Schlichting and Gersten 2000). Prandtl envisioned the mixing length concept, which provides a simple model of the Reynolds stresses in shear flows. In the mixing length concept, the velocity fluctuations that make up the Reynolds stresses are associated with turbulent eddies of particular size ℓ_t, the *turbulent mixing length*. These eddies describe the effective transfer of momentum within the flow field and are directly responsible for the resulting large-scale characteristics of the flow, such as the mean velocity at each location and the corresponding local velocity gradient. For flow over a solid bed, the Reynolds stress expressing shear between vertical flow layers is given by

$$\tau_{xz} = -\rho\overline{u'_{\mathrm{x}}u'_{\mathrm{z}}}. \tag{2.13}$$

If the only gradient in the flow field is over depth (i.e. $\partial u/\partial z$), then velocity fluctuations in streamwise (x) and vertical (z) directions are associated with eddies of size λ in the vertical plane, with eddy-axis perpendicular to the mean flow direction. This view leads to the relations

$$\sqrt{(u'_{\mathrm{x}})^2} = \lambda\frac{\partial u}{\partial y}, \quad \sqrt{(u'_{\mathrm{z}})^2} = \lambda\frac{\partial u}{\partial y}. \tag{2.14}$$

Consequently, using the mixing length concept, the Reynolds shear stress is represented by

$$\tau_{xy} = \rho\lambda^2\left(\frac{\partial u}{\partial y}\right)^2. \tag{2.15}$$

This model for the Reynolds stress can be used in equation (2.4) to describe relatively simple shear flows (e.g. Rodi 1980).

For wall-bounded flows, Von Kármán (1930) hypothesized that the mixing length λ is proportional to the distance from the wall z

$$\lambda = \kappa z, \tag{2.16}$$

where Von Kármán's constant κ has a universal value, experimentally determined as $\kappa \simeq 0.4$. It can be shown that for steady uniform flow, the mixing length model in combination with Von Kármán's hypothesis leads to a logarithmic velocity profile as (e.g. Townsend 1976)

$$u(z) = \frac{u_*}{\kappa} \ln\left(\frac{z}{z_0}\right), \tag{2.17}$$

where the *zero-plane displacement* z_0 is defined as the height where the flow velocity reduces to zero, i.e. $u(z_0) = 0$. Furthermore, the *friction velocity* u_* is defined as

$$u_* = \sqrt{\tau_b/\rho}, \tag{2.18}$$

where τ_b reflects the equivalent bed shear stress required to balance the driving force

$$\tau_b = \rho g h i. \tag{2.19}$$

Next, the average flow velocity U is obtained by integrating the velocity profile in equation (2.17) over the flow depth h, which yields

$$U = \frac{u_*}{\kappa} \ln\left(\frac{h}{\mathrm{e} z_0}\right). \tag{2.20}$$

Experiments by Nikuradse (1933) have shown that the zero-plane displacement z_0 can be characterized by an equivalent roughness height k_N as $z_0 \simeq \frac{k_N}{33}$, where k_N reflects the size of irregularities on the channel bed.

An important characteristic of the logarithmic velocity profile is that its shape is determined by turbulent mixing, irrespective of viscosity, and thus reflects fully turbulent flow (where viscous effects are negligible). Therefore, in wall-bounded flows, a distinction is made between situations where flow near the wall is mainly viscous (a *smooth wall*) or where flow remains turbulent (a *rough wall*). Using the results of Nikuradse and the definitions of the hydraulic resistance coefficient and hydraulic radius, equations (2.11) and (2.12), Keulegan (1938) provides an expression for the hydraulic resistance coefficient for fully turbulent flow over a rough channel bed

$$\frac{1}{\sqrt{f}} = \frac{1}{\kappa} \log \frac{R}{k_N} + 2.21 \qquad \text{(hydraulically rough)}, \tag{2.21}$$

and also for flow over a smooth channel bed

$$\frac{1}{\sqrt{f}} = \frac{1}{\kappa} \log(\mathrm{Re}\sqrt{f}) \qquad \text{(hydraulically smooth)}. \tag{2.22}$$

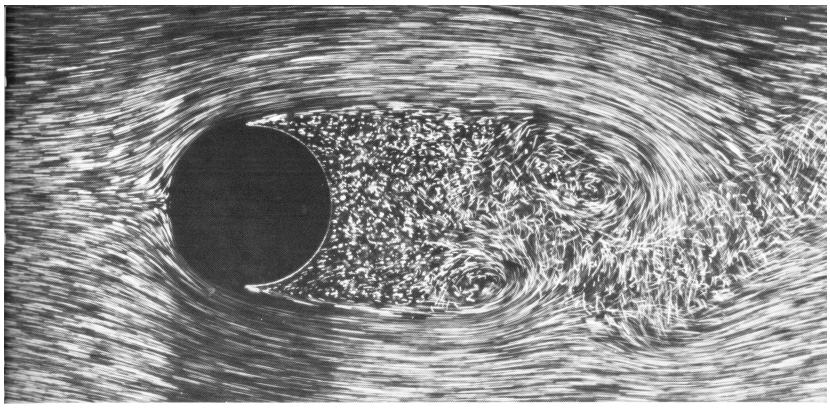

Figure 2.2: Wake turbulence behind a cylinder at Re = 2000. Visualization is by air bubbles in water (Werlé and Gallon 1972, photograph courtesy of ONERA *French Aerospace Lab*).

In relation to Kolmogorov's theory of turbulence, experimental observations have shown that the large-scale turbulent motions are more isotropic for hydraulically rough flow than for hydraulically smooth flow (Poggi et al. 2003). The energy spectrum in rough channel flows thus exhibits the $-5/3$ power law across a relatively large range of wave-numbers, spanning a range of associated length-scales from the forcing scale-size (i.e. flow depth) to the equivalent roughness height.

Flow past an obstructing object: form drag

Flow past an obstructing object may cause turbulent vortices in the wake of the object (see Figure 2.2). Due to the confined region where enhanced turbulent mixing takes place, it is more difficult to make scaling assumptions of the Reynolds stresses throughout the flow field (e.g. Townsend 1949), as was shown for simple shear flows. Therefore, the effect of form drag is more commonly expressed by empirical methods (Williamson 1996), using general scaling assumptions. By spatially-averaging the time-averaged Reynolds equations, it can be shown that the drag term appears in the flow equation as a result of heterogeneity of the time-averaged flow (e.g. Raupach and Shaw 1982, Nikora et al. 2001).

Drag caused by an obstructing object can be understood in terms of a pressure drop in the wake. The larger the wake, the larger the region with lower pressure, yielding a larger effective drag force. The cross-sectional extent of the wake is roughly equal to the blockage area of the obstructing object. Therefore, drag caused by an obstructing object is closely related to its blockage area. The *drag coefficient* C_D is defined based on the drag force F_D an object with blockage area a experiences in a flow field having mean velocity U (e.g. Heddleson

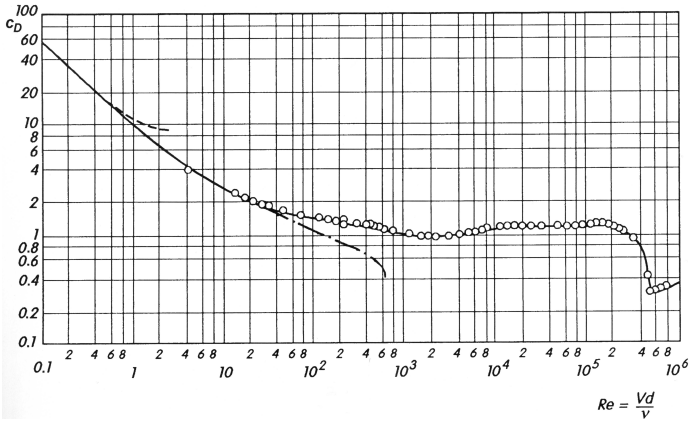

Figure 2.3: The drag coefficient C_D of flow around a cylinder, as function of the Reynolds number Re (Schlichting and Gersten 2000).

et al. 1957, Hoerner 1965)

$$C_D = \frac{F_D}{\frac{1}{2}\rho a U^2}. \tag{2.23}$$

Figure 2.3 gives an overview of empirically determined drag coefficients for a cylinder at different turbulent flow regimes (e.g. Schlichting and Gersten 2000). In laminar flow, it is found that C_D is approximately inversely proportional to Re, up to a Reynolds number of Re $\sim$ 10. At larger Reynolds numbers (Re $> 10^2$), the drag coefficient remains nearly constant at a value of $C_D \simeq 1$. This trend confirms that the blockage area of an obstructing object is indeed a suitable scaling parameter for describing drag. At high Reynolds numbers ($10^5 <$ Re $< 10^6$) a sudden drop in drag coefficient is observed. This decreased drag is commonly referred to as the *drag crisis*, which may be understood in terms of a compressed wake-size at highly turbulent flows (Singh and Mittal 2005).

The energy spectrum of turbulent flow in the wake of a cylinder shows a -5/3 power law dependence on wave number, with most energy contained in eddies associated with the size-scale of the cylinder diameter (e.g. Ninni et al. 1999). However, if the cylinders are placed in shallow flows, then the presence of the bed suppresses formation of large eddies in the vertical plane. In such cases a steeper -3 power law exponent is observed in the energy spectrum (e.g. Jirka 2001, Uijttewaal et al. 2001), which is associated with quasi-two-dimensional turbulence (Kraichnan 1967).

2.3 Computations of turbulent flows in presence of vegetation

A brief overview was given of current understandings of turbulent flows. Ideally, flows are modeled by using the Navier-Stokes equation, as this equation provides

the most general and complete description of fluid flows. However, due to the non-linearity of the Navier-Stokes equation, detailed flow calculations are complicated. For practical applications it is therefore inevitable to derive simplified flow descriptions, as in the case of simple shear flows or drag-dominated flows, or to apply numerical solution techniques (or use a combination of the two). Next, practical properties of different techniques to calculate fluid flows are briefly described, and how they may be used to include the hydraulic response caused by vegetation.

2.3.1 Solving the Navier-Stokes equation

Direct Numerical Simulation (DNS)

In Direct Numerical Simulation (DNS) the Navier-Stokes equations are resolved to the smallest details of fluid flow. The associated Kolmogorov micro-scales, given by equations (2.7) and (2.8), prescribe the required spatial and temporal resolutions to capture all relevant flow patterns (e.g. Pope 2000). At scales smaller than the Kolmogorov micro-scales, molecular forces govern energy losses, which, for common flow situations, are well represented by an energy sink based on viscosity.

For turbulent flows with relatively small Reynolds numbers and in simple geometric domains, DNS has already been applied successfully (Vincent and Meneguzzi 1991, Moin and Mahesh 1998, Breugem 2004, Williams and Singh 2004). However, clear disadvantages of DNS are the large computational cost, which increases with Re^3 (Pope 2000), and the amount of memory capacity needed. A simple calculation reveals that passage of a flood wave over a distance of 1 km in a typical lowland river could easily require tens or hundreds of years of DNS computation time[‡].

Large-Eddy Simulation (LES)

In Large Eddy Simulations (LES) the Navier-Stokes equation is also directly solved, but without describing all spatial and temporal scales of turbulent flow (e.g. Meneveau and Katz 2000). The required computational time of LES is therefore significantly smaller than in DNS, because the time-consuming small-scale motions are "filtered out"[§]. As a consequence of filtering small-scale motions, an additional model is needed to represent turbulent effects that are no longer explicitly resolved. For this purpose, turbulent viscosity models may be used (*explicit filtering* of small-scale turbulence). If no explicit filter is used,

[‡]An average flow velocity of 0.5 [m/s] over a flow depth of 5 [m] yields Kolmogorov microscales of $\eta_\kappa = 80$ [μm] and $\tau_\kappa = 6$ [ms]. If the channel width is 50 [m] and length is 1000 [m] then DNS requires a grid of $5 * 10^{17}$ cells. Traversing the channel at a flow velocity of 0.5 [m/s] takes about half an hour, of which the flow characteristics have to be determined at intervals of the Kolmogorov timescale τ_κ. This yields a total of $15 * 10^{22}$ calculation steps. Using today's fastest computer, the IBM BlueGene/L System capable of 280.6 TFlops (*teraflops*, or 10^{12} calculation steps per second), the calculation would take at least 20 years.

[§]More than 99.9 % of the computational effort in DNS is spent on resolving the small-scale motions in the energy dissipation range (Pope 2000).

then the computational grid and discretization technique limits the scale of the smallest motions (*implicit filtering*). Gullbrand and Chow (2003) give an overview of different filtering techniques of LES for channel flows, and Piomelli and Balaras (2002) of wall-turbulence models that may be used in combination with LES.

A particular example of wall-turbulence modeling used in combination with LES is known as Detached Eddy Simulation (DES), as first proposed by Spalart et al. (1997). In near-wall flows, the dynamically important motions become smaller, thus increasing the required resolution of a LES approach. Therefore, in DES the boundary layer near the wall is solved with the Reynolds-averaged Navier-Stokes equation and the motions in the separated outer layer with LES. As a result, the large computational effort that LES requires to solve near-wall flow is avoided, but still the energetically relevant motions in the outer flow are described.

Incorporating vegetation flow resistance

Nadaoka and Yagi (1998) applied LES to model shallow flow over vegetation, by treating vegetation as an array of equally spaced cylinders. As a turbulence model they adopted an energy transport equation (K-ε model) that also incorporated vegetation drag, by means of a standard drag force term. The model was able to reproduce turbulence characteristics at the top of the vegetation layer and gave good agreement with measured mean flow velocities in between and above the vegetation. A similar approach, using an explicit turbulence filter that includes cylinder drag, is presented in Cui and Neary (2002), who also obtain good agreement with reference laboratory flow measurements. Stoesser and Rodi (2004) applied LES to flow over cylinders without incorporating the empirical drag coefficient, but imposed the no-slip boundary conditions on all solid boundaries, including the surfaces of the cylinders. That way, turbulent flow structures generated by the presence of protruding cylinders are explicitly described by the model, effectively yielding form drag of the cylinders. In the study of Stoesser and Rodi (2004) it is shown that the shape of the roughness elements is of significance to the properties of the turbulent flow field, a result that is also well-known from empirical determinations of form drag coefficients (e.g. Heddleson et al. 1957, Hoerner 1965).

2.3.2 Solving the Reynolds-averaged Navier-Stokes equation

In the Reynolds-averaged Navier-Stokes (RANS) equation, equation (2.4), only the behavior of the mean flow field is described, and all mixing patterns are absorbed into a separate turbulence model. Turbulent motions are thus no longer explicitly described, reducing the required computation time even further (compared to LES). Several turbulence models have been proposed for the Reynolds stresses, each having their own particular advantages (e.g. Rodi 1980, Rodi 1995). Consequently, application of particular turbulence models are restricted to specific types of flow situations. Simple shear flow can often be described by adopting a simple turbulence model, for example Prandtl's mixing layer concept.

More complex flow configurations require more generally applicable turbulence models, such as transport equations for the turbulent kinetic energy.

Incorporating vegetation flow resistance

The vertical structure of the flow field over vegetation has been modeled by various researchers using the RANS equations (e.g. Shimizu and Tsujimoto 1994, López and García 2001, Neary 2003, Uittenbogaard 2003, Choi and Kang 2004). In each of these works a spatially-averaged form drag description is included in the RANS equations to include the effect of flow obstruction by vegetation. By calibration on the drag coefficient good agreement with measured flow velocities were obtained, while agreement with turbulence characteristics is sometimes poor (e.g. Defina and Bixio 2005). Kutija and Hong (1996) also incorporated flexibility of vegetation by including a cantilever beam theory to calculate an effective height of the vegetation. Unfortunately, the effect of flexibility was not validated by comparison with laboratory flow data. Fisher (2001) and Choi and Kang (2006) use the 3D RANS equations to model flow in channels that are partly vegetated, both studies yielded good agreement with measured mean flow characteristics. The particular advantage of these models is that they include the effect of lateral exchange mechanisms between vegetated and non-vegetated flow regions, which may provide insight into optimal planting locations to reduce stream bank erosion (Choi and Kang 2006).

2.3.3 Using spatially-averaged flow descriptions

The Saint-Venant equation, equation (2.3), describes the behavior of the spatially-averaged flow field (as averaged over width, depth or both), and all small-scale flow effects are included in the resistance coefficient. The computational effort required to solve the Saint-Venant equation is smaller than for the RANS equation, as the resolution of the flow description is reduced. If flow is (nearly) steady and uniform, also the longitudinal component of the flow model can be averaged-out, yielding '0D' flow relations. Examples of such '0D' relations are the well-known Chézy, Manning and Darcy-Weisbach equations (e.g. Yen 2002).

A disadvantage of the spatially-averaged approach is that the resistance coefficient is often case-specific and not always well-understood. Therefore, in many practical applications of spatially-averaged flow models, the hydraulic resistance coefficient is used as calibration parameter (e.g. Wasantha Lal 1995). Alternatively, the hydraulic resistance coefficient is determined under controlled conditions, and attributed to specific properties of the flow domain (as for example the roughness height for flow over a solid surface). As a result of such studies, values for hydraulic resistance coefficients have been established that are related to surface and geometry characteristics (e.g. Chow 1959).

Incorporating vegetation flow resistance

Traditionally, the hydraulic resistance of vegetated river sections is estimated using empirically determined (Manning) resistance coefficients (Chow 1959),

based on the premise that vegetation resistance may be treated as an equivalent bed roughness. However, these resistance coefficients appear to be case- and flow-specific (US Soil Conservation Service 1954) and are therefore difficult to apply to new situations. Alternatively, Petryk and Bosmajian (1975) propose a model that uses a vegetative drag force, in analogy to cylinder drag. By adjusting the drag coefficient accordingly, the drag-force approach is able to describe flow through vegetation accurately. Fischenich and Dudley 2000 provide an extensive list of vegetation-specific drag coefficients. Fathi-Maghadam and Kouwen (1997) use dimensional analysis supported by experimental results (regression analysis) to arrive at an expression that also includes vegetation flexibility and presence of leaves. Also Järvelä (2004) acknowledges the influence of plant flexibility, which is included as a correction factor on the drag coefficient.

Flows *over* vegetation are not necessarily drag-dominated nor do they follow a clean logarithmic velocity profile. Therefore, other methods have been proposed that describe the hydraulic impact of vegetation based on *adjusted* boundary layer velocity profiles (e.g. Kouwen and Unny 1973, Klopstra et al. (1997), Stephan and Gutknecht 2002, Van Velzen et al. 2003). A common feature in these methods is that flow through the vegetation is described by means of an effective drag force, and that flow over vegetation is described by means of an effective wall-roughness. In particular the estimation of an equivalent wall roughness based on vegetation characteristics still poses problems (e.g. Klopstra et al. 1997, see also Chapter 3). Therefore, even though these methods provide an appealing, qualitatively sound representation of flows over vegetation, the poor understanding of flow-dependent roughness parameters still limits their range of applicability.

2.4 Appropriate flow detail for river-reach models

In section 2.3, different methods are described to solve fluid flow problems. Figure 2.4 gives an overview of the different approaches, showing the respective properties regarding physics of flow and associated model resolution. The axes in the graph represent three (relative) properties of the respective modeling techniques:

1. The level of description (e.g. Pope 2000). This axis describes the completeness of the adopted laws of fluid motion (i.e. physics of the flow model).

2. The (numerical) resolution. This axis describes the spatial and temporal detail of the adopted computational domain (i.e. grid size, time steps).

3. Flow-dependent parameters in the model equations. This axis reflects the relative amount of flow processes that are not explicitly described, but absorbed into (flow-dependent) coefficients, parameterizations or turbulence models.

The sketch in Figure 2.4 illustrates that the level of description and the numerical resolution of a flow model are closely related. A high level of descrip-

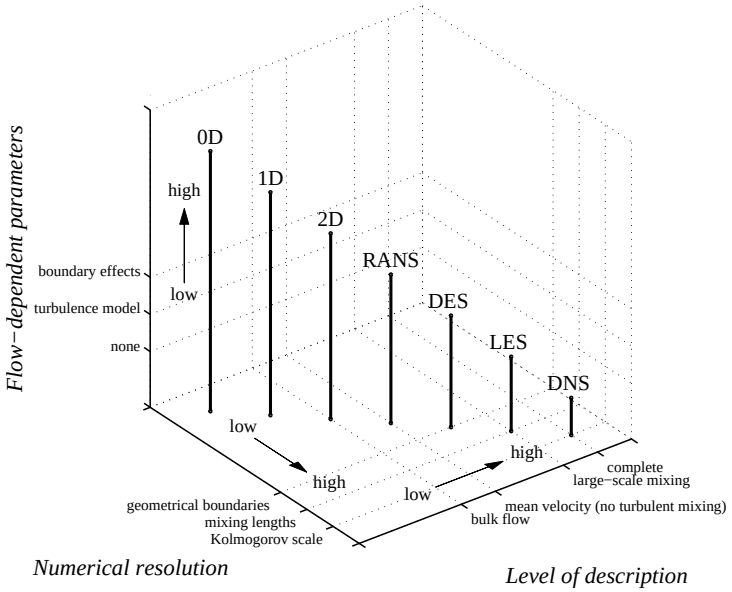

Figure 2.4: Conceptual overview of the level of description and (numerical) resolution of a flow modeling technique, and the corresponding flow-dependent parameters in the model (Noordam and Huthoff 2006). See section 2.3 for explanation of the different modeling techniques (0D-DNS).

tion requires a high (numerical) resolution, due to the relevance of small-scale flow patterns in fluid motions. This interconnection is the key to complications associated with flow modeling techniques. Detailed flow modeling techniques require correspondingly detailed input data to warrant the accuracy of their predictions (e.g. Willems et al. 2000). Also, detailed flow models generally lead to large computational efforts. Therefore, the desired application objective of a particular model has to be weighed against the necessary detail of required input (and the availability thereof) and acceptable computational effort.

For river engineering purposes, in particular when related to discharge capacity studies, it is essential that the mean flow field is represented accurately, while details of turbulence characteristics are of minor importance. In principle, all methods shown in Figure 2.4 have the capability of calculating the mean flow velocity. The reliability of a particular method depends on the availability of input data (resolution of geometrical domain), and the understanding of flow-dependent parameters. In DNS and LES techniques, the content of flow-dependent parameters is smallest (or even completely absent). However, these methods require a resolution of geometrical boundaries on the scale of turbulent mixing lengths, which is a practical impossibility for river-reach scales. Moreover, with modern computing capabilities, the large computation times of these methods are still not suitable for practical use.

Nicholas and Mitchell (2003) constructed a river flow model using a digital elevation model with a spatial resolution of 1×1 m. Such resolution is the highest still possible at river-reach scales, without the necessity of specifying details of every single obstructing object. The detail of flow characteristics in a flow model is constrained by the resolution of the geometrical boundaries. Therefore, flows at river-reach scales can be most accurately described using the RANS equation[♮]. The RANS approach requires that for each computational node a turbulence model is defined that describes the influence of sub-grid surface properties. Topographic features that are captured by the resolution of the geometrical domain naturally enter the flow behavior in the model. Therefore, the resolution of a flow model can be chosen such that it captures only the presence of *important* geometrical variations, without increasing the need for additional flow-dependent parameters. Regarding this issue, Wheater (2002) points out that the level of hydraulic model complexity that is appropriate to the available data of channel geometry requires further research attention. Roughly speaking, geometrical variations may be assumed to have important influence on the flow field if their size-scale is of the same order of magnitude as the flow boundaries. In other words, the presence and relative magnitude of geometrical variations in the channel dictate the desired spatial resolution of the flow model.

Simplified (spatially-averaged) flow-descriptions are still very popular in engineering studies as detailed input data is not always available, and because of the development and computational effort associated with high-resolution mod-

[♮]If turbulent mixing motions in river flows are expected to be larger than the model grid-size, then the outer flow can, in principle, also be modeled using LES (effectively yielding a DES river model).

eling (e.g. Werner and Lambert 2007). However, as modern computing capabilities and large-scale data-gathering techniques advance (Stelling and Verwey 2005), simplified flow-descriptions only remain attractive if they are widely applicable and yield similarly accurate outcomes. Therefore, if the resolution of input data does not describe the important variations of the flow domain, then the associated hydraulic effects should be included in (flow-dependent) model parameters. Processes to be included in such parameterizations are:

- In a depth-averaged parameterization: any process that affects the vertical velocity profile, such as bed friction, protruding large objects, surface shear (e.g. due to wind).
- In a width-averaged parameterization: any process that affects lateral velocity profiles, such as lateral variability of bed level or bed friction, meandering, and side-wall friction.
- In a longitudinally-averaged parameterization (in streamwise direction): any process that affects the mean streamwise velocity, such as bed forms, channel widening/narrowing, inclination changes, and bed roughness variability.

If spatially-averaged hydraulic resistance parameters are used to calibrate a model (e.g. Wijbenga et al. 1998), then caution should be taken if the model is applied outside the calibration range. The extrapolated effect of poorly understood parameters may introduce unrealistic behavior.

2.5 Vegetation resistance in rivers: is a generally applicable description possible?

As argued before, the highest practically attainable flow-resolution for river-reach models is achieved in RANS-modeling. Focussing on the hydraulic response to vegetation, RANS-based approaches yield good predictions of the mean flow field through vegetation, provided that an appropriate value for the drag coefficient is chosen. Therefore, the crucial component in such methods is the drag force term. In case of a spatial vegetation density of m vegetation stems of per unit surface area, the drag force per unit volume at height z above the bed is characterized by (e.g. Baptist 2005)

$$\mathrm{F}_D(z) = \frac{1}{2}\rho m(z) C_D(z) D(z) u(z)|u(z)|, \tag{2.24}$$

where D is the stem diameter of the vegetation. In spatially-averaged, or adjusted boundary layer methods, vegetation drag enters the flow description in the same manner. Therefore, the choice of flow modeling technique and numerical resolution (depending on availability of topographic information and geometrical variations thereof), does not alter the methodology of describing vegetation drag.

Reliability of modeling mean flow in the layer occupied by the vegetation is thus equally reliable between modeling techniques that apply the drag force approach. The main difference between these methods is the way in which flow over vegetation is treated. In RANS models, detailed transport equations of turbulent energy may account for the mean flow profile in the surface layer (i.e. above the vegetation), which do not require additional flow-dependent parameters that reflect vegetation influence (e.g. Neary 2003). By using a RANS-model with a simple shear turbulence model (e.g. the mixing layer concept) or a simplified adjusted-boundary-layer model for surface layer flow, the respective characteristic mixing length or equivalent roughness height require specification. So far, general applicable parameterizations of the mixing length or equivalent roughness height have not been achieved, as their dependencies on vegetation characteristics remain ambiguous. Raupach et al. (1996) proposes to scale the mixing length for flow over vegetation with the vegetation height, while Ghisalberti and Nepf (2004) point out that shear stress near the top of the vegetation layer is affected by vegetation density. In Klopstra et al. (1997) an equivalent roughness height is proposed depending on vegetation height and flow depth, in Van Velzen et al. (2003) the equivalent roughness height depends only on vegetation height. Neither of these proposed methods is calibrated on flow and vegetation characteristics that covers the full range of situations that may be encountered in the field. Therefore, the challenge remains to find a simple, general method for parameterizing flow *over* vegetation. Possible ways to achieve this are (i) to analyze data of a wide range of flows over vegetation or (ii) to obtain simplified theoretical descriptions of the general physical laws that govern flow over vegetation.

The analytical vegetation resistance model proposed by Klopstra et al. (1997) seems a promising starting point towards finding a simple, theoretically sound description of flow over vegetation. The method is based on fundamental physical principles and only includes one parameter that, despite its known physical meaning (i.e. the turbulent length-scale), is not well understood in terms of vegetation and flow dependencies. Also, in the Netherlands the model by Klopstra et al. (1997) is the current method used to compute vegetation resistance in studies used for river engineering purposes (Van Velzen et al. 2003). A close inspection of its properties is thus essential.

2.6 Conclusions

Except in DNS and LES of turbulent flows, where the effect of vegetation may be treated by imposing no-slip on solid boundaries, a spatially averaged drag-coefficient is always necessary to describe flow through the vegetation layer. As it is practically impossible to gather the necessary input data for river-reach DNS or LES models, the highest attainable resolution of river-reach flow models is by using the RANS equation. Therefore, flow within the vegetation layer needs to be described using a (spatially-averaged) drag force approach.

To warrant general applicability of a river flow model including vegetation drag, in a RANS-based model a generally applicable energy-transport turbu-

lence model could be chosen. That way, the flow model naturally describes flow over vegetation, without further need for vegetation-parameterizations. For simpler (spatially-averaged) flow models, the drag force approach yields an equally reliable and widely applicable method to describe flow *through* vegetation (i.e. for emergent vegetation). However, spatially-averaged flow models require an additional vegetation resistance parameterization to describe flow *over* vegetation. Several such parameterizations have been proposed before, but none is generally applicable. As spatially-averaged flow models are still the primary tool for river engineering purposes, it is recommended to resolve this issue by either investigating a wide range of flow data, or by a closer inspection of theoretical implications of simplified fluid flow laws. In particular, the method proposed by Klopstra et al. (1997) seems promising for general applicability in river-reach models. However, to obtain such a qualification, a better understanding of all its model components is required.

Chapter 3

An integrated velocity profile method for flow with submerged cylindrical vegetation

In this chapter an analytical velocity profile for flow in presence of submerged vegetation is presented and evaluated. The demonstrated method is, to a large extent, based on the findings of Klopstra et al. (1997), who derived an analytical solution of the velocity profile through an array of homogeneously distributed rigid cylinders (see also Khublaryan et al. 2004, Baptist 2005, Defina and Bixio 2005). The hydraulic response of vegetation is thus studied in an idealized form, avoiding complications associated with the shapes of plants and their natural variability, the presence of leaf foliage and bending or streamlining effects. Understanding the flow behavior in such idealized situations may contribute to a description of flow for more realistic cases involving natural vegetation.

A key constituent of the derived analytical velocity profile is the required turbulent length scale α. Two existing closure relations for this length scale α seem inappropriate; one is dimensionally incorrect and the second gives unrealistic behavior in limiting conditions. Here, we propose a new closure relation that does not have these disadvantages. A comparison between the average flow velocity determined from laboratory flow experiments and results of depth-integration of the proposed velocity profile, shows that the proposed method is only weakly sensitive to the required turbulent length scale α. This finding suggests that the level of detail of the flow model can be further reduced, without loosing much of its predictive capability.

Furthermore, even though experimental results show very good agreement with the analytical flow velocity profile, it is shown that some characteristics of the model are unrealistic. Firstly, the no-slip boundary condition near the channel bed is not met, and secondly, the turbulence model at the top of the vegetation layer is inconsistent with flow in the surface layer. Consequences of these properties are discussed by comparison with a more detailed model of the flow field, which required numerical solution techniques.

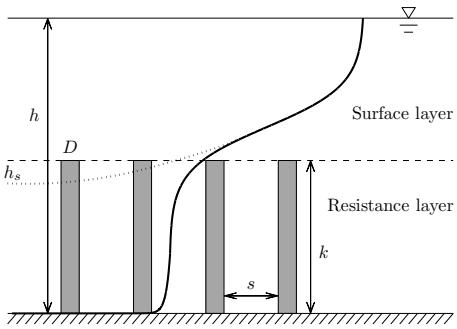

Figure 3.1: A schematic view of the geometrical parameters involved when describing flow in presence of rigid cylinders. Also shown is the typical shape of the velocity profile of flow in presence of submerged (cylindrical) vegetation.

3.1 Introduction: vegetation as cylinders?

Different species of vegetation come in many different shapes and sizes. Correspondingly, laboratory and field measurements have yielded many different empirical relations that describe the hydraulic response to obstructing vegetation in a flow field (e.g. Copeland 2000, Freeman et al. 2000). These relations are suitable when modeling the hydraulic response to exactly those vegetation types (and distributions) that were studied, but what to use in different situations with other plant species? Is there a way to describe the effect of vegetation in a flow field in a more general way, such that the model can be more widely applied? When attempting such a venture one should keep in mind all the relevant processes at play when vegetation becomes overflown. James et al. (2004) points out that resistance at the channel bed may be small compared to the stem drag caused by vegetation, but this hardly simplifies matters. The interplay mechanisms between vegetation and the flow field could cause bending or streamlining effects, thereby continually changing the effective drag force. Moreover, due to the natural variability in plant height, stem width, surface density and the amount of leaf foliage, hydraulic drag may vary significantly from place to place.

Despite such complications, several attempts have been made to describe the hydraulic resistance of vegetation in a simplified way. Some use as determining factor the effective cross-sectional blocking area of the vegetation (e.g. Petryk and Bosmajian 1975), others the effective porosity (e.g. Tsujimoto et al. 1996, Hoffmann and van der Meer 2002), others still the effective stem diameter and ground surface coverage (e.g. Kaiser 1984, Stone and Shen 2002). While providing overall dependencies between plant dimensions and properties of the flow field, many of these descriptions still include poorly understood empirical parameters or parameters that are difficult to determine in the field. We choose to avoid the latter disadvantage, and develop a description that is based on readily measurable quantities. Therefore, we adopt the rigid cylinder analogy (see Fig-

ure 3.1). Thus, vegetative flow resistance is restricted to cylinder-type species, such as reed or tall grasses. Figure 3.1 shows a schematic view of the geometric parameters that are involved in flow near submerged cylinders: cylinders are nonflexible (stiff), have constant diameter D and are homogeneously distributed over the bed with surface density m (with spacing between vegetation elements s).

3.2 Analytical velocity profile

In this section an analytical velocity profile is proposed for flow near an array of homogeneously distributed cylinders, where flow in-between and flow above the cylinders is treated separately. The flow layer above the cylinders is referred to as the *surface layer* and the layer that is penetrated by the rigid cylinders as the *resistance layer* (see Figure 3.1). First, in section 3.2.1 an assumed velocity profile for the surface layer is presented. Secondly, in section 3.2.2 a profile is derived based on physical principles for the resistance layer. Also, in section 3.2.2 it is shown how the profiles in the resistance and surface layer match at their common interface. The velocity profile contains a closure parameter α, which represents a turbulent length scale and may be used as calibration parameter. In section 3.3 laboratory measurements are used to determine a new relation that predicts values of α.

3.2.1 Flow in the surface layer

In the layer above the cylinders it is assumed that the flow field resembles that of flow over a rough solid bed. The roughness characteristics of the artificial bed are related to the properties of the actual presence of vegetation. Turbulent flow over a rough bed is traditionally described by a logarithmic velocity profile, with the skin friction represented by an equivalent roughness height (Nikuradse 1933, Keulegan 1938). If flow over a solid bed is described, the flow velocity near the bed reduces to zero, as postulated by the no-slip boundary condition (Lauga et al. 2005). However, in the case of flow over vegetation, the flow velocity in the resistance layer is non-zero. Therefore, we adopt a logarithmic velocity profile that is superimposed on a non-zero base velocity u_k [⋆]:

$$u = u_k + \frac{u_*}{\kappa} \ln\left(\frac{z - k + h_s}{h_s}\right), \text{ for } (k \leq z \leq h)\,. \tag{3.1}$$

Where u_k is the velocity at the top of the resistance layer, h_s the artificial roughness height that characterizes the artificial rough bed and κ is the Von Kármán constant ($\kappa = 0.41$). The friction velocity is denoted by u_* and is defined as

$$u_* = \sqrt{g\,(h - k)\,i}. \tag{3.2}$$

⋆The assumed velocity profile in equation (3.1) is equivalent to the modified logarithmic profile adopted by Klopstra et al. (1997). See also Stephan and Gutknecht (2002) for alternative modified logarithmic velocity profiles.

Where g is the gravitational acceleration and i the slope of the channel (the inclination). In order to describe flow over vegetation or an array of cylinders realistically, the artificial roughness height h_s is chosen such that the logarithmic velocity profile makes a smooth transition with the velocity profile in the resistance layer (at $z = k$).

3.2.2 Flow in the resistance layer

Following Klopstra et al. (1997), the velocity profile in the resistance layer is based on a force balance between the gravitational driving force F_g (per unit volume) and momentum losses due to the turbulent shear stress τ and drag caused by the protruding cylinders:

$$\frac{\partial \tau}{\partial z} = \mathrm{F}_D - \mathrm{F}_g. \tag{3.3}$$

The *Boussinesq hypothesis* is commonly adopted to describe energy dissipation in turbulent flows by introduction of an eddy viscosity ν_ϵ. The shear stress in turbulent flows is related to ν_ϵ, similar to the kinematic viscosity in case of laminar flows (e.g. Pope 2000):

$$\tau = \rho \nu_\epsilon \frac{\partial u}{\partial z}. \tag{3.4}$$

Whereρ is the water density. The eddy viscosity is generally not well-represented by a constant value, but is related to the local mean flow velocity or gradients in the mean flow field. Two commonly used models to describe the distribution of the eddy viscosity are based on (i) Prandtl's mixing length concept and (ii) Prandtl's free shear layer concept (e.g. Rodi 1980). In mathematical form, these two turbulence models are represented as

$$\text{Mixing layer}: \quad \nu_\epsilon = \lambda^2 \frac{\partial u}{\partial z} \tag{3.5}$$

$$\text{Free shear}: \quad \nu_\epsilon = \alpha u. \tag{3.6}$$

Where both α and λ are characteristic turbulent length scales, relating to the respective turbulence model. The height above bed level is given by z and u is the mean longitudinal velocity (at height z). The mixing layer concept, leading to equation (3.5), is based on the idea that turbulent fluctuations cause displacements of small fluid volumes over a characteristic *mixing length* λ. The methodology proved to be particularly useful for flows that have only one significant velocity gradient (Rodi 1980). The free shear model, equation (3.6), is a simplification of the mixing layer model, where the velocity gradient $\frac{\partial u}{\partial z}$ is estimated as the mean velocity u relative to a characteristic length scale α. Because of its simplicity, the free shear model is often preferred for practical predictions of turbulent flows (e.g. Tsujimoto and Kitamura 1990, Vionet et al. 2004). Also in the current work we adopt the free shear model for the eddy

viscosity. Subsequently, combining equations (3.4) and (3.6) yields for the shear stress

$$\tau = \rho\alpha u\frac{\partial u}{\partial z}. \tag{3.7}$$

In the discussion (section 3.5) we reflect on consequences of adopting the free shear turbulence model as alternative to the mixing layer model given in equation (3.5).

Next, standard expressions of the streamwise component of the gravitational force F_g and for the drag force F_D (Schlichting and Gersten 2000) are given by (both F_g and F_D are per unit volume):

$$\mathrm{F}_g = \rho g i \tag{3.8}$$

$$\mathrm{F}_D = \frac{1}{2}\rho m D C_D u^2 \tag{3.9}$$

In the expression for the drag force, equation (3.9), m represents a surface density of vegetation elements (vegetation elements per m^2) that have a diameter D. Finally, C_D is the dimensionless drag coefficient which needs to be determined experimentally.

Inserting equations (3.7), (3.9) and (3.8) into the force balance given in equation (3.3) results in

$$\frac{\partial^2 u^2}{\partial z^2} - \frac{u^2}{l^2} + \frac{U_{r0}^2}{l^2} = 0, \tag{3.10}$$

where the length scale l and the characteristic velocity U_{r0} are defined as

$$l = \sqrt{\frac{\alpha}{mDC_D}}, \tag{3.11}$$

$$U_{r0} = \sqrt{\frac{2gi}{mDC_D}}. \tag{3.12}$$

By introducing an additional length scale b, the *drag length*, as

$$b = \frac{1}{mDC_D}, \tag{3.13}$$

equations (3.11) and (3.12) may be written as

$$l = \sqrt{\alpha b}, \tag{3.14}$$

$$U_{r0} = \sqrt{2gib}. \tag{3.15}$$

The length scale b reflects the flow resistance due to cylinder form drag. The flow velocity U_{r0} is found in situations where bottom or surface layer effects are not influencing the flow field. In such cases, the shear stress term vanishes from the force balance (3.3), which results in a constant vertical velocity profile of

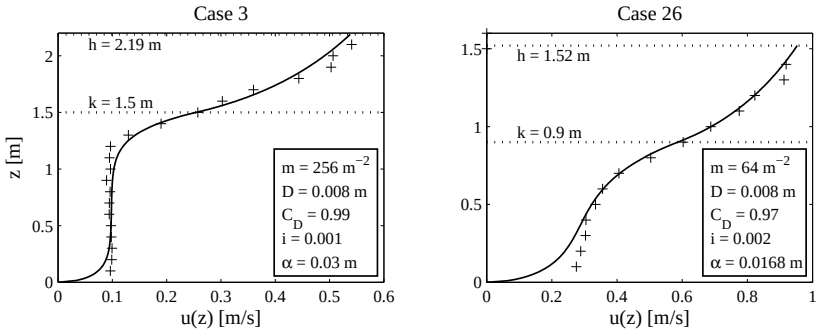

Figure 3.2: The derived analytical velocity profile using a no-slip boundary condition at the bed, as compared to two laboratory cases from experiments by Meijer (1998b).

magnitude U_{r0}. The general solution to equation (3.10) is given by (Klopstra et al. 1997, Khublaryan et al. 2004):

$$u = \sqrt{U_{r0}^2 + \mathrm{C}_1 \mathrm{e}^{z/l} + \mathrm{C}_2 \mathrm{e}^{-z/l}}, \quad \text{for } z \leq k. \tag{3.16}$$

Choosing appropriate boundary conditions now enables quantification of the unknown constants C_1 and C_2 (Klopstra et al. 1997). A natural choice for a bed level boundary condition is the no-slip condition (i.e. $u(0) = 0$). A second boundary condition is imposed at the top of the resistance layer by setting the shear stress to

$$\tau_k = \rho g \, (h - k) \, i, \tag{3.17}$$

which corresponds to the shear stress required to balance the gravitational force that acts on the surface layer. Applying the no-slip boundary condition at the bed, and the shear stress condition from equation (3.17) at the interface between resistance and surface layer, yields for equation (3.16)

$$u = U_{r0} \sqrt{1 - \mathrm{e}^{z/l} + \left(\frac{h-k}{l} + \mathrm{e}^{k/l} \right) \frac{\sinh\left(z/l\right)}{\cosh\left(k/l\right)}}, \quad \text{for } z \leq k, \tag{3.18}$$

which completes the derivation for the velocity profile in the resistance layer. Correspondingly, the velocity at the top of the resistance layer (if $z = k$) becomes

$$u_k = U_{r0} \sqrt{1 - \mathrm{e}^{k/l} + \left(\frac{h-k}{l} + \mathrm{e}^{k/l} \right) \tanh\left(k/l\right)}. \tag{3.19}$$

In Figure 3.2 the derived velocity profile, equation (3.18), is shown as it is matched with the logarithmic velocity profile in the surface layer. For this purpose, the artificial roughness height h_s, as given in equation (3.1), is chosen such that the logarithmic velocity profile fits the boundary condition at the top

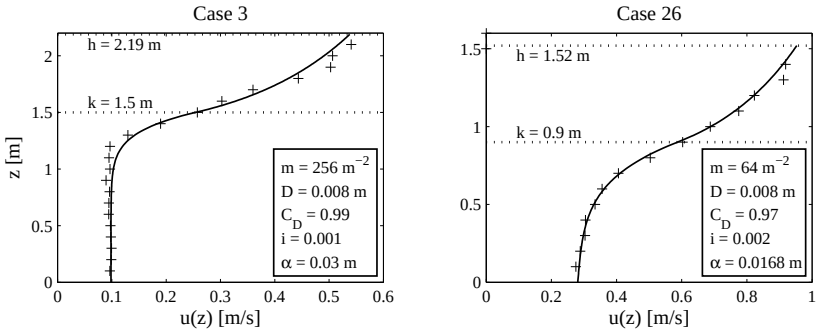

Figure 3.3: The derived analytical velocity profile using a complete-slip boundary condition at the bed, as compared to the two laboratory cases also shown in Figure 3.2.

of the resistance layer; equation (3.17). Based on a turbulence model according to equation (3.7), the roughness height h_s is equal to

$$h_s = \frac{\alpha}{\kappa}\frac{u_k}{U_{r0}}\sqrt{\frac{2b}{h-k}}. \tag{3.20}$$

Finally, the analytical profile is matched to measured velocity profiles (experiments by Meijer 1998b) using the turbulent length scale α as a calibration parameter. Overall, by calibration of α, good agreement can be achieved between the derived and measured profile, only near the channel bed a large difference remains between model and experiment (see Figure 3.2). The flow experiments show that the bed boundary layer is much smaller than predicted by the velocity profile model. Apparently, in combination with the free shear turbulence model, given in equation (3.6), the no-slip bed boundary condition forces the velocity profile into unrealistic behavior.

Alternatively, we neglect the bed boundary layer entirely, and evaluate how well the velocity profile of flow through vegetation can be described when the only resistance to flow is caused by form drag of the vegetation stems. Therefore, by imposing (the physically unrealistic) *complete* slip as bed level boundary condition (i.e. when $u(0) = U_{r0}$), the general solution given in equation (3.16) becomes

$$u = U_{r0}\sqrt{1 + \left(\frac{h-k}{l}\right)\frac{\sinh(z/l)}{\cosh(k/l)}}, \quad \text{for } z \leq k. \tag{3.21}$$

which yields a velocity at the top of the resistance layer of

$$u_k = U_{r0}\sqrt{1 + \left(\frac{h-k}{l}\right)\tanh(k/l)}. \tag{3.22}$$

Figure 3.3 shows that the velocity profile given in equation (3.21) agrees much better with measured velocities. This may seem a surprising result because

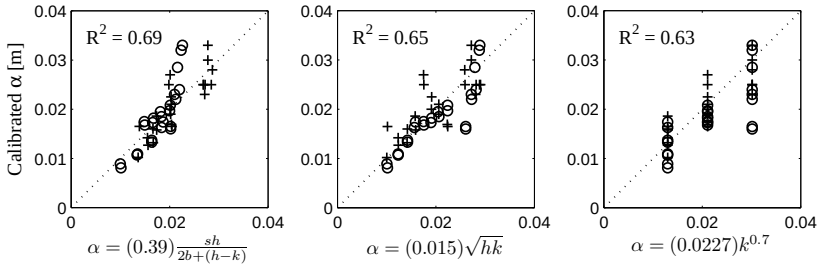

Figure 3.4: Performance of three closure relations for turbulent length scale α. Different symbols correspond to experiments with different cylinder surface densities: for '$\circ$' $m = 64$ m^{-2} and for '+' $m = 256$ m^{-2}.

numerous experiments have shown that the no-slip boundary condition is a universal property of wall-bounded flows (e.g. Lauga et al. 2005). In the discussion in section 3.5 we reflect on this apparent contradiction.

3.3 Calibration of the analytical velocity profile

In previous studies it was found that the turbulent length scale α correlated with the depth of flow and the height of the resistance layer. The following empirical expressions were found to describe the relation between α, the depth h and vegetation height k reasonably well:

$$\alpha = 0.015\sqrt{hk}, \tag{3.23}$$

$$\alpha = 0.0227k^{0.7}. \tag{3.24}$$

Equation (3.23) is proposed by Meijer (1998b) and equation (3.24) by Van Velzen et al. (2003). Unfortunately, for the expressions above no justification is given based on physical principles. A disturbing observation is also that equation (3.24) is not dimensionally correct. Nevertheless, equation (3.24) is used by the Dutch Institute for Inland Water Management and Waste Water Treatment (Van Velzen et al. 2003) for large-scale river flow modeling. The reason for this choice lies in the more realistic behavior of relation (3.24) at large flow depths. Equation (3.23) predicts an increasing length scale α with increasing depth h, which gives unrealistically high hydraulic resistances for large relative flow depths. On the other hand, at all flow depths equation (3.24) remains a measure of vegetation characteristics only.

Because of the shortcomings of both closure relations given in equations (3.23) and (3.24, we aim at deriving a new closure for α that is both dimensionally correct and shows realistic behavior when the depth of flow becomes large. In analogy to a method often used for flow through porous media (e.g. Bentz and Martys 1995), we will look whether the geometric boundaries in the flow field are suitable for constructing a spacing hydraulic radius (R_s) that scales

with the turbulent length scale α. In the study of Tollner et al. (1982), who investigated sediment transport processes in flow through a field of cylinders, the introduction of such a spacing hydraulic radius already proved successful. The following expression represents the general form of a spacing hydraulic radius (R_s = area/perimeter)

$$R_s = \frac{\gamma_i \gamma_i}{2\gamma_i + \gamma_i}. \tag{3.25}$$

By using the format of equation (3.25) in finding a new closure relation for α, dimensional correctness is guaranteed. Here γ_i may reflect any of the six geometrical length scales h, k, b, s, D and $h - k$ that are present in the studied situation. Consequently, a total of 756 spacing hydraulic radii may be constructed with equation (3.25). Among the used geometrical dimensions, the separation between cylinders s is calculated from the surface density m and stem diameter D as:

$$s = \frac{1}{\sqrt{m}} - D \tag{3.26}$$

In addition to the property that all combinations of constructed spacing hydraulic radii carry the dimension [m], the format proposed in equation (3.25) also allows direct proportionality to any of the six length scales (when all γ_i are the same geometrical parameter). Next, the calibrated values of α, corresponding to best agreement between measured and modeled velocity profile (maximum R^2), are correlated to each of the 756 constructed hydraulic radii as

$$\alpha = K_R R_s, \tag{3.27}$$

where K_R is a proportionality constant.

From all the constructed hydraulic radii using equation (3.25), the four that gave best agreement with the observed trend in calibrated α-values are listed in Table 3.1 (based on highest coefficients of correlation R^2). Also listed are the two previously existing relations, equations (3.23) and (3.24). None of the newly derived closures for α is significantly better than the existing relations. However, the highest coefficient of correlation (R^2) is found for the relation

$$\alpha = (0.39)\frac{sh}{2b + (h - k)}, \tag{3.28}$$

which gives predictions for α that are as good as those by equations (3.23) and (3.24). Figure 3.4 shows the performance of equation (3.28) as compared with experimentally derived values for the turbulent length scale α, in comparison with the performance of equations (3.23) and (3.24).

In the limiting case that the water depth is much larger than the vegetation height (if $h >> k$), and in cases that k, s and b are of the same order of magnitude ($k \simeq s \simeq b$), all four of the new expressions in Table 3.1 reduce to $\alpha \simeq k$. The turbulent length scale α in situations of large flow depths, with small but densely packed roughness elements, therefore represents the roughness height k. This property is also present in the dimensionally inhomogeneous relation given by equation (3.24). Because of this property, equation (3.24)

Table 3.1: Characteristics of functions to predict α.

α-function	R^2	R^2 significance (95% Conf. int.)	Dimensionally correct?	Limit correct? (for $h >> k$)
(0.39)$\frac{sh}{2b+(h-k)}$	0.69	(0.51 - 0.81)	ok	ok
(0.82)$\frac{kh}{2k+h}$	0.62	(0.41 - 0.76)	ok	ok
(0.04)$\frac{ks}{2b+k}$	0.62	(0.41 - 0.76)	ok	ok
(0.09)$\frac{k(h-k)}{2(h-k)+h}$	0.60	(0.40 - 0.75)	ok	ok
(0.015)$\sqrt{hk}$	0.65	(0.46 - 0.79)	ok	
(0.0227)$k^{0.7}$	0.63	(0.43 - 0.77)		ok

(although dimensionally incorrect) is often favored above equations (3.23), which is proportional to the square root of the flow depth.

In summary, Table 3.1 shows that the newly proposed expressions for the turbulent length scale α give equally good predictions as the existing ones (compared to the experimental data by Meijer 1998b). However, the newly proposed formulas comprise the property of being dimensionally correct with the advantage that at large flow depths the turbulent length scale α reduces to an equivalent roughness height. Therefore, all four of the new closure relations for α provide an improvement to the expressions given in equations (3.23) and (3.24). Because the closure relation proposed in equation (3.28) gives the best correlation with calibrated values of α, is dimensionally correct and gives a realistic value when the depth of the surface layer is small, it is recommended as best closure relation for the turbulent length scale α.

It remains difficult to attribute a physical explanation to the turbulent length scale as given in equation (3.28). The effective area of the spacing hydraulic radius, given by the numerator of equation (3.28) 'sh', reflects the cross-sectional flow area between two neighboring cylinders. The (wetted) perimeter, typically reflecting the boundaries where most turbulent energy is dissipated, is given by the denominator '$2b + (h - k)$'. For flow through emergent cylinders, the drag length b is indeed the length scale that is associated with turbulent energy losses. Likewise, for wall-bounded flow the typical scale of turbulent eddies is associated with the flow depth. For the surface layer, treated as flow over an equivalent rough bed, the typical length scale associated with energy losses is thus '$h - k$'. Therefore, it is not a complete surprise that the length scale associated with energy losses at the interface between surface layer and resistance layer is constructed from the equivalent cross-sectional flow area 'sh', and the two

length scales that are typical of turbulent energy losses.

3.4 Depth-averaged flow velocity based on vertical velocity profile

In some studies, details about the velocity profile of the flow field through vegetation are of great importance. For example the velocity gradient near the bed determines the intensity of local shear, relevant in erosion studies and morphodynamic modeling (e.g. Baptist 2005). However, for discharge capacity studies (i.e. conveyance studies) the depth-averaged flow velocity is of main interest. Having established a relation that describes the vertical velocity profile through submerged vegetation, the average flow velocity can now be determined by integration over depth. Treating the velocity profile in and above the resistance layer separately, the overall average flow velocity is calculated as:

$$U_T = \frac{k}{h}U_r + \frac{h-k}{h}U_s \tag{3.29}$$

Where U_r and U_s are the average velocities in and above the resistance layer, respectively. These will be determined separately in sections 3.4.1 and 3.4.2.

Again, the laboratory flow experiments by Meijer (1998b) serve as a comparison to averaged velocities based on depth-integration of the velocity profile function. In the used experiments, streamwise flow velocities were measured at depths 10 cm apart. Reference average velocities were calculated from trapezoidal interpolation between the measured points of the velocity profile.

3.4.1 Depth-averaged velocity in the surface layer

The depth-averaged velocity in the surface layer is determined by depth-integration of the logarithmic velocity profile as given in equation (3.1):

$$U_s = \frac{1}{h-k}\int_k^h u\mathrm{d}z = u_k + \frac{u_*}{\kappa}\left(\frac{h-k+h_s}{h-k}\ln\left(\frac{h-k+h_s}{h_s}\right)-1\right) \tag{3.30}$$

Where u_*, h_s and u_k are given by equations (3.2), and (3.20) (3.22), respectively. Both the artificial roughness height h_s and the velocity at the top of the resistance layer u_k depend on the turbulent length scale α.

Figure 3.5 shows that for the three different closure relations for α, equations (3.23), (3.24) and (3.28), the predicted velocity in the surface layer, equation (3.30), agrees very well with the average velocities measured in the laboratory experiments. Even though the three investigated closure relations for α show considerable differences (see Figure 3.4), their effects on depth-averaged flow velocities in the surface layer are quite the same (as can be seen in Figure 3.5). Apparently, sensitivity of U_s on α is weak, and an accurate description for the closure of α is not required.

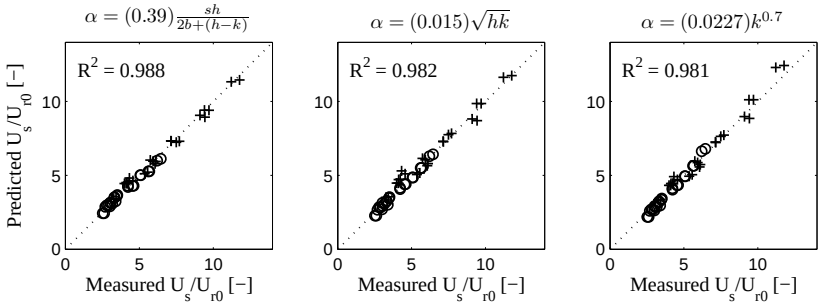

Figure 3.5: Average velocities in the surface layer based on equation (3.30), using three different closure relations for turbulent length scale α ($\circ$ $m = 64$ m^{-2}, $+$ $m = 256$ m^{-2}).

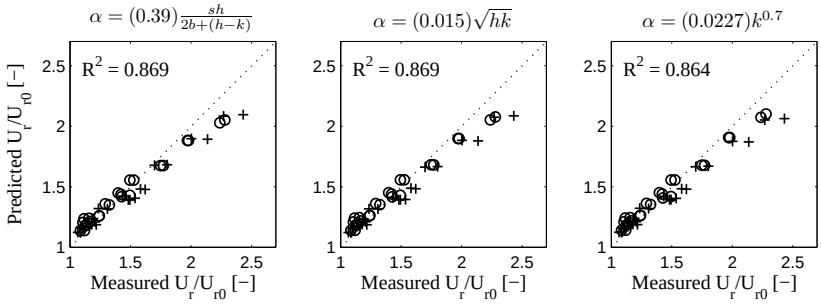

Figure 3.6: Average velocities in the resistance layer based on numerical integration of equation (3.21), using three different closure relations for turbulent length scale α ($\circ$ $m = 64$ m^{-2}, $+$ $m = 256$ m^{-2}).

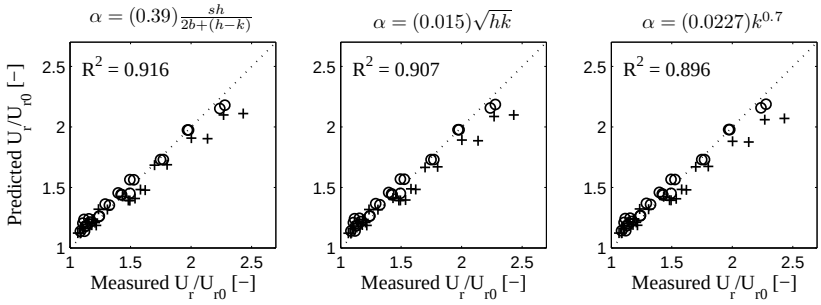

Figure 3.7: Average velocities in the resistance layer based on equation (3.34), using three different closure relations for turbulent length scale α ($\circ$ $m = 64$ m^{-2}, $+$ $m = 256$ m^{-2}).

3.4.2 Depth-averaged velocity in the resistance layer

The average velocity in the resistance layer is determined by depth-integration of the analytical velocity profile, as given by equation (3.21). Unfortunately, there is no exact analytical solution to the integral of equation (3.21), therefore the predicted values shown in Figure 3.6 are the result of a numerical integration procedure.

An analytical solution for the depth-averaged velocity in the resistance layer clearly has computational advantages. Therefore, simplifying assumptions are made that allow for such an analytical analysis. Following Klopstra et al. (1997), a simplification is made by assuming that in the definitions of $\sinh(z/l)$ and $\cosh(k/l)$ the exponential function $\mathrm{e}^{-z/l}$ is negligible compared to $\mathrm{e}^{z/l}$ and that $\mathrm{e}^{-k/l}$ is negligible compared to $\mathrm{e}^{k/l}$:

$$\sinh(z/l) = \frac{\mathrm{e}^{z/l} - \mathrm{e}^{-z/l}}{2} \approx \frac{1}{2}\mathrm{e}^{z/l} \tag{3.31}$$

$$\cosh(k/l) = \frac{\mathrm{e}^{k/l} + \mathrm{e}^{-k/l}}{2} \approx \frac{1}{2}\mathrm{e}^{k/l} \tag{3.32}$$

These approximations are allowed for $z >> l$ and $k >> l$, which is reasonable unless the resistance layer is shallow or the separation between vegetation elements is large. The velocity profile in the resistance layer, equation (3.21), now becomes:

$$u \simeq U_{r0}\sqrt{1 + \left(\frac{h-k}{l}\right)\mathrm{e}^{(z-k)/l}}, \text{ for } 0 \leq z \leq k. \tag{3.33}$$

It is now possible to integrate equation (3.33) analytically, which yields (see Klopstra et al. 1997):

$$U_r = U_{r0}\frac{2l}{k}\left(\Upsilon + \frac{1}{2}\ln\frac{\Upsilon - 1}{\Upsilon + 1}\right)_{\Upsilon_0}^{\Upsilon_k} \tag{3.34}$$

where the integration boundaries are given by:

$$\Upsilon_k = \sqrt{1 + \left(\frac{h-k}{l}\right)} \tag{3.35}$$

$$\Upsilon_0 = \sqrt{1 + \left(\frac{h-k}{l}\right)\mathrm{e}^{-k/l}} \tag{3.36}$$

Note that the expressions in equations (3.35) and (3.36) reflect the (dimensionless) velocities at the top of the resistance layer and the bed respectively (normalized to U_{r0}), when using the adapted velocity profile as given by equation (3.33). Figure 3.7 shows the average velocities in the resistance layer based on the approximated analytical solution in equation (3.34).

A comparison between Figure 3.6 and Figure 3.7 reveals that the approximated velocity profile given by equation (3.33) gives even better agreement with measured depth-averaged flow velocities than the original profile from equation (3.21).

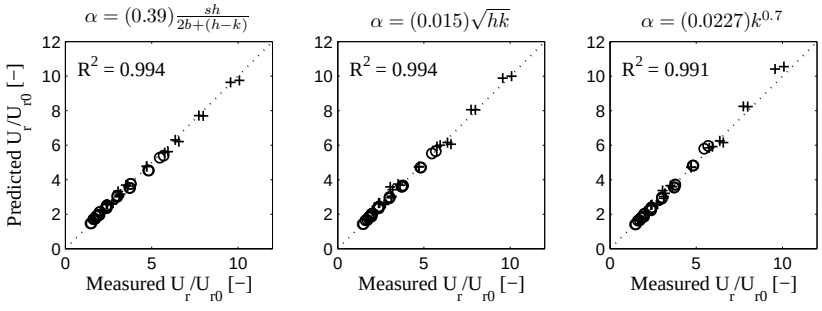

Figure 3.8: Average velocities over the total flow depth, based on depth-integration of an analytical velocity profile ($\circ$ $m = 64$ m^{-2}, $+$ $m = 256$ m^{-2}).

3.4.3 Overall depth-averaged flow velocity

Inserting equations (3.30) and (3.34) into equation (3.29) gives a description of the depth-averaged velocity for flow through submerged vegetation. In the obtained flow resistance model the only parameter that cannot be directly measured in the field is the turbulent length scale α. In order to make the model suitable for practical use, in section 3.3 several closure relations for α are presented. Figure 3.8 shows how three different closure relations for α affect the modeled overall average flow velocity. As can be seen, differences between methods are only very small. This may not be surprising since all three α-closures were calibrated on the same data set, which is also the set that is finally used for comparison in Figure 3.8. Nevertheless, the graphs in Figure 3.4 show that the three closure models for α behave significantly different. Apparently, the average velocities as predicted by the depth-averaged velocity profile, are not very sensitive to the variations in turbulent length scale α, as concluded also for the separate flow layers.

3.5 Discussion: complete slip and turbulence models

It was found that the derived analytical velocity profile with a complete-slip boundary condition at the channel bed gave better results than with the no-slip condition. This result must be interpreted in view of an essential property of the velocity profile: a constant turbulent length scale α. Such a constant turbulent length scale may be a reasonable assumption for most parts of the resistance layer, but near the channel bed this is probably no longer valid. Boundary layer theory proposes near-wall turbulent length scales that are proportional to the distance from the wall (e.g. Schlichting and Gersten 2000). Consequently, the near-wall behavior of the velocity profile proposed in 3.2.2 is based on a turbulent length scale that is too large, because it is not bounded by the distance to the wall. This effect can be compensated when choosing a bed boundary condition that also does not account for the presence of the wall: the complete-slip.

Alternatively, if α is allowed to vary with depth, then the original force

balance in equation (3.3) no longer yields an analytical solution of the velocity profile. Therefore, if an analytical treatment of the flow in the resistance layer is no longer possible, we also do not have to adopt the simplified turbulence model as given in equation (3.6). A more realistic turbulence description is provided by Prandtl's mixing length model, given by equation (3.5). The mixing length concept allows theoretical justification of the logarithmic velocity profile over a rough wall (e.g. Nikuradse 1932 and citations therein), and is thus naturally associated with flow in the surface layer. Therefore, a consistent treatment of turbulent flow in presence of submerged vegetation requires the application of one turbulence model throughout the flow field, i.e. the same model in both the surface and the resistance layer.

Using the mixing length concept to model the turbulent eddy viscosity, as given by equation (3.5), the corresponding shear stress description becomes:

$$\tau = \rho\lambda^2 \left(\frac{\partial u}{\partial z}\right)^2 \tag{3.37}$$

In the resistance layer it seems natural that the size of eddies is restricted by the available space between vegetation elements, and therefore, that λ remains constant throughout the resistance layer. One could argue that this is no longer the case for natural vegetation because the presence of leaves may vary along the height of the plant. Assuming λ constant results in the force balance (i.e. substitution of equation (3.37) into equation (3.3))

$$\frac{\partial u}{\partial z}\frac{\partial^2 u}{\partial z^2} - \frac{u^2}{4b\lambda^2} + \frac{gi}{2\lambda^2} = 0\ , \quad \text{for } z \leq k. \tag{3.38}$$

Near the bed λ is no longer restricted by the separation between vegetation elements but by the distance to the bed z. The hypothesis of Von Kármán states that in the bed boundary layer the parameter λ is proportional to the distance from the bottom (Schlichting and Gersten 2000)

$$\lambda = \kappa z. \tag{3.39}$$

For the region where z is smaller than the separation between vegetation elements s, the force balance becomes (using equation (3.39))

$$\frac{\partial u}{\partial z}\frac{\partial^2 u}{\partial z^2} - \frac{u^2}{4b\kappa^2 z^2} + \frac{gi}{2\kappa^2 z^2} + \frac{1}{z}\frac{\partial u}{\partial z} = 0\ , \quad \text{for } \kappa z < s. \tag{3.40}$$

Figure 3.9 shows the numerical solutions for u combining equations (3.38) and (3.40), and adopting the no-slip bed boundary condition. It can be seen that the predicted profile agrees very well with measurements from flume experiments, as opposed to the performance of the analytical profile when no-slip at the bed is used (Figure 3.2). Therefore, we conclude that due to oversimplified turbulence modeling in section 3.2.2, the physically verified no-slip boundary condition performs badly in combination with the derived analytical velocity profile through vegetation. Nevertheless, since bed roughness only plays a minor role in the overall hydraulic resistance of a vegetated field, the analytical

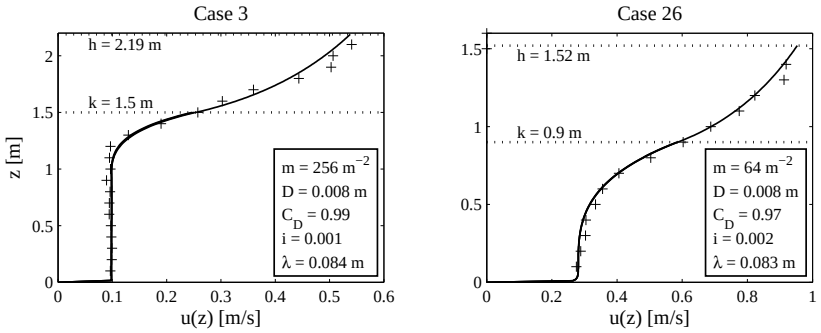

Figure 3.9: The solution of the numerically found velocity profile based on a turbulent length scale λ and a no-slip boundary condition at the channel bed, as compared to two laboratory cases.

solution with the complete-slip boundary condition still gives good predictions of the depth-averaged flow velocity. In effect, the analytical solution for flow with submerged vegetation over-predicts flow velocities near the bed. This error may have severe implications if the model is used in morphological studies. However, for calculating discharge capacities in vegetated areas, errors of flow velocities near the channel bed have negligible influence.

3.6 Conclusions

The analytical velocity profile for flow over submerged cylinders as originally proposed by Klopstra et al. (1997) gives a good description of the *depth-averaged* flow velocity. However, two unrealistic properties of the analytical model are identified: (*i*) the no-slip condition at the channel bed does not give good results (instead, complete slip is adopted), and (*ii*) the used turbulence model in the vegetation layer is inconsistent with the turbulence model in the surface layer. Alternatively, numerical analysis of flow through vegetation, using a more detailed turbulence model that is consistent with flow in the surface layer, shows that the no-slip condition gives realistic results. Comparison with the analytical model revealed that unrealistic flow predictions due to an oversimplified turbulence model may be compensated by imposing an unrealistic bottom boundary condition: complete slip.

Despite the mentioned shortcomings of the analytical flow model, it is shown that the model gives accurate predictions of depth-averaged flow velocities in flow affected by obstructing cylinders. To serve such a practical purpose, a closure relation is required for the turbulent length scale α that is included in the model. A new closure relation is put forward that is dimensionally correct and yields realistic limiting values, which is subsequently compared with the performance of two closure relations that are proposed in other works. It is shown that even though the different closure relations are significantly different, their effect on predicted average velocities is very small. This observation suggests

that the level of detail of the flow model may be further reduced without much loss of accuracy. Possibly, a more general model that does not include turbulent scales, or does not resolve the entire velocity profile, may still be sufficient for accurate predictions of depth-averaged flow velocities.

Chapter 4

A bulk flow model including vegetation resistance*

A new model for the depth-averaged velocity for flow in presence of submerged vegetation is developed. The model is based on a two-layer approach, where flow above and through the vegetation layer is described separately. Vegetation is treated as a homogeneous field of identical cylindrical stems and the flow field is considered stationary and uniform. It is demonstrated that scaling considerations of the bulk flow field can be used to avoid complications associated with smaller scale flow processes, and that still the behavior of depth-averaged flow over vegetation is described accurately. The derived scaling expression of the average flow field is simple in form, it follows fundamental laws of fluid flow and it shows very good agreement with laboratory flume experiments. The new model can be used for quick evaluation of a river's hydraulic response in cases where vegetated floodplains are inundated.

4.1 Introduction

The presence of vegetation in floodplains may have significant influence on the overall discharge capacity of a river (e.g. Darby 1999). In particular if floodplains are relatively wide compared to the main channel, realistic predictions of stage-discharge relations rely strongly on accurate knowledge of floodplain flow. Therefore, it is crucial to understand the processes that contribute to floodplain resistance, and the hydraulic impacts these processes may have.

The interplay between walls or solid objects and the flow field causes vortices and swirling motions at various length scales. Trying to represent these detailed flow characteristics is an immense task, which even with the most modern equipment is impossible for spatial and temporal scales that are relevant in river engineering studies. Consequently, depth-averaged quantities and scaling considerations are often used to arrive at bulk flow descriptions. Several such relations exist that relate the average flow velocity to surface characteristics, for example by means of a roughness height (Strickler 1923, Nikuradse 1933,

*This chapter has been published as a separate paper: Huthoff, F., D. C. M. Augustijn and S. J. M. H. Hulscher (2007). Analytical solution of the depth-averaged flow velocity in case of submerged rigid cylindrical vegetation. *Water Resources Research* 43(W06413), doi:10.1029/2006WR005625.

Keulegan 1938). However, if the irregularities, or resistance elements are of the same order of magnitude as the flow depth, available methods to predict flow resistance are no longer valid (e.g. Smart et al. 2002, Stone and Shen 2002). If, for example, a flow field is penetrated by vegetation, turbulent vortices are created in the wakes downstream of the protruding stems (e.g. Akilli and Rockwell 2002). The associated energy losses of the mean flow field cause the flow to slow down. These drag effects can even become more important than energy losses due to friction at the channel bed (e.g. James et al. 2004). Therefore, conventional resistance equations (based on wall roughness) are no longer appropriate when describing flow through vegetation. In such cases, both bed resistance and drag effects have to be taken into account in order to arrive at a representation of hydraulic resistance that covers a wide range of conditions realistically.

Several previous investigations have focussed on effects of vegetative resistance in river flows. Experimental campaigns have been set up to measure flow resistance in natural vegetated fields (e.g. Green 2006). Experiments in laboratory flumes have been carried out, with some recent studies by Stephan and Gutknecht (2002), Järvelä (2002), Wilson et al. (2003), and Armanini et al. (2005). Also, detailed numerical simulations of flow through vegetation were performed (e.g. Shimizu and Tsujimoto 1994, Erduran and Kutija 2003, Neary 2003, Choi and Kang 2004). As a result of such studies, several relations were proposed that describe flow resistance caused by vegetation. Some of these relations are empirical (Ree and Crow 1977, Kouwen and Fathi-Moghadam 2000), others have stronger theoretical foundations (Petryk and Bosmajian 1975, Stone and Shen 2002). Also, there are methods that are based on modified logarithmic-velocity profiles (e.g. Kouwen and Unny 1973, Stephan and Gutknecht 2002), which are a well-established experimental characteristic of turbulent wall-bounded flows and find theoretical justification in similarity arguments (e.g. Schlichting and Gersten 2000). Klopstra et al. (1997) combined methodologies by treating flow over vegetation in a two-layer approach, where the flow in two layers is described separately. They combined a modified logarithmic velocity profile in the surface layer with a newly derived velocity profile that is present in between the vegetation.

Among the existing vegetation-resistance relations, the empirical ones have the advantage of being simple in form. On the other hand, empirical relations have the drawback that their applicability is limited to the range of conditions for which they were derived. Theoretical descriptions often are complex. Besides, they may require poorly understood closure parameters and sometimes pose practical difficulties when gathering required input data.

In the current work a new scaling expression of the average flow field is proposed that combines advantages of existing flow equations: (*i*) it is simple in form, (*ii*) it is based on fundamental (flow) principles, (*iii*) it depends on readily measurable quantities and, most importantly, shows excellent agreement with experimental data. The method is based on a two-layer approach, similar as done by Klopstra et al. (1997), where flow in and above the vegetation is treated separately. However, here we only consider bulk characteristics of the flow field by which we avoid difficulties associated with depth-averaging of flow velocities.

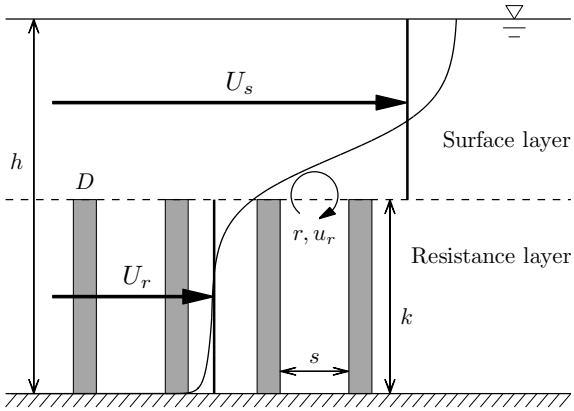

Figure 4.1: In the two-layer approach for flow with submerged vegetation, the height of the vegetation k marks the interface between the resistance layer and the surface layer (h is the total flow depth). The average velocity in the resistance layer U_r is determined by a balance between the streamwise component of the gravitational force, bed resistance, form drag and shear stress due to flow over the vegetation (section 4.3). Flow in the surface layer (U_s) is described with an equivalent bed roughness model (section 4.4).

Vegetation is replaced by cylindrical stems that are homogeneously distributed and have identical geometrical and material properties. Furthermore, the vegetated channel is considered to be sufficiently wide, such that side-wall effects can be neglected. An improved understanding of processes in these idealized conditions will eventually lead to a better description of flow through natural vegetation.

In section 4.2 the concept of the two-layer approach is explained. Next, in section 4.3 and 4.4 the proposed velocity descriptions for the two flow layers are derived. A comparison with selected data from flume experiments is made in section 4.5, which subsequently yields the new calibrated model for the depth-averaged velocity of flow with submerged vegetation.

4.2 The two-layer approach

In a flow field over a solid boundary the force balance between gravitation and flow resistance leads to an equilibrium flow state, which can be associated with a characteristic average flow velocity. For steady uniform flow this condition is expressed as

$$\rho g h i = \rho f U^2 \tag{4.1}$$

where the streamwise component of the gravitational force (per unit length and width) depends on the density of water ρ, the gravitational acceleration g, the depth of flow h and the channel slope i. Dimensional analysis requires that for a dimensionless bed-friction function f the average flow velocity enters the bed

resistance term as U^2. For flow over a solid boundary several formulations for f have been proposed to reflect energy losses due to wall friction (see Yen 2002 for an overview). Strickler (1923) proposed a power-law dependence on the relative roughness height k_S/h, where k_S reflects the height of irregularities at the bed:

$$f_S = \tfrac{1}{64}\left(\frac{k_S}{h}\right)^{1/3}. \tag{4.2}$$

A theoretical justification for equation (4.2) is given by Gioia and Bombardelli (2002), who have shown that the given power-law dependence is valid for turbulent flow over a hydraulically rough bed. This condition is usually met in natural rivers.

However, in the situation of flow over vegetation not only the bed friction slows down the flow but also the drag caused by the vegetation. Therefore, an additional resistance term F_D (force per unit area) is added to the force balance from equation (4.1), which results in (e.g. Petryk and Bosmajian 1975, Wu et al. 1999, Stone and Shen 2002)

$$\rho g h i = \rho f U^2 + F_D. \tag{4.3}$$

Equation (4.3) describes the force balance in a flow layer that is penetrated by vegetation.

If the vegetation is submerged in a flow field, then flow *above* the vegetation is not directly obstructed by the individual plants. The flow in this particular layer experiences resistance due to a slower flowing region in between the vegetation. The resistance to flow in the surface layer can therefore be described by an equivalent bed shear stress. Hence, the depth-averaged velocity in this surface layer is determined by a force balance equivalent to equation (4.1).

In summary, assuming that all vegetation has the same height, for overflown vegetation two distinct flow layers can be distinguished that have different characteristic flow velocities (see Figure 4.1):

(i) the flow layer that is penetrated by the vegetation (i.e. the *resistance layer*) with average velocity U_r and

(ii) the flow layer above the vegetation (i.e. the *surface layer*) with average velocity U_s.

The average flow velocity of the entire flow depth (U_T) is found by proportionally adding the average flow velocities of the resistance layer U_r and the surface layer U_s:

$$U_T = \frac{k}{h}U_r + \frac{h-k}{h}U_s, \tag{4.4}$$

where the height of the vegetation k only partly penetrates the total depth of flow h.

4.3 The resistance layer

4.3.1 Emergent vegetation

To derive the average flow velocity in the resistance layer, we first consider the situation where the vegetation is not completely overflown. By replacing the vegetation with a homogeneous field of identical cylindrical stems, the additional resistance F_D in equation (4.3) can be replaced by a standard drag force term (*stem drag*, see Schlichting and Gersten 2000) to yield:

$$\rho g h i = \rho f {U_{r0}}^2 + \tfrac{1}{2}\rho C_D m D h {U_{r0}}^2. \tag{4.5}$$

The average velocity for flow through emergent vegetation is now denoted by U_{r0}. Individual stems have a diameter D [m], a bed surface density m [m^{-2}] and are characterized by a dimensionless drag coefficient C_D. The separation between neighboring stems follows from $s = 1/\sqrt{m} - D$ (i.e. s is measured edge-to-edge). Since U_{r0} is a depth-averaged value, parameters m, s, D and C_D should be treated accordingly.

The force balance in equation (4.5) can easily be extended to also take the solidity of the vegetation into account, i.e. a factor is introduced that corrects for the surface area and volume occupied by the vegetation (e.g. Kaiser 1984, Stone and Shen 2002, James et al. 2004). However, James et al. (2004) found that such a solidity correction can usually be neglected. The correction on flow velocities and water levels is proportional to D^2/s^2 (Huthoff and Augustijn 2006). Therefore, only when the stem diameter of the vegetation is of the same order of magnitude as the separation between individual plants, then equation (4.5) yields significant loss in accuracy (for $h < k$).

The product $C_D m D$ in equation (4.5) carries the dimension [1/m]. For further simplification we therefore introduce a new length parameter (the *drag length*)

$$b = \frac{1}{C_D m D}. \tag{4.6}$$

The drag length b represents the downstream distance over which the mean flow momentum is dissipated due to cylinder drag. Based on equation (4.5), and using the definition for the drag length from equation (4.6), the average velocity for flow through emergent vegetation U_{r0} is written as (see also Petryk and Bosmajian 1975)

$$U_{r0} = \sqrt{\frac{2bgi}{1 + \frac{2b}{h} f}}, \qquad \text{for } h \le k. \tag{4.7}$$

The average flow velocity U_{r0} can now be determined if the bed resistance function f is known, for example by using Strickler's relation as given by equation (4.2).

4.3.2 Submerged vegetation

When the cylindrical elements become submerged, the flow in the surface layer will have a higher average velocity as in this layer no drag due to the stems

is experienced. The energy losses in the surface layer will be entirely due to a shear stress near the top of the resistance layer, which balances the streamwise component of the gravitational force that drives the flow. The shear stress between the surface layer and the resistance layer (i.e. the *interface shear* τ_k, at height k) will also cause the flow in the resistance layer to speed up. If we introduce the extra shear stress component τ_k due to flow in the surface layer, and realize that the height of the resistance layer is now given by k, the force balance from equation (4.5) modifies to

$$\tau_k + \rho g k i = \rho f {U_r}^2 + \tfrac{1}{2}\rho C_D m D k {U_r}^2. \tag{4.8}$$

The velocity in the resistance layer for *submerged* vegetation is now denoted by U_r. Also, we have assumed that the drag coefficient for an emergent stem is identical to that of a submerged stem, which is reasonable unless the cylinders have small aspect ratios k/D (see Sumner et al. 2004, who finds distinctly different wake structures if $k/D < 5$).

The shear stress at the top of the resistance layer τ_k balances the gravitational force that acts on the water volume in the surface layer, given as

$$\tau_k = \rho g (h - k) i. \tag{4.9}$$

Inserting equation (4.9) into equation (4.8) yields the force balance for flow in a submerged resistance layer:

$$\rho g h i = \rho f {U_r}^2 + \tfrac{1}{2}\rho C_D m D k {U_r}^2. \tag{4.10}$$

The contribution on the left-hand-side of equation (4.10) is due to the gravitational force that acts both on the surface and the resistance layer. The drag force now acts over a depth k, as opposed to the total flow depth h in the force balance that describes flow through emergent vegetation (equation (4.5)). Rearranging terms in equation (4.10) gives a new description for the average velocity in the resistance layer for submerged conditions:

$$\frac{U_r}{U_{r0}} = \sqrt{\frac{h}{k}}, \qquad \text{for } h \geq k. \tag{4.11}$$

A similar relation to equation (4.11) has been proposed by Bentham and Britter 2003, where the average velocity in the resistance layer is proportional to $\sqrt{h}$. Also, Smart et al. 2002 point out that with increasing relative roughness, a conceptual drag coefficient model would lead to a square-root law of the flow resistance.

The average velocity in the resistance layer U_r logically reduces to U_{r0} if no free flowing layer above the cylindrical stems is present (i.e. if $h = k$). After inserting Strickler's bed resistance function f_S as given in equation (4.2) into equation (4.10) the scaling velocity U_{r0} is written as:

$$U_{r0} = \sqrt{\frac{2bgi}{1 + \frac{b}{32k}\left(\frac{k_S}{h}\right)^{1/3}}}, \qquad \text{for } h \geq k. \tag{4.12}$$

Considering that the roughness height k_S is usually much smaller than the flow depth h, the contribution of bed resistance is often negligible. From equation (4.12) it follows that the average velocity in the resistance layer U_{r0} is practically equal to

$$U_{r0} \approx \sqrt{2bgi}, \qquad \text{if } k_S << h. \tag{4.13}$$

The average flow velocity in the resistance layer can be estimated from equation (4.13) if there is no information available about the properties of the channel bed. Such an estimate is reasonable for dense or tall emergent vegetation in relatively deep flows (small drag length b, and large vegetation height k and flow depth h). For sparse vegetation distributions (large drag lengths), bed resistance may become the dominant source of flow resistance. This effect is also included in equation (4.11), which for extremely large drag length b ultimately transforms to Manning's well-known relation for flow over a rough bed.

4.4 The Surface Layer

4.4.1 Shear stress in the surface layer

In steady flow over a rough bed, the shear stress at the bed surface balances the gravitational force on the water body. Similarly, for flow over vegetation, resistance to flow in the surface layer is due to a shear stress that originates at the top of the resistance layer. An expression for this shear stress is already given in equation (4.9). From the Reynolds Averaged Navier-Stokes equation (RANS) it follows that the (Reynolds) shear stress at any location in the flow is determined by the magnitude of fluctuations in the velocity field (e.g. Pope 2000)

$$\tau_{xz} = \rho\overline{v_x v_z} \tag{4.14}$$

where v_x and v_z denote turbulent velocity fluctuations in streamwise and vertical direction (i.e over depth), respectively.

In the theoretical derivation of Manning's law for rough channel flow, Gioia and Bombardelli (2002) assume that streamwise velocity fluctuations v_x scale with the average flow velocity U_s, and that vertical fluctuations v_z are determined by eddies between the roughness elements. It is assumed that a characteristic spatial scale r and characteristic velocity u_r can be associated with these eddies. Following Gioia and Bombardelli (2002), the interface shear stress at the artificial bed (i.e near the top of the resistance layer, see Figure 4.1) scales as

$$\tau_k \sim \rho U_s u_r. \tag{4.15}$$

Together with the expression for the interface shear stress as given in equation (4.9) this yields

$$\rho g(h-k)i \sim \rho U_s u_r. \tag{4.16}$$

To find a relation for the average velocity in the surface layer U_s, an independent expression for u_r needs to be found. For that purpose, a methodology similar to the one demonstrated by Gioia and Bombardelli (2002) is used, which is based

on the condition of a constant turbulent energy dissipation rate from large to smaller flow scales (*Kolmogorov scaling*).

4.4.2 Turbulent energy and Kolmogorov scaling

In the Kolmogorov view on turbulent flow, turbulent energy is created through external forcing at the largest scale of the system (energy containing range) and is dissipated to successively smaller scales until eventually viscosity damps the smallest flow patterns (e.g. Pope 2000). The rate of production of turbulent kinetic energy per unit mass is denoted by ε [m^2/s^3] and, at large scales, is independent from the viscosity (Kolmogorov's second similarity hypothesis). For the energy input at the largest scale, a scaling expression for ε is obtained that is composed of representative geometrical parameters and the representative flow velocity. For surface layer flow as depicted in Figure 4.1, it seems natural to choose the depth of the surface layer $(h - k)$ for the geometrical spatial parameter, and the average surface velocity U_s for the representative velocity. Dimensional analysis yields

$$\varepsilon \sim \frac{U_s^3}{h-k}. \tag{4.17}$$

Furthermore, the concept of an energy cascade, in which turbulent energy is transferred from large to smaller spatial scales, requires that energy dissipated at small spatial scales equals production at the largest scale of the system (e.g. Pope 2000). In our particular case, if it is assumed that eddies of size r and velocity u_r dominate the flow field near the artificial rough bed (i.e. at the top of the vegetation), the dissipation rate scales as

$$\varepsilon \sim \frac{u_r^3}{r}. \tag{4.18}$$

Now ε is related to the characteristic velocity u_r and a length scale r, which represents the extent of local eddies. The characteristic velocity in the resistance layer can be related to the average velocity in the surface layer as (using eqs. (4.17) and (4.18))

$$u_r \sim U_s \left(\frac{r}{h-k} \right)^{1/3}. \tag{4.19}$$

The scaling relation for flow in the surface layer, equation (4.19), is only valid if there is no length scale between scales $h - k$ and r where significant additional sources of turbulent energy occur that affect the energy cascade (i.e. existence of a spectral gap, e.g. Pouquet et al. 1983, Nikora et al. 1997). For flows over vegetation, convincing evidence has been found for enhanced turbulent energy production at length scales associated with wake dimensions (e.g. Raupach et al. 1986, Nezu and Onitsuka 2001 and Naden et al. 2006). However, these features seem to be most pronounced at depths well into the resistance layer (e.g. Poggi et al. 2004), and thus do not have severe implications for the assumptions leading to equation (4.19).

Next, equation (4.19) is inserted into equation (4.16), which yields a scaling expression for the average velocity in the surface layer:

$$U_s \sim \left(\frac{h-k}{r}\right)^{1/6} \sqrt{g(h-k)i}. \tag{4.20}$$

Note that equation (4.20) reduces to the Manning/Strickler equation (Manning 1889, Strickler 1923) if the spacing hydraulic radius r is independent of flow depth. It is well-established that for turbulent flow over rough-walls the relation between the average flow velocity and wall-characteristics is represented by Manning's formula (Chow 1959, Silberman et al. 1963, Yen 2002). This will be used as a limiting condition, in case the depth of the surface layer becomes much larger than the roughness elements.

4.4.3 Similarity considerations

The velocity in the surface layer can be treated as a dimensionless quantity by scaling U_s to the characteristic velocity in the resistance layer U_{r0}. The same scaling methodology was followed to arrive at equation (4.11) for the dimensionless velocity in the resistance layer. Assuming that the dimensionless velocity in the surface layer shows similarity with respect to the surface layer depth $(h-k)$, the following power law asymptotic is defined:

$$\frac{U_s}{U_{r0}} \sim \left(\frac{h-k}{\ell}\right)^{\eta}. \tag{4.21}$$

An unknown scaling length ℓ is introduced in equation (4.21), which is determined from comparison with experimental data (section 4.5).

If in equation (4.20) r indeed reflects an equivalent roughness height, at large depths the power law exponent in equation (4.21) must have the value $\eta = 2/3$:

$$\frac{U_s}{U_{r0}} \sim \left(\frac{h-k}{\ell}\right)^{2/3}, \quad \text{for } h >> k. \tag{4.22}$$

However, a property of equation (4.22) is that U_s reduces to zero when the surface layer vanishes (i.e. when h approaches k). This behavior is not realistic because the average flow velocity in the surface layer should *always* be larger than the flow velocity in the resistance layer (U_{r0}), even if the surface layer is extremely shallow. Essentially, the power law in equation (4.22) does not give realistic results when the depth of the surface layer, $h-k$, becomes close to or smaller than the scaling length ℓ. This can be solved if we assume *incomplete* similarity in the surface layer depth $h-k$, and no kind of similarity in the relative depth h/k (see Barenblatt 2003 for theory on complete and incomplete similarity). Assuming incomplete similarity in $h-k$, we allow the power exponent η in equation (4.21) to be variable (depending on the relative flow depth h/k):

$$\frac{U_s}{U_{r0}} \sim \left(\frac{h-k}{\ell}\right)^{\eta(h/k)}. \tag{4.23}$$

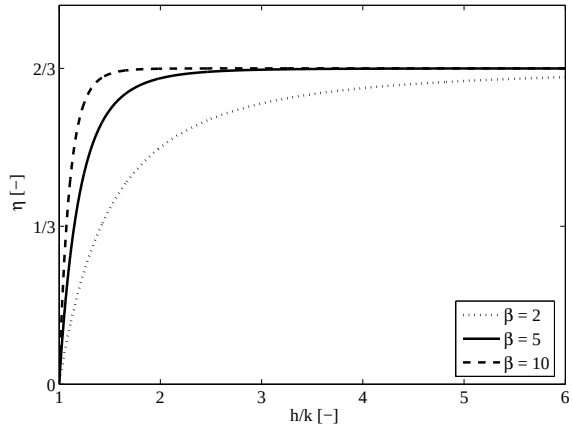

Figure 4.2: Possible functions of the exponent η in equation (4.23), when assuming incomplete similarity between the dimensionless flow velocity in the surface layer (U_s/U_{r0}) and the depth of the surface layer $h-k$. Larger values for β result in faster transitions from $\eta = 0$ to $\eta = 2/3$ (see equation (4.24)).

We have already argued that for large depths the power exponent η should approach 2/3, in correspondence with Manning's resistance law. However, as h approaches k the velocity in the surface layer U_s should approach U_{r0}, which requires that η vanishes. In summary:

(i) if $h/k >> 1$ then $\eta \to 2/3$,

(ii) if $h/k \to 1$ then $\eta \to 0$.

These conditions are met when η is defined as

$$\eta = \frac{2}{3}\left(1 - \left(\frac{h}{k}\right)^{-\beta}\right), \qquad \text{for } \beta > 0. \tag{4.24}$$

Equation (4.24) describes the transition from a power exponent $\eta = 2/3$ to $\eta = 0$ as the depth of the surface layer decreases (i.e. as h approaches k). The exponent β determines how quickly η makes this transition (Figure 4.2).

Inserting equation (4.24) into the scaling equation for the average velocity in the surface layer, equation (4.23), yields

$$\frac{U_s}{U_{r0}} \sim \left(\frac{h-k}{\ell}\right)^{\frac{2}{3}\left(1-\left(\frac{h}{k}\right)^{-\beta}\right)}. \tag{4.25}$$

Thus, we have derived a new model for the average velocity in the surface layer. For large flow depths, equation (4.25) transforms to Manning's law. For shallow surface layer flows it approaches the drag-dominated velocity in the resistance layer.

Table 4.1: Model results to predict the average velocity in the surface layer using Equation (4.25). For different geometric quantities to describe the scaling length ℓ, the optimal value for exponent β is determined (in case $\ell = Ks$ five values for β are shown).

ℓ [m]	K [-]	β [-]	R^2	(99% Conf. int.)
Ks	0.87	3	0.94	(0.88 - 0.97)
Ks	0.95	4	0.975	(0.95 - 0.99)
Ks	0.99	5	0.981	(0.96 - 0.99)
Ks	1.00	6	0.977	(0.95 - 0.99)
Ks	1.00	7	0.97	(0.93 - 0.98)
Kb	0.093	4	0.85	(0.70 - 0.93)
KD	9.5	5	0.60	(0.33 - 0.79)
KC_DD	9.8	5	0.59	(0.31 - 0.78)
Kk	0.13	50	0.33	(0.07 - 0.60)

4.5 Comparison to data from flume experiments

4.5.1 The flume experiments

For model calibration we use the experimental data from Meijer and van Velzen (1998) (for data see also Baptist 2005). The available experimental data comprise 48 flow experiments with homogeneously distributed cylindrical stems that all have the same stem diameter ($D = 8$ mm). The cylinder height k varied between three distinct values ($k = 0.45$, 0.9 or 1.5 m), and flow depths h were varied such that relative depths were in the range from $h/k = 1.3$ to $h/k = 5.5$. Half of the total set of experiments was carried out with a surface density m of 256 cylindrical stems per square meter ($s = 5.45$ cm), the other half with a surface density of $m = 64$ m^{-2} ($s = 11.7$ cm).

For each of the experiments, flow velocities were measured at depths 0.10 m apart with an Acoustic Doppler Velocimeter (ADV). Using linear interpolation, the average flow velocity for the surface layer U_s and the resistance layer U_r were estimated separately (see Figure 4.3). The characteristic velocity U_{r0} was determined by depth-averaging the flow velocity in the lower part of the resistance layer, which was unaffected by the flow in the surface layer.

Based on four flow experiments without artificial vegetation, the roughness height k_S of the flume bed was determined $k_S = 2.3 \pm 0.6$ mm. Also, from eight experiments with emergent cylinders, drag coefficients were determined from measured flow velocities and measured surface slopes (using equation 4.5). The resulting drag coefficients were compared with values predicted for flow around isolated cylinders. For this purpose, local Reynolds numbers were calculated from the measured average velocities in the resistance layer (Re $\sim 3{\cdot}10^4 - 4{\cdot}10^4$) and subsequently, the drag coefficients C_D for the circular cylinders. Standard works on fluid mechanics (e.g. Schlichting and Gersten 2000) report that in such a flow regime the drag coefficient remains fairly constant with a value of nearly 1. Measured C_D values were quite evenly spread around predicted values, and it was concluded that the observed deviation from the predicted

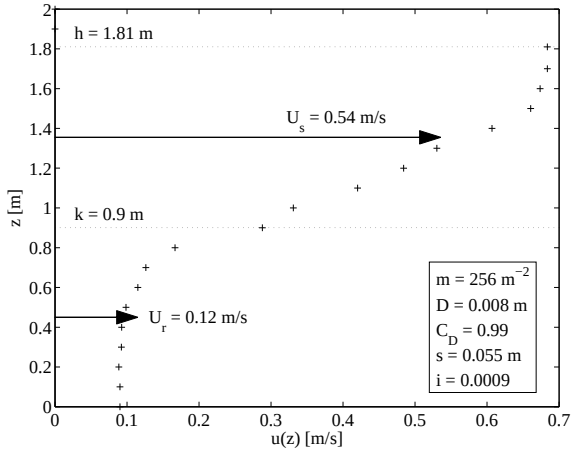

Figure 4.3: Measured velocity profile ('+') for one of the 48 flow experiments with rigid cylindrical vegetation (Meijer and van Velzen 1998). Arrows depict the magnitude of the depth-averaged velocities in the surface layer U_s and the resistance layer U_r.

drag coefficients was largely due to measurement errors in the surface slope (Meijer 1998b). No significant variations in the drag coefficient were observed that could be attributed to sheltering effects for objects placed in an array (e.g. Raupach 1992, Nepf 1999). Consequently, for the remaining 48 experiments with submerged cylinders, predicted C_D values were adopted and surface slopes were corrected to match the measured characteristic velocity U_{r0} in the lower resistance layer.

4.5.2 Average velocities in the two flow layers

Figure 4.4 shows the measured average velocities in the resistance layer as compared to the ones predicted by equation (4.11). Although for slow flows the velocities are slightly overestimated, the overall agreement between equation (4.11) and measured values is very good ($R^2 = 0.94$).

The scaling expression for the velocity in the surface layer, equation (4.25), consists of two unknown parameters; the scaling length ℓ and the transition exponent β. Table 4.1 shows some model results using different geometrical quantities for the scaling length ℓ, and the corresponding values for β that fit the measurements best (maximum R^2). It turns out that for $\ell = Ks$ the proposed scaling law gives best agreement with laboratory data. This particular scaling approach is not very sensitive to changes in β, as any β-value in the range 4-7 still yields a coefficient of determination larger than 0.97 if compared to laboratory data. The maximum of R^2 occurs when β is very close to 5 ($R^2 = 0.98$), with a corresponding coefficient of proportionality K practically equal to unity. Therefore, we propose the following expression for the scaling length ℓ in the surface layer:

$$\ell = s. \tag{4.26}$$

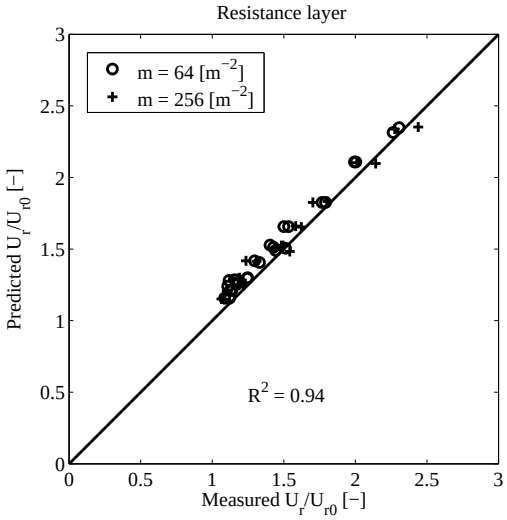

Figure 4.4: Comparison between the proposed model for the depth-averaged velocity U_r in the resistance layer (equation (4.11), on vertical axis) and results from laboratory flume experiments (m = number of cylindrical stems per m^{-2} on the bed surface).

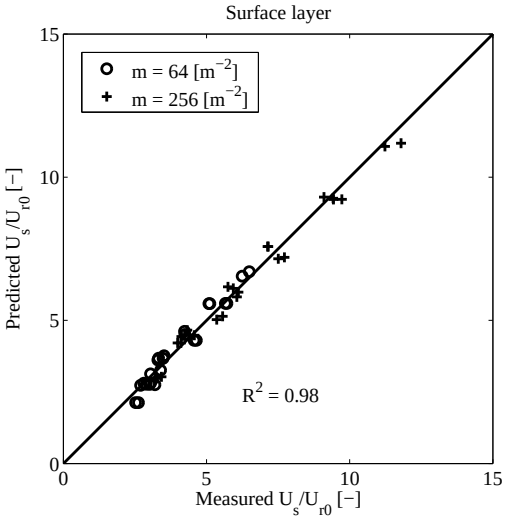

Figure 4.5: Measured and predicted values (equation (4.27)) of the depth-averaged velocity U_s in the surface layer.

In combination with a value for the transition exponent of $\beta = 5$ in equation (4.24), the new scaling relation for the flow velocity in the surface layer becomes

$$\frac{U_s}{U_{r0}} = \left(\frac{h-k}{s}\right)^{\frac{2}{3}\left(1-\left(\frac{h}{k}\right)^{-5}\right)} . \tag{4.27}$$

Figure 4.5 shows how the predictions of the calibrated scaling expression, equation (4.27), compare to the measured flow velocities. Surface layer velocities are predicted accurately for the entire data set of 48 experiments.

As shown in section 4.4.2, theory predicts a depth-independent scaling length ℓ, and a constant power of 2/3, when the depth of the surface layer is large. By comparison with experimental data (with relative depths in the range $h/k = 1.3 - 5.5$) we found that shallow flows are also well described by introducing a transition exponent of $\beta = 5$ in equation (4.24). This value for β implies that the exponent η only deviates significantly from 2/3 for relative flow depths $h/k < 2.5$ (see Figure 4.2). Therefore, even though the scaling relation given in equation (4.22) was only expected to give realistic results for deep surface layer flows, it also performs well for flows in relatively shallow surface layers when using the scaling length $\ell = s$ (equation (4.26)). If we would assume complete similarity between flow velocity and depth of the surface layer (i.e. by using a constant exponent $\eta = 2/3$ in equation (4.25)), small values of U_s/U_{r0} are predicted less accurately, but still a coefficient of determination of $\mathrm{R}^2 = 0.94$ is found.

4.5.3 A two-layer scaling model for the entire flow depth

By using the newly proposed flow velocity models for the resistance layer (equation (4.11)) and the surface layer (equation (4.27)), the expression for the average velocity of the entire flow depth (equation (4.4)) becomes:

$$\frac{U_T}{U_{r0}} = \sqrt{\frac{k}{h}} + \frac{h-k}{h}\left(\frac{h-k}{s}\right)^{\frac{2}{3}\left(1-\left(\frac{h}{k}\right)^{-5}\right)} \tag{4.28}$$

In Figure 4.6, the predictions of the new two-layer velocity scaling model for the entire flow depth (equation (4.28)) are compared to the measured average flow velocities. The combined performance of the velocity models in the resistance and surface layer (eqs. (4.11) and (4.27)) is even better than their separate predictions, yielding a coefficient of determination $\mathrm{R}^2 = 0.99$.

In section 4.5.2 it was addressed that the variable power exponent η in the surface layer only affects predicted flow velocities for relatively shallow surface layers (if $h/k < 2.5$). For the average velocity over the entire depth (equation (4.28)), this effect is even further suppressed because for shallow surface layers the overall flow field is largely determined by flow in the resistance layer. Therefore, predictions of depth-averaged flow velocities are not very sensitive to the choice of parameter β in equation (4.25).

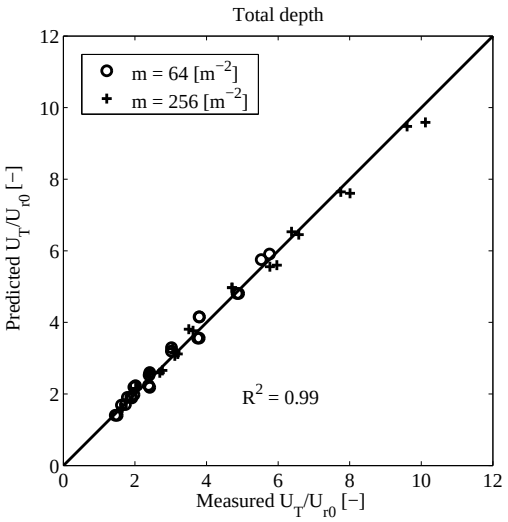

Figure 4.6: The predicted depth-averaged velocity over the entire flow depth (U_T as in equation (4.28), on vertical axis) vs. measured average velocities.

4.6 Discussion

4.6.1 Length scales in the surface layer

The scaling length ℓ, reflecting the flow resistance that the surface layer experiences due to the cylindrical elements, is well-represented by the spacing between the cylindrical stems s. This may seem a surprising result since earlier studies have shown that the shear length scale at the interface between surface and resistance layer (defined as $L = U(\partial U/\partial z)^{-1}$ at $z = k$) reflects the turbulent length scale that is responsible for most vertical momentum transfer (e.g. Raupach et al. 1996, Ghisalberti and Nepf 2004). While correlations between L and k (the vegetation height) sometimes yield good results (Raupach et al. 1996), in general, a scaling relation $L \sim k$ cannot be correct. This conclusion is supported by observations of flow over tall resistance elements with only limited extent of the shear layer (e.g. Ghisalberti and Nepf 2004). Also in Figure 4.3 a limited shear layer is shown: in the lower half of the resistance layer the velocity profile is practically vertical. In the region of vertical velocity profile, neither bed effects nor surface layer effects significantly influence the flow field. Thus, energy losses are due to cylinder drag. Departure from a vertical velocity profile in the upper half of the resistance layer is due to flow in the surface layer, but is entirely detached from bed roughness effects. Therefore, if bed effects have negligible influence on the mean flow in the resistance layer, the shape of the velocity profile at the top of the cylinders is not controlled by the distance to the bed.

If a general scaling length exists for flow over tall objects, then it can only be related to scales that are present at the top of the resistance layer, such as

the stem diameter, or the spacing between neighboring elements. Both Raupach et al. (1996) and Ghisalberti and Nepf (2004) acknowledge that the interface shear, or conversely, the shear scaling length L, is related to vegetation density. In view of these observations, the drag length b, which depends on vegetation density and reflects momentum dissipation due to cylinder drag, appears to be a suitable candidate for a turbulent length scale. Furthermore, Table 4.1 shows that $\ell = b$ also yields good results when compared to laboratory data ($R^2 = 0.85$). Here we reflect on some implications associated with choosing $\ell = b$ instead of $\ell = s$.

First of all, it is important to note that the scaling length ℓ is merely introduced to make equation (4.21) dimensionally correct, as it seems natural to scale the flow velocity in the surface layer to the characteristic velocity U_{r0} in the resistance layer. The turbulent length scale r in equation (4.20) reflects the equivalent size of eddies responsible for the momentum transfer in the resistance layer. Combining equations (4.13), (4.20) and (4.22) reveals that both length scales are related as

$$r \sim \frac{\ell^4}{b^3} \tag{4.29}$$

Next, we consider the drag length b and the spacing between cylinders s as possible values for the scaling length ℓ:

1. If $\ell = b$ then $r \sim b$.
2. If $\ell = s$ then $r \sim s^4/b^3$.

The drag length b can be expressed as

$$b = \frac{(s+D)^2}{C_D D} \tag{4.30}$$

(see equation 4.6), which yields for the turbulent length scales:

1. If $\ell = b$ then $r \sim (s+D)^2/(C_D D)$.
2. If $\ell = s$ then $r \sim (C_D D)^3/(s+D)^2$.

Assuming that the turbulent scale r reflects the equivalent length scale where most momentum transfer takes place (an equivalent 'roughness height', see equation (4.20)), then a larger r is associated with larger resistance to flow. In terms of cylinder geometry and distribution, larger resistance is associated with *increasing* diameter D and *decreasing* separation s. This behavior is found in option 2, while option 1 gives the opposite behavior (if $s > D$). Therefore, it is concluded that the drag length b cannot be a suitable value for the scaling length ℓ.

Having discarded b as suitable scaling length for ℓ, the alternative $\ell = s$ remains a likely candidate. The analysis above has shown that $\ell = s$ is associated with a turbulent length scale r that increases with increasing stem diameter and

vegetation density. Such general trends are indeed expected, but the exact form of the scaling function for r is not well understood.

Also, interpreting the turbulent scale r as an equivalent roughness height (for surface layer flow), it seems natural to assume that r may not exceed the height of the cylinders k. Subsequently, ℓ should always be smaller than $(kb^3)^{1/4}$ for $\ell = s$ to be valid. Further investigations with different geometrical properties of the cylinders, and different spatial distributions, should be carried out to study these situations.

4.6.2 Hydraulic resistance of natural vegetation

Complications arise when we want to represent hydraulic resistance of *natural* vegetation with the newly proposed two-layer flow model. In the proposed flow model, the plant height k is considered fixed and identical for all individual plants. A fixed value for the plant height k allowed us to define two distinct flow layers. Is this still possible when the plant height is spatially variable, or when in case of flexible vegetation bending effects decrease the depth of the resistance layer? An average plant height is possibly still appropriate for defining two flow layers if plant height variability is concentrated around a well-pronounced mean value. If, however, the distribution of different heights shows distinct peaks then more flow layers should be defined, each associated with an average flow velocity. Plant flexibility not only changes the effective height of the vegetation but may also alter the effective drag force due to streamlining. Järvelä (2004) has proposed a solution to this problem by introducing the vegetation parameter χ, that serves as a correction factor on the drag force.

Also, the spacing parameter s, that reflects the spatial density of the vegetation, is easily determined for a homogeneous field of identical stems. However, which value should be used for a representative plant separation if the spatial distribution of individual plants is not homogeneous, or when variability between plants exists and side branches with leaves also obstruct the flow? For flow through emergent vegetation this problem is more easily solved because the drag coefficient C_D can be adjusted to match flow measurements for a specific choice of plant separation (or similarly, a choice of frontal plant area, see e.g. Fischenich and Dudley 2000). Whether it is justified to use this same plant separation value to determine the flow velocity in the surface layer when the vegetation becomes overflown is questionable. Relating to this issue, Järvelä (2004) proposed a method to estimate an effective diameter for branched vegetation. Along the same lines, it would be interesting to investigate whether an effective plant separation allows for application of the new model to real vegetation. Van Velzen et al. (2003) gives a list of effective surface densities and stem diameters for a range of typical floodplain vegetation types. Comparing the effective ratios k/D and s/D for natural vegetation with the ranges investigated in the present study, shows that the proposed hydraulic resistance model potentially covers a wide range of vegetation types, including grasses, reed, sedges and several types of bushes (Table 4.2).

Table 4.2: Effective geometrical parameters of selected floodplain vegetation types (Van Velzen et al. 2003). Also listed are geometrical parameters of the cylindrical stems used in the current study.

Vegetation type	m [m^{-2}]	D [m]	s [m]	k [m]	s/D [-]	k/D [-]
Natural grassland	4000-5000	0.003	0.011-0.013	0.1-0.2	4	33-67
Sedges	200	0.006	0.065	0.3	11	50
Thistle bushes	1000-3000	0.003	0.015-0.029	0.3	5-10	100
Bramble bushes	112	0.005	0.089	0.5	18	100
Pipe grass	300	0.004	0.054	0.5	13	125
Reed-mace	20	0.018	0.21	1.5	11	83
Reed	80	0.005	0.11	2.5	22	500
Orchards	0.16	0.1-0.2	2.3-2.4	2-3	11-24	15-20
Softwood shrub	3.8	0.034	0.48	6	14	176
Dense cylinders	256	0.008	0.055	0.45-1.5	6.9	45-188
Sparse cylinders	64	0.008	0.117	0.45-1.5	14.6	45-188

4.7 Conclusions

In the present study, flow over large-scale roughness elements is described by an average-velocity model where distinct flow characteristics are attributed to two separate flow layers. By describing flow by its bulk behavior, we avoided the necessity of integration over depth and the associated complications of depth-dependent turbulence intensities. Predictions of the new expression for the depth-averaged velocity for flow with submerged rigid vegetation gives excellent agreement with measured flow velocities (coefficient of determination $R^2 = 0.99$).

The new proposed models that describe the depth-averaged flow velocity in the two flow layers separately, also each show very good agreement with measured flow velocities. It was shown that depth-averaged flow in the resistance layer is adequately described by means of a simple bulk-force balance. Apart from the drag coefficient that is particular to the shape of the resistance elements, no further calibration parameter is needed for the resistance layer model. For the surface layer, a comparison with results from flume experiments shows that the scaling length ℓ, required in the depth-averaged velocity relation, is well-represented by the spacing between the cylindrical stems. A depth-dependent power law exponent is used to force the scaling law to a realistic limiting value for relatively shallow surface layer flows. This adaptive power exponent improves predicted velocities in the surface layer if the vegetation penetrates about half of the total water column, until vegetation becomes emergent (and the surface layer vanishes). For relatively larger depths of the surface layer, average flow velocities follow Manning's resistance law.

The proposed flow resistance model is based on idealized vegetation characteristics with homogeneous geometrical and material properties. Because of its accurate predictions for such conditions, it may serve as a reliable basis for describing the hydraulic response to natural vegetation.

4.8 Appendix: A tentative explanation for the turbulent length scale of flow over vegetation

In this appendix[†], a scaling expression is derived for the turbulence scale r. The key assumption in the derivation is that turbulent motions generated in the wake of the cylinders are responsible for energy losses to the mean flow field. A spatially-averaged eddy length-scale is derived to represent these losses.

First of all, the product '$C_D mD$' in the drag force, see equation (4.5), represents the effective blockage area per unit volume. Its inverse, the drag length $b = 1/(C_D mD)$, represents an effective longitudinal length-scale over which the mean flow energy is dissipated to wake turbulence. Next, the spatially-averaged eddy length-scale r is estimated by longitudinally averaging dominant turbulent

[†]This appendix is not included in the publication by Huthoff, F., D. C. M. Augustijn and S. J. M. H. Hulscher (2007) in *Water Resources Research* 43(W06413).

scales that are present within the drag length

$$r = \frac{1}{b}\int_0^b r(x)dx, \tag{4.31}$$

where $r(x)$ is the size of dominating eddy at location x downstream of the cylinder, which locally contains most turbulent energy.

Immediately downstream of the cylinder the dominating eddies typically have sizes of the order of the cylinder diameter, which remains the case up to the formation length L_f (e.g. Williamson 1996). Momentum dissipation due to cylinder drag is largely determined by the wake-generated eddies within the formation length. Downstream of the formation length L_f, the presence of wake-generated eddies rapidly diminishes (Raupach 1992, Williamson 1996). Hence, we assume that

$$\text{if} \quad x < L_f, \text{ then } r \sim D, \tag{4.32}$$

$$\text{if} \quad x > L_f, \text{ then } r \simeq 0, \tag{4.33}$$

which yields for the spatially-averaged eddy length-scale

$$r \sim \frac{1}{b}\int_0^{L_f} D dx = \frac{DL_f}{b}. \tag{4.34}$$

The formation length typically scales with the width of the cylinder $L_f \sim D$ (e.g. Chen and Jirka 1995). Subsequently, the eddy length-scale r scales as

$$r \sim \frac{D^2}{b} \sim \frac{D^3}{(s+D)^2}, \tag{4.35}$$

which is equal to the scaling function found for r in section 4.6.1, associated with the empirical result $l = s$.

Chapter 5

Evaluation of bulk flow model against measurements in natural vegetated waterways*

In this chapter the vegetation bulk flow model from Chapter 4 is compared to results from flow experiments conducted in natural waterways. Two field case studies with flow over vegetation are considered: (i) fixed-point flow measurements in a Green River and (ii) vessel-borne flow measurements along a cross-section with floodplains in the river Rhine. Analysis of the two cases shows that the simple flow model is consistent with measured flow velocities and the present vegetation characteristics, and predicts a realistic Manning resistance coefficient. From flow measurements in the river floodplain (case 2) an estimation of the equivalent height of the drag dominated vegetation layer was made based on flow characteristics only. The resulting height corresponds well with the height of vegetation in the floodplain. The expected depth-dependency of the associated Manning resistance coefficient for relatively shallow flows could not be detected due to lack of appropriate data. Furthermore, it was shown that topographical variations in the floodplain may have important impact on the flow field.

5.1 Introduction: Hydraulic resistance due to vegetation in natural waterways

In various studies it was shown that if vegetation penetrates a significant part of the water column then a constant Manning resistance value is no longer adequate to describe the hydraulic resistance with changing water levels (e.g. Cook and Campbell 1939, US Soil Conservation Service 1954, Green and Garton 1983, Wilson and Horritt 2002, García Díaz 2005). These studies have shown that the hydraulic resistance due to vegetation (in terms of Manning's n) tends to decrease with increasing water level. A general, easily applicable, methodology to describe such behavior is still lacking despite intense research efforts in the

*This chapter has, in slightly revised form, been submitted for publication as a separate paper: Huthoff, F., M. Straatsma, D. C. M. Augustijn and S. J. M. H. Hulscher (2007). Evaluation of a simple hydraulic resistance model using flow measurements collected in vegetated waterways. Submitted to *Hydrological Processes*.

recent years. This is partly due to the difficulties associated with isolating the effect of vegetation on a flow field (e.g. Gendelman 1981). Hydraulic resistance parameters determined in the field are unavoidably contaminated with additional external influences, such as geometrical variations of the channel, density currents, sediment interactions, wind or surface waves (e.g. Lightbody and Nepf 2006). Furthermore, collecting flow data in natural vegetated waterways is in itself a tricky task: the presence of vegetation obstructs detailed flow velocity sampling (Green 2005). In particular when vegetation is abundant and has a large impact on the flow field, accurate data sampling is difficult. As a result, studies where flow characteristics and the influence of vegetation are measured in natural rivers are relatively scarce (e.g. Sukhodolova et al. 2004), they are case-specific and, due to the complexity of the environment, are quite difficult to interpret (see Lee et al. 2004, where flume studies are used as a reference to field measurements).

Most experimental studies relating to the hydraulic resistance of vegetation are conducted in laboratory flumes, where it is possible to minimize hydraulic impacts due to other external influences (e.g. Järvelä 2002, Shi and Hughes 2002, Wilson et al. 2003, Armanini et al. 2005). That way, investigations of vegetative hydraulic resistance allow isolation of the impact of specific vegetation characteristics (such as stem width, height, flexibility). These studies have revealed that flow through vegetation is difficult to describe based on geometrical conditions of the vegetation only, even if vegetation is described in a simplified way as cylindrical stems. A recurring complication of these hydraulic resistance models is the need for a general representation of energy losses associated with turbulent mixing patterns. Such energy-loss representations may enter the flow models in the form of a turbulent mixing length, which reflects the typical size of the largest and dominating mixing patterns (e.g. Murota et al. 1984, Tsujimoto et al. 1991, Klopstra et al. 1997, Velasco et al. 2005). Flow descriptions that include the mixing length concept only have practical value if the mixing length is directly related to measurable quantities. Such relations have been proposed (Klopstra et al. 1997, Meijer and van Velzen 1998, Khublaryan et al. 2004), but due to lack of theoretical justification their general applicability remains questionable. Other more general applicable attempts include so-called $\mathrm{K}-\epsilon$ models, which explicitly describe the transport of turbulent kinetic energy (Shimizu and Tsujimoto 1994, López and García 2001, Defina and Bixio 2005). However, these methods require considerably larger computational effort, in particular if applied in models on a river-reach scale.

Alternatively, in Chapter 4 a simple vegetation resistance model is proposed that includes only measurable quantities. The model requires knowledge of a vegetation drag coefficient C_D, the average vegetation height k, stem diameter D and a representative spacing between neighboring plants s. Among these, only the drag coefficient cannot be directly obtained from geometrical dimensions, but is to be determined in laboratory flow experiments with emergent vegetation. Hence, species specific C_D-values absorb the impact of presence of foliage and vegetation flexibility and streamlining (for extensive list of vegetation drag coefficients, see Fischenich and Dudley 2000).

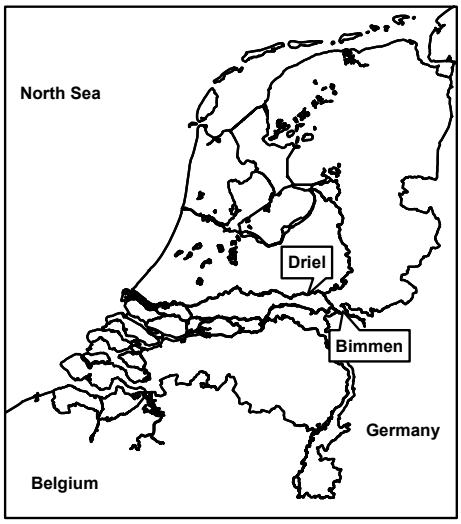

Figure 5.1: A map of the Netherlands indicating the two study locations: the Green River at Driel and the floodplain near Bimmen.

In the current work we investigate whether the simplified model from Chapter 4 is consistent with flow measurements in the field, and whether it provides a potential candidate for integration with river-wide flow models. Two case-studies with flow in vegetated waterways are considered. First, in section 5.2, measured flow velocities and vegetation characteristics in a Green River are evaluated against predictions of the hydraulic resistance model. It is shown that the model provides an acceptably accurate estimate of the average flow velocity, as based on general vegetation characteristics. Next, in section 5.3, flow velocities are measured in a natural floodplain at different discharge magnitudes. In this case-study no detailed information about the post-flood vegetation is available. Therefore, we evaluate whether the measured dynamic behavior of the hydraulic resistance is consistent with the vegetation resistance model. It is shown that the proposed model describes the vegetation resistance well. However, as for the considered case the dynamic behavior of hydraulic resistance is only weak, a simple wall-roughness model may also be used (such as Manning's equation for rough channel flow).

5.2 Fixed-point measurements in a Green River (Driel, the Netherlands)

5.2.1 The study location

In February 2005 a high-discharge event in the Rhine caused a *Green River*[†] near Driel to be deployed for additional discharge capacity. Due to its rela-

[†]A Green River is a secondary waterway that is only deployed for additional discharge if the discharge in the main river channel reaches a particular high level. The bed of a Green

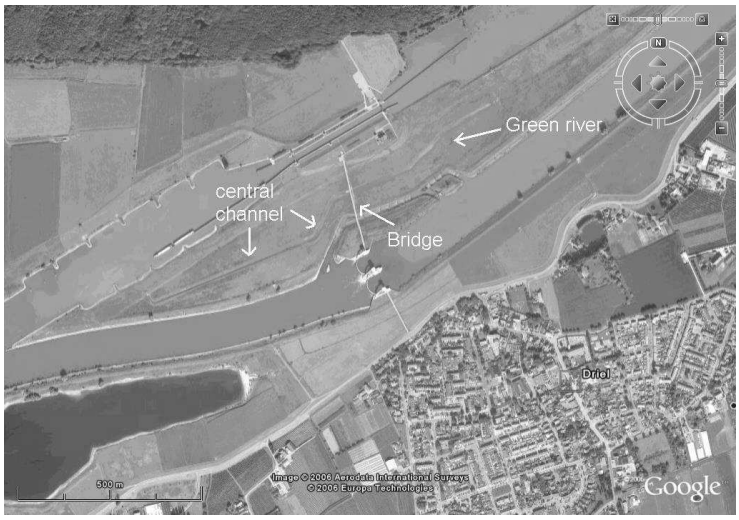

Figure 5.2: Aerial picture showing the Green River at Driel and the bridge that was used to take the flow measurements from (picture: Google Earth).

Table 5.1: Vegetation characteristics as measured in the field (February 2005) at the study location at Driel.

k [m]	D [m]	m [m^{-2}]	s [m]
0.375	0.0037	51	0.136

tive homogeneous geometrical boundaries, this location is particularly suitable for measurements of the hydraulic effect of the present vegetation. The aerial picture in Figure 5.2 shows the surroundings of the study area, including the bridge from where measurements were performed, the weir in the main channel and the village of Driel. The flow direction in this picture is from east (right) to west (left). Figure 5.3 shows the presence of vegetation on the channel bed of the Green River, as observed when no surplus discharge is directed through the Green River. Note that the Green River includes a central sub channel that also contains water when the Green River is not deployed. The sub channel is closed at both ends, and therefore does not carry *flowing* water. In Figure 5.3 (right picture) the sub channel is just visible, but can be more clearly discerned from the aerial picture in Figure 5.2.

5.2.2 Methodology & Results

The bridge that spans the Green River was used to suspend a measurement device from, to record the flow velocities below. Figure 5.4 shows a picture of

River is commonly covered with grass (hence, *green*) and used for agriculture purposes if not flooded.

Figure 5.3: The vegetation that covers the channel bed in the Green River at Driel (see Table 5.1 for vegetation characteristics). Below the large bridge that spans the entire Green River at Driel, a small bridge crosses the central deeper channel, as seen in the right picture (pictures by Menno Straatsma).

Figure 5.4: The measurement location at Driel during the high discharge event on the 17th of February 2005 (picture by Menno Straatsma).

the bridge over the flooded Green River on the 17th of February 2005, the day that data was collected. Three locations along the bridge were used for measurements: one in the central sub channel of the Green River (location 2) and two locations well separated to either sides of the central sub channel (location 1 and 3). These latter two locations have similar bed coverage characteristics (as seen in figure 5.3) and are thus expected to be hydraulically equivalent.

An *RD Instruments* Acoustic Doppler Current Profiler (ADCP) was used to record flow velocity profiles in the Green River, which was immersed into the flow field from the bridge that spans the channel. The ADCP resolves the three-dimensional flow vector at various user-defined depths. Due to the size of the ADCP itself, and the inability of the ADCP to measure flow velocities immediately below the device, flow velocities were measured from 46 cm below the water surface downwards, at depths 10 cm apart. An average ensemble interval of nearly 6 s was used to determine the mean streamwise velocity.

Figure 5.5 shows the measured flow velocity profiles for the three locations along the bridge. The graphs also show the profile of the average streamwise velocity, together with 16 and 84 percentile error boundaries. These boundaries correspond to a 1σ standard deviation if errors were distributed normally (i.e. a Gaussian distribution). Also, the total depth of flow h is measured independently by the ADCP, as stated above the graphs of Figure 5.5.

In Figure 5.5 it can be seen that in the flow layer of about 30 cm above the channel bed large fluctuations in flow velocities were measured. The enhanced scatter in these flow measurements near the bed is likely due to the presence of vegetation. Vegetation height was independently measured, which on average yielded a height of $k \simeq 37.5$ cm. Table 5.1 gives an overview of the local vegetation characteristics as measured in comparable circumstances later in February 2005 (during dry conditions of the Green River). Figure 5.5 also states the depth-averaged flow velocities of the flow layer above the vegetation U_s (in the *surface layer*), as based on the ADCP-measurements. These values were determined by taking the average value (and corresponding 16- and 84 percentile boundaries) of all flow velocity measurements from above the vegetation. The absence of flow measurements in the upper part of the water column is not corrected for, as the velocity profiles do not show a strong velocity increase towards the water surface. Nevertheless, this simplification introduces a small bias in the average flow velocities, giving slightly underestimated values for U_s.

The graphs in Figure 5.5 show that, between the three measurement locations, the depth-averaged flow velocity in the deepest location (Location 2) is not significantly larger than for the other two locations (in fact, it is slightly smaller). This may seem an unexpected result, because in general one would expect larger flow velocities at larger depths (for equal bed resistance), and also because of the expected lower hydraulic resistance of the central sub channel (because of the absence of vegetation). However, it must be kept in mind that not the entire water column in the central sub channel contributes to discharge capacity. As the channel is closed at both ends, the fluid layer below surrounding banks does not flow freely. Another effect that causes the flow in the central channel to slow down is the presence of a small second bridge that obstructs

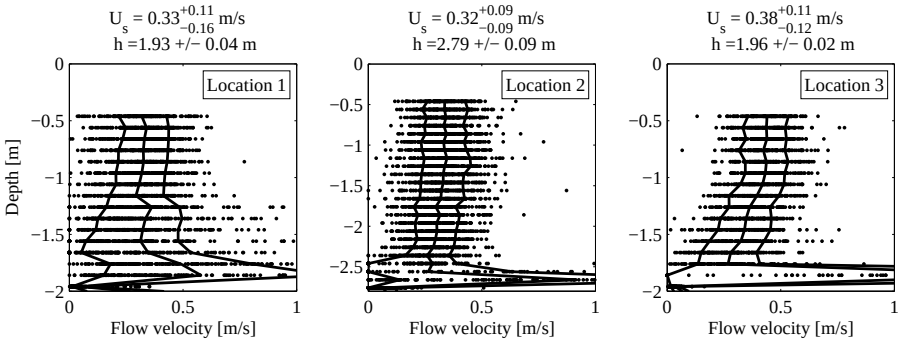

Figure 5.5: ADCP measurements at three different locations near the bridge at Driel. For each location, separate flow measurements of flow velocities at different depths are shown. Stated above each graph, U_s is the depth-averaged flow velocity in the surface layer and h the depth of flow. The average velocity profile and 16 and 84 percentile boundaries are also shown in each of the graphs.

the flow locally. In Figure 5.3 (right picture) the small bridge is clearly visible. This bridge was entirely flooded during the high-discharge event in February 2005 (see Figure 5.4), thus obstructing flow near the central sub channel. Consequently, we consider the flow measurements corresponding to the shallower regions in the Green Channel (e.g. velocity profiles of Location 1 and Location 3 in Figure 5.5) most representative of the hydraulic response due to bed vegetation. In the remainder, the measurements from Location 2 in the central sub channel are therefore discarded for the analysis of hydraulic resistance due to vegetation.

Finally, the energy slope i was determined by tracking a float that was set free in the flow field with a *total station* located at a fixed point on the river bank (for float tracking methodology, see Straatsma 2007). This resulted in an average value for the energy slope of $i = 9.2 \times 10^{-5}$, having a relative error of about 20%.

5.2.3 Comparison to model predictions

Based on approximated physical laws for fluid flows over an array of homogeneously distributed cylinders, Huthoff et al. (2007) propose a simple flow model to describe the hydraulic resistance of vegetation (see Chapter 4). The flow velocity in the vegetation layer (or *resistance layer*) U_r is described separately from flow in the surface layer U_s. Together, they give an estimate of the average flow velocity over the total depth U_T:

$$U_T = \frac{k}{h} U_r + \frac{h-k}{h} U_s. \tag{5.1}$$

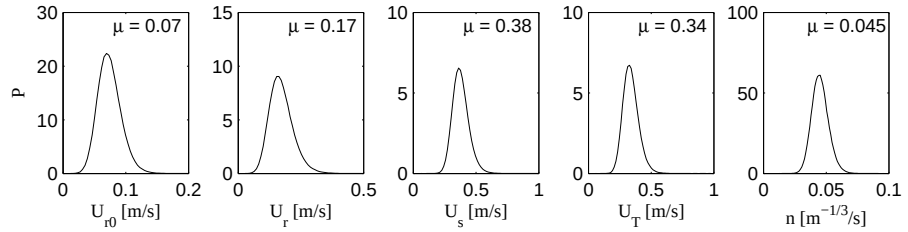

Figure 5.6: Probability densities of predicted flow velocities based on the vegetation characteristics (Table 5.1) and geometrical characteristics of the channel (mean values are given by μ) and a drag coefficient of $C_D = 1.8 \pm 0.18$.

The depth-averaged flow velocity in the surface layer is represented by the power law:

$$U_s = U_{r0} \left(\frac{h-k}{s} \right)^{\frac{2}{3}\left(1-(k/h)^5\right)}. \tag{5.2}$$

Where U_{r0} is the flow velocity for situations with emergent vegetation and s a representative separation between vegetation elements. If the total depth of flow h is at least twice as large as the vegetation height k, then the power exponent in equation (5.2) reduces to a constant value of 2/3. In between the vegetation the average flow velocity is estimated as

$$U_r = U_{r0} \sqrt{\frac{h}{k}}. \tag{5.3}$$

For both equations (5.2) and (5.3) the characteristic scaling velocity U_{r0} is given by

$$U_{r0} = \sqrt{\frac{2gi}{mDC_D}}, \tag{5.4}$$

with g the gravitational acceleration, i the (energy) slope, m the number of vegetation elements per unit area (on the channel the bed), D the stem diameter and C_D the dimensionless drag coefficient. For homogeneously distributed cylindrical vegetation elements the separation s is calculated as (Huthoff et al. 2007):

$$s = \frac{1}{\sqrt{m}} - D. \tag{5.5}$$

Using the vegetation parameters from Table 5.1, flow velocities at certain depths of flow can be predicted, according to equations (5.1)-(5.5). The only unknown parameter is the drag coefficient C_D, which is a function of the Reynolds number (e.g. Wu et al. 1999), stem aspect ratio (Sumner et al. 2004), vegetation distribution density (Nepf 1999, Raupach 1992) and foliage and streamlining effects (e.g. Fathi-Maghadam and Kouwen 1997, Kouwen and Fathi-Moghadam 2000, Järvelä 2004). However, for flow through an array of equally spaced cylinders, a constant value of $C_D = 1$ is a reasonable value (e.g. Stone and Shen

Table 5.2: Predicted flow characteristics (with standard deviations) near the bridge at Driel (at Location 3) for three different assumed values for the drag coefficient C_D. Flow velocities were predicted using equations (5.1)-(5.5).

	Predicted values				
C_D [-]	U_{r0} [m/s]	U_r [m/s]	U_s [m/s]	U_T [m/s]	n 10^{-2}[$m^{-1/3}$s]
1.0 ± 0.10	0.10±0.02	0.23±0.06	0.51±0.08	0.45±0.08	3.4±0.5
1.5 ± 0.15	0.08±0.02	0.19±0.05	0.41±0.07	0.37±0.06	4.1±0.6
1.8 ± 0.18	0.07±0.02	0.17±0.04	0.38±0.06	0.34±0.06	4.5±0.7

2002, Huthoff et al. 2007). For natural vegetation usually higher values for C_D are reported. Van Velzen et al. (2003) propose a value of $C_D = 1.5$ or $C_D = 1.8$ for natural vegetation types, while DVWK (1991) recommends $C_D = 1.5$. The latter value is also adopted by Järvelä (2004).

Table 5.2 shows the predicted flow velocities for the resistance layer, the surface layer and the entire flow depth using three different values for the drag coefficient. To calculate the uncertainty in predicted flow velocities we assumed a 20% standard deviation in the parameters from Table 5.1 and a 10% standard deviation in C_D. The corresponding probability densities for predicted flow velocities are illustrated in Figure 5.6.

Comparing the measured values for the surface velocity $U_s \simeq 0.38$ m/s in Figure 5.5 with the predicted values in Table 5.2, shows that the vegetation resistance model proposed by Huthoff et al. (2007) gives good results when a drag coefficient close to $C_D = 1.8$ is adopted for the herbaceous vegetation in the studied Green River. This value for the drag coefficient is consistent with values reported in literature for natural vegetation.

5.2.4 Discussion

Measured flow velocities in the Green Channel were only obtained in the surface layer, as no reliable values could be extracted from the flow layer that is penetrated by the vegetation (see Figure 5.5). Therefore, we have no reference measurements to evaluate the predicted depth-averaged flow velocities of the resistance layer U_r or the total flow depth U_T (given in Table 5.2). However, using the predicted values for U_T, a Manning resistance parameter n can be calculated, which can subsequently be compared to values cited in literature for grassed channels. Manning's equation is given as (Manning 1889):

$$U_T = \frac{R^{2/3}}{n}\sqrt{i}, \tag{5.6}$$

which has the property that the resistance coefficient n is practically constant for hydraulically rough turbulent flow over a fixed bed (e.g. Yen 2002). Inserting the measured flow depth (at Location 3, see Figure 5.5) and the predicted values for U_T yields Manning resistance coefficients as stated in Table 5.2. The resistance parameter $n = 0.045 \pm 0.007$ $m^{-1/3}$s, obtained with U_T that includes

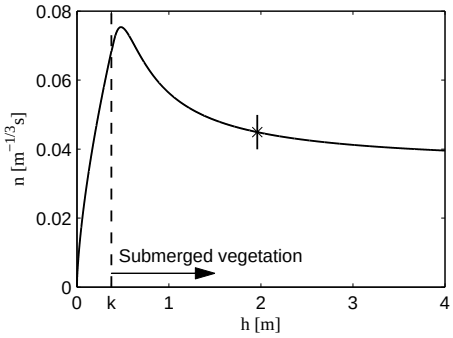

Figure 5.7: Depth-dependency of the Manning's resistance coefficient n as predicted by the model equations (5.1)-(5.5), using a drag coefficient $C_D = 1.8$. The '$\times$' symbol corresponds to the average conditions as found at Location 3 in the Green River ($\pm\sigma$ error bounds shown).

a drag coefficient $C_D \simeq 1.8$, appears to be the most realistic value because the associated surface layer velocity U_s agrees well with the measured value. Also, the value $n = 0.045 \pm 0.007$ is consistent with the Manning value cited in literature for grassed floodplains. For floodplain vegetation classification *high grass* Chow (1959) states a general value of $n = 0.035$, with a lower boundary of $n = 0.030$ and an upper boundary of $n = 0.050$ $\mathrm{m}^{-1/3}\mathrm{s}$. For flow over vegetation, n does not remain constant because a drag-dominated layer makes up a considerable part of the water column, and because of vegetation streamlining effects. Therefore, by describing vegetative hydraulic resistance in terms of a Manning's n value, a resistance-dependency on flow depth reflects departure from the conceptual model of flow over a solid rough boundary. Figure 5.7 shows how the model equations (5.1)-(5.5) together with Manning's law, equation (5.6), lead to a depth-dependent Manning coefficient. Considering flow along a particular vertical, the hydraulic radius R in equation (5.6) is replaced by the flow depth h.

In Figure 5.7 it can be seen that, taken the uncertainty bounds in the determined Manning coefficient, no significant changes in n are expected in the Green River for deeper flows than for the situation that was sampled. The study of Wilson and Horritt (2002) on the flow resistance of grass also shows that the Manning coefficient becomes practically constant if the depth of flow is several times larger than the vegetation height (if relative submergence $h/k > 3$). On the other hand, shallower flows are expected to yield considerable higher resistance values for n. Unfortunately, in the current experiment only flow measurements were collected for one discharge event. Therefore, we are unable to further analyze the dependency of n on flow depth.

We conclude that the model proposed in Chapter 4 gives a good representation of the measured flow velocity in the Green River when adopting a drag coefficient typical for natural vegetation. Also, at the considered flow depth (rel-

Figure 5.8: The research vessel while measuring flow velocities in the Dutch Upper Rhine in November 1998 (left). The picture on the right shows the ADCP as it is attached to the side of the ship (pictures by *Aqua Vision*).

ative submergence $h/k \simeq 5.3$) the model equations yield a Manning resistance value that agrees with the value cited in literature for *high grass* in floodplains (Chow 1959). It seems reasonable to adopt the determined value for the Manning coefficient $n = 0.045 \pm 0.007$ m$^{-1/3}$, also for larger depths of flow.

5.3 Vessel-borne flow measurements in the Dutch Upper Rhine

5.3.1 The study location

In 1998 a high-discharge event occurred on the Rhine with a recorded maximum discharge magnitude of 9413 m^3/s at station Lobith on November 4th (`www.waterbase.nl`). The station at Lobith marks the location where the Rhine enters the Netherlands, flowing in from Germany. During the November 1998 high-discharge event, vessel-borne ADCP measurements were carried out by the Dutch consultancy company *Aqua Vision* along different transects in the Rhine branches near the Dutch-German border (Eij 2004). See Figure 5.8 for one of the used research vessels. In the previous section, where measurements from a fixed point in a Green River were presented, it was shown that ADCP measurements produce relatively large uncertainty bounds for mean velocity magnitudes. Therefore, to be able to isolate the hydraulic response due to vegetation, it is essential to consider study locations where as little as possible unknown disturbances affect the flow. For that reason we only consider the flow measurements collected in the fairly homogeneous floodplain of the Dutch Upper Rhine.

Figures 5.9 and 5.10 show aerial pictures of the Dutch Upper Rhine section near river km 863.9. In the shown area, the river axis marks the German-Dutch border, where the southern bank is German territory and the northern bank belongs to the Netherlands. Water flows from the east to the west, which in Figure 5.9 is from the lower right to the upper left. Just downstream of the German village of Bimmen (see Figure 5.9) both banks along the river are

Figure 5.9: An aerial picture of the study area (April 2006, Google Earth). The white line shows the representative transect with a length of approximately 800 m, along which depth and velocity measurements were collected.

Dutch territory. The floodplain on the southern bank is clearly visible in both pictures, as is the embankment that separates it from the main channel. Groynes are present on the northern bank and further upstream also on the southern bank. The floodplain is covered with grassland and near the bank reed bushes are found (classification from `www.ecotopenkaarten.nl`). The white line in the two figures depicts the trajectory along which the flow data was collected during the November 1998 campaign.

5.3.2 Methodology & Results

Flow data was collected in the Dutch Upper Rhine at river km 863.9 on four consecutive days from the 3rd to the 6th of November and then again from the 9th to the 11th of November. The discharge peak occurred at November 4th and decreased quite rapidly after this day. On the 9th of November the water level had dropped to a level that flow measurements were no longer possible in the floodplain. The final three measuring days were thus restricted to flows in the main channel. On each day, flow measurements were repeated several times by traversing the river cross-section back and forth. Figure 5.11 shows the total set of trajectories that were covered by the research vessel during the entire November 1998 campaign. Even though the different trajectories do not overlap perfectly, a fairly confined cross-sectional strip of the channel was sampled for flow data. In Figure 5.11 an *equivalent transect* is shown (dotted line) which is determined as the best straight-line fit to all locations where flow measurements were collected. To be able to combine measurements collected in subsequent sampling runs, all measurements are mapped onto the equivalent

Figure 5.10: Aerial picture of the study area taken in the summer of 2003. In the background the bifurcation of the Rhine at *Pannerdensche Kop* is clearly visible (Picture by Bert Broekhoven, courtesy of RWS RIZA).

transect by perpendicular translation (i.e. shift over shortest distance from sampling location to equivalent transect). All further analysis thus relates to a representative channel cross-section defined by the equivalent transect.

In Figure 5.12 an example is shown of one of the sampling runs, with collected data shown along the equivalent transect. With the used ADCP, flow velocities were measured below the research vessel at depths 25 cm apart with the shallowest measuring depth 1.32 m below the water surface. Lateral sampling separations were on average 4 m, depending on the speed and the path of the research ship. On average, a flow region of 60 cm above the channel bed could not be reliably sampled for flow velocities, due to presence of obstructing objects (vegetation) or debris.

Figure 5.12 clearly shows that lower flow velocities occur in the shallower regions and higher flow velocities in deeper parts of the cross-section. However, a striking feature is that almost straight above the *deepest* part of the channel cross-section a local minimum in flow velocities is found (near the lateral coordinate of 380 m). This feature is also observed in the remaining measurement runs (not shown here). The overview pictures of the study area in Figures 5.9 and 5.10 may provide an explanation for this observation. Just upstream of the channel cross-section a small channel merges with the Rhine on its southern bank. The local dip in flow velocities may be due to enhanced mixing patterns in the wake of the confluence zone and to a vortex street originating behind the upstream groyne.

The ADCP measurements shown in Figure 5.12 were performed in a so-called *bottom track mode*. This means that, even though the ADCP may be moving (because being attached to a moving station), measured flow velocities

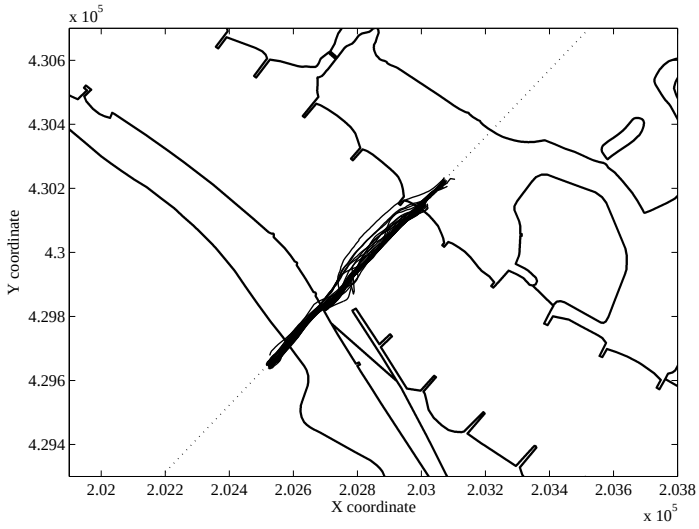

Figure 5.11: All trajectories in the Rhine at location river km 863.9 where flow measurements were performed in November 1998. The dotted line depicts the equivalent transect along which all data is mapped for analysis.

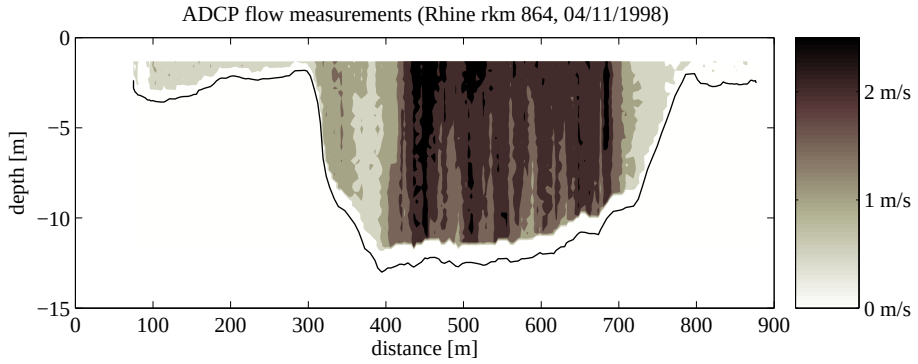

Figure 5.12: ADCP velocity measurements for one of the measurement runs shown in Figure 5.11, plotted along the representative transect.

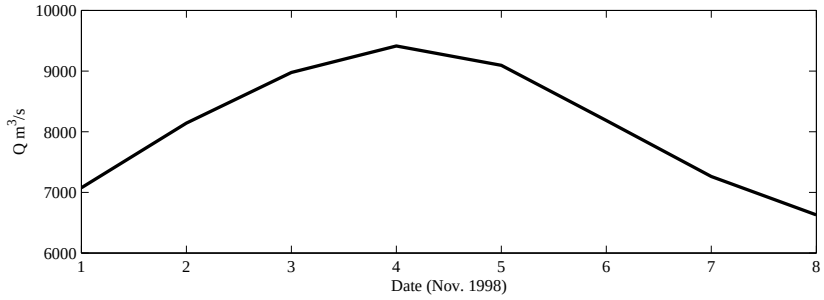

Figure 5.13: Recorded discharge time series in the Dutch Upper Rhine at station Lobith for the discharge peak in November 1998.

are given with respect to a detected fixed bed. In principle, this methodology yields flow velocities relative to channel bed. However, during high discharges a layer of sediment and mud may be dragged along with the flow. In such cases the ADCP interprets the moving bottom layer as being a fixed bed, and thus yields a systematic underestimation of the measured flow velocities (systematic errors in flow velocity may be a few dm/s, Eij 2004). The measurements used here are corrected for this effect by comparison with independent GPS data of the research vessel. Details of this procedure are described in the experimental report by *Aqua Vision* (Eij 2004).

Averaging procedures of measured ADCP data

To be able to compare the measured flow velocities in the vegetated flood plains to model predictions of vegetation resistance, we depth-averaged the measured flow velocities and grouped all data collected on the same day (which were in fact collected within a time frame of a few hours), assuming that within this time-frame no significant hydraulic changes have occurred in the system (for reference, see hydrograph in Figure 5.13). Figure 5.14 shows the resulting set of depth and depth-averaged velocity measurements collected on the 4th of November 1998. Velocity depth-averaging is performed by taking the mean of all velocities measured in the water column, within width-intervals of 10 m. Also shown are the 16 and 84 percentile error bounds around the mean value. This method does not take the unknown velocities near the surface and the bed channel into account (see measurement gaps in Figure 5.12). For the deep flow section in the river's main channel this procedure yields quite accurate estimates of the depth-averaged flow velocities, because the unsampled part of the water column is relatively small. However, in the floodplains typically half of the water column remains undetectable for flow velocity measurements. Therefore, the determined average flow velocities do not necessarily give a realistic representation of flow over floodplain vegetation. In the next section a correction procedure is described to account for floodplain flow velocities in the unsampled parts of the water column.

The bottom graph in Figure 5.14 shows the function $h^{2/3}/U$ set out against the lateral coordinate. Looking at equation (5.6), this value represents a measure for flow resistance, namely $n/\sqrt{i}$. Therefore, if we assume that the downstream slope i is equal across the equivalent transect, then the bottom graph in Figure 5.14 reflects a relative hydraulic resistance across the channel. From Figure 5.14 it thus appears as if the hydraulic resistance of the main channel is nearly equal to that of the floodplain ($n/\sqrt{i} \simeq 3.5$).

By including the slope in a parameter to reflect hydraulic resistance ($n/\sqrt{i} = h^{2/3}/U$), we avoid the uncertainties due to slope determination when analyzing temporal or lateral variability of the hydraulic resistance. On the other hand, it is implicitly assumed that at all lateral locations, and at all times, the (surface) slope remains the same. Since flow measurements were in fact collected during non-stationary conditions (i.e. during passing of a flood wave), the condition of constant surface slope is, strictly speaking, not met. However, in the Appendix it is shown that a constant surface slope may be assumed without significant loss of accuracy.

Next, the hydraulic characteristics (depth, flow velocity, relative equivalent flow resistance) are spatially-averaged over a chosen lateral distance. In Figure 5.14 four vertical bars are drawn that mark the regions over which the hydraulic conditions are averaged. The chosen regions are all 50 m wide. Two regions in the floodplain are selected; 'fp1' corresponding to a region of lower bed level than region 'fp2'. Two regions to represent flow in the main channel are 'mc1' and 'mc2'. Figure 5.15 shows how the averaged hydraulic conditions in these four regions change during the measurement period. Note again that conditions in the floodplain were only measured during four days around the discharge peak on the Rhine. At lower discharges it was no longer possible to enter the floodplain for flow velocity sampling.

In Figure 5.15 the change in flow depths in the floodplain and in the main channel clearly reflects passing of the peak of the flood wave. Corresponding flow velocities also show a maximum during the flood wave peak and lower velocities at shallower flow depths. The relative equivalent hydraulic resistance (bottom graph) exhibits quite large uncertainties for the floodplain. Nevertheless, it is clear that floodplain regions 'fp1' and 'fp2' have significant different hydraulic resistance characteristics. The hydraulic resistance in the main channel can be quite accurately determined because of the small relative errors in flow velocities and flow depths. After the flood wave has passed, the relative hydraulic resistance in the main channel seems to have increased. This observation is in line with results from studies by Wilbers (2004), who shows that high-discharge events cause large bed forms on the channel bed, which increases the hydraulic resistance.

Correction of depth-averaged flow velocities for incomplete sampling

The ADCP only samples flow velocities in a confined part of the water column, generally leaving out the top 1.3 m and the bottom 0.6 m. Therefore, the flow velocities in Figures 5.14 and 5.15 have a bias due to this shortcoming. In

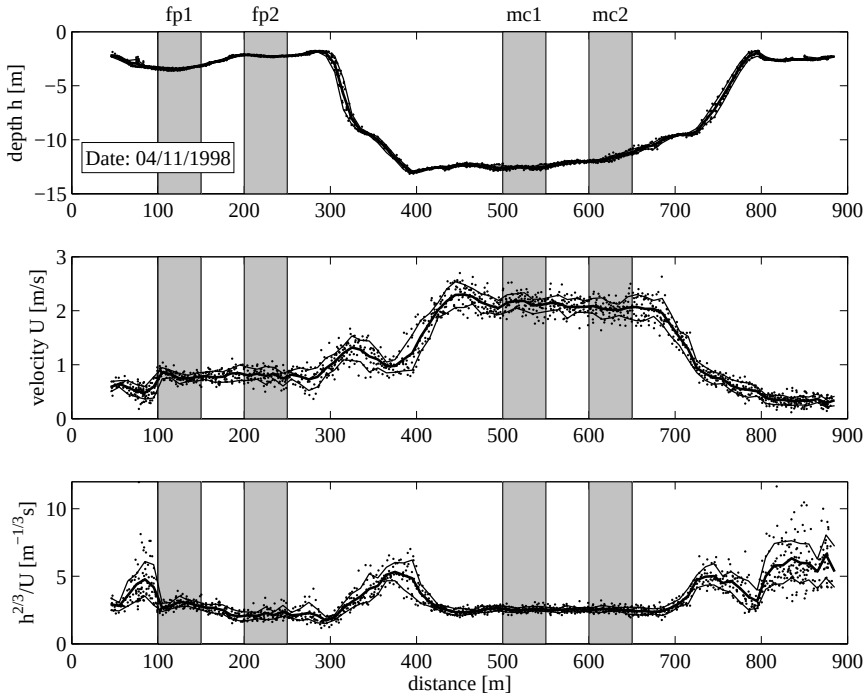

Figure 5.14: Measured depths (top graph) and depth-averaged flow velocities (middle graph) along the representative transect. The bottom graph depicts the profile of the equivalent hydraulic resistance. Also shown are the mean values, surrounded by 16 and 84 percentile boundaries (determined from all measurements within parallel bins of width 10 m). The 4 vertical bars show which regions are used for lateral averaging of measured values.

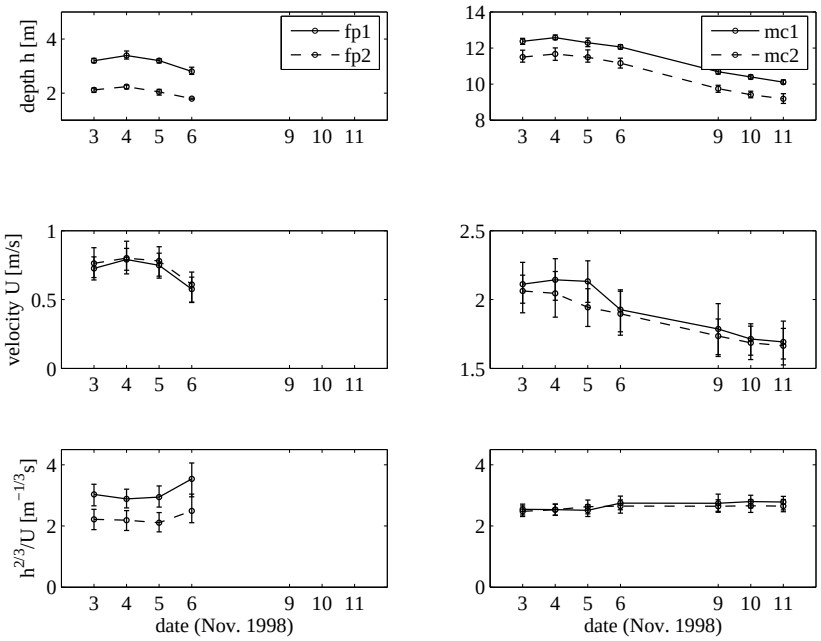

Figure 5.15: Time-dependency of the hydraulic characteristics within the chosen regions in the floodplain ('fp1' and 'fp2') and the main channel ('mc1' and 'mc2', see figure 5.14). Also shown are $\pm\sigma$ error bounds.

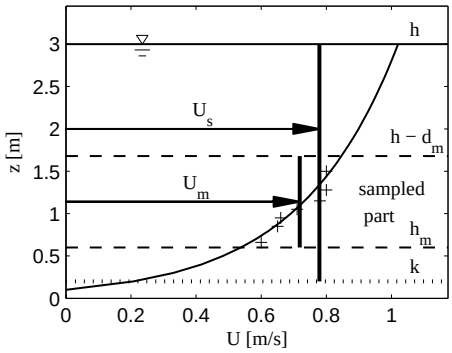

Figure 5.16: Sketch to illustrate the correction procedure of measured flow velocities by the ADCP, assuming a logarithmic velocity profile in the surface layer. The measured depth-averaged velocity U_m, corresponding to part of the surface layer ($h_m < z < h - d_m$), is corrected to represent the flow velocity in the entire surface layer U_s (for $k < z < h$).

deep flow sections, as in the main channel where the flow depth easily exceeds 10 m, the unsampled part of the water column is relatively small. Therefore, reasonably reliable values of depth-averaged flow velocities are obtained when averaging the measured velocity magnitudes. However, the absence of measured flow velocities near the bed and near the water surface poses a problem for the analysis of relatively shallow floodplain flows. In order to evaluate whether idealized vegetation resistance models may be used to describe flow in floodplains, we therefore make some assumptions to achieve more realistic values of 'measured' depth-averaged flow velocities:

- We assume that the flow field *above* the vegetation follows a vertical logarithmic velocity profile that corresponds to a (Nikuradse) roughness height of $k_N = 0.1$ m (a reasonable assumption for grassed bed cover according to Van Velzen et al. 2003).
- The assumed profile is made to fit the measured average flow velocity U_m for the sampled flow depth ($h_m < z < h - d_m$). Where h_m and d_m represent the height above the channel bed and the depth below the water surface where no flow measurements could be collected, respectively.
- From the fitted profile, the average velocity in the surface layer U_s is determined, assuming a resistance layer height of $k = 0.06$ m (representative value for floodplain grass in winter conditions according to Van Velzen et al. 2003).

Figure 5.16 illustrates the procedure for correcting flow velocities in the surface layer. Effectively, the correction-procedure described above and in Figure 5.16 corresponds to multiplying the measured depth-averaged flow velocity U_m by a factor Φ:

$$U_s = \Phi U_m \tag{5.7}$$

where

$$\Phi = \frac{h - d_m - h_m}{h - k} \frac{\int_k^h \ln \frac{z}{k_N} \mathrm{d}z}{\int_{h_m}^{h-d_m} \ln \frac{z}{k_N} \mathrm{d}z}. \tag{5.8}$$

The first measurement point by the ADCP is 1.32 m below the water surface while the measurement point closest to the bed is approximately at 0.6 m above bed level. Measurement depths were 25 cm apart, therefore the equivalent measuring range of the ADCP is confined by a height from the bed level $h_m = 0.6 - \frac{0.25}{2}$ m and a depth below the water surface $d_m = 1.32 - \frac{0.25}{2}$ m. Figure 5.17 (top graph) shows the corrected velocities when multiplying the measured average flow velocities by the factor Φ from equation 5.8. As expected, the correction is largest for flow measurements in shallow regions.

5.3.3 Comparison to model predictions

Having determined representative values for floodplain flow velocities in the surface layer (U_s), we evaluate their correspondence to the flow model proposed

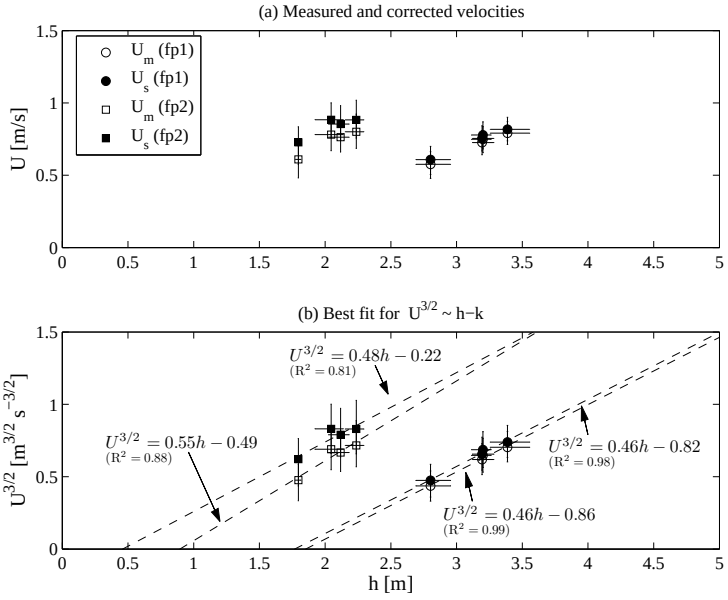

Figure 5.17: Top graph: Relation between the depth-averaged velocity U and the depth of flow h for locations 'fp1' and 'fp2' in the floodplain (filled symbols depict corrected flow velocities). Bottom graph: best fit straight lines when plotting flow depths against velocities to a power 3/2.

Table 5.3: Equivalent vegetation heights k determined by matching flow measurements with the vegetation resistance model given by equation (5.10).

Location	U	A	B	$k = \mathrm{B/A}$	R^2
	[m/s]	$[\mathrm{m}^{3/2}\mathrm{s}^{-3/2}]$	$[\mathrm{m}^{5/2}\mathrm{s}^{-3/2}]$	[m]	[–]
fp1	U_m	0.46	0.86	1.9	0.99
fp1	U_s	0.46	0.82	1.8	0.98
fp2	U_m	0.55	0.49	0.9	0.88
fp2	U_s	0.48	0.22	0.4	0.81

in Chapter 4. If the depth of the surface layer $(h-k)$ is more than three times the vegetation height, then the flow velocity in the surface layer is described by a simple scaling law (see also section 5.2.3):

$$U_s = U_{r0}\left(\frac{h-k}{s}\right)^{2/3}. \tag{5.9}$$

This expression can be rearranged to yield:

$$U_s^{3/2} = \mathrm{A}h - \mathrm{B}, \qquad \text{where } \mathrm{A} = \frac{U_{r0}^{3/2}}{s} \text{ and } \mathrm{B} = \mathrm{A}k. \tag{5.10}$$

The bottom graph in Figure 5.17 shows the measured and corrected velocity values $U_m^{3/2}$ and $U_s^{3/2}$ set out against the depth of flow h. For each data set also a best fit straight line is shown. Following equation (5.10), the fraction B/A from the best fit straight lines in Figure 5.17 yield an equivalent vegetation height k, which reflects the height of the drag dominated flow layer. Table 5.3 gives an overview of these values.

The results given in Table 5.3 show that for location 'fp2' an equivalent height for the drag dominated resistance layer is found of $k = 0.4$ m, if using corrected flow velocities for U_s. A vegetation height of 0.4 m is higher than expected for the floodplain under consideration, but is still acceptable considering the few measurement points used for fitting in Figure 5.17. For location 'fp1' an equivalent vegetation height of 1.8 m is found, which is unrealistically high, taken that vegetation characteristics are fairly uniform in the floodplain.

5.3.4 Discussion

Varying hydraulic resistance in a homogeneously vegetated floodplain?

Previous sections have shown that two investigated locations in the floodplain had quite different hydraulic properties, despite the apparent homogeneity of floodplain vegetation cover. A closer inspection of the geometry of the considered floodplain shows that the flow depth at location 'fp1' is about 1.3 m deeper than at location 'fp2' (Figure 5.15), and that in the deeper region water does not flow freely over the entire depth. Figure 5.18 shows the floodplain shortly after a flooding event in 2007, depicting a clearly confined pool that corresponds to location 'fp1'. Therefore, the larger depth in the floodplain is a local topographical effect, which also impacts the local hydraulic resistance.

Focusing only on the shallower part of the floodplain ('fp2'), which is not affected by local topographical effects, an estimate of vegetation resistance can be made. Adopting a vegetation spacing of $s = 1$ cm for grassed floodplains (see Van Velzen et al. 2003) yields an approximate characteristic velocity of $U_{r0} = 0.03$ m/s. If a channel slope of $i = 10^{-4}$ is assumed, which is a representative value for the considered Rhine section (e.g. Julien et al. 2002), Figure 5.19 shows the predicted trend of Manning values, using model equations (5.1)-(5.3). It can be seen that for shallow flows the Manning value can be as high as

Figure 5.18: A picture of the studied floodplain along the river Rhine. A clearly confined pool can be discerned in the deeper part of the floodplain (Picture by Fredrik Huthoff, 14 March 2007).

$n = 0.15$ depending on the vegetation height, while for flow depths $h > 1.5$ m a Manning value in the range $n = 0.02 - 0.025$ is predicted. This value is slightly lower than the value stated in Chow (1959), who gives $n = 0.030 \pm 0.005$ for short grass types in floodplains.

Consequences for modeling of floodplain flows.

It was found that local variations of hydraulic properties could be attributed to topographic variations in the floodplain. Depth-averaged flow models based on the *De Saint-Venant equations* and mass-continuity such as 1D SOBEK (WL|Delft Hydraulics 1993) or 2D WAQUA (MX.Systems 2005, WL|Delft Hydraulics 2005) reproduce these effects realistically, as long as the presence of the important topographical variations are captured by the spatial resolution of the model (see also Nicholas and Mitchell 2003). However, in flow models that compute the local equilibrium velocity and depth (e.g. 1D K-WERT, Busch et al. 1999) the bed resistance in a local bed level depression would yield overestimated flow velocities. To correct for this effect it is recommended to explicitly distinguish between discharge-carrying regions and water storage regions *within* separate river cross-sections. A simple method to achieve this in the flow model could be by raising the bed level of local depressions to the bed level of the surrounding higher regions.

It was shown that the vegetation resistance model proposed by Huthoff et al. (2007) may account for the hydraulic resistance due to vegetation in the shallower part of the floodplain. The dynamic behavior predicted by the vegetation resistance model could not be clearly identified, due to the weak dependence on flow depth at relatively large depths. It is expected that Manning's n of the

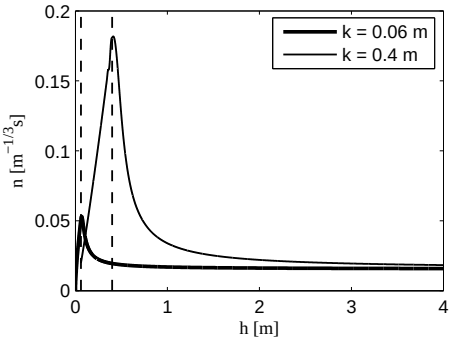

Figure 5.19: The depth-dependency of Manning's n according to model equations (5.1)-(5.3) adopting (i) a characteristic velocity of $U_{r0} = 0.03$ m/s in the vegetation layer, (ii) a vegetation height $k = 0.06$ or $k = 0.4$ m, (iii) a vegetation spacing $s = 1$ cm and (iv) channel slope $i = 10^{-4}$.

floodplains only changes significantly at relatively shallow flows in the floodplain (if $h \simeq k$), such measurements were not available. In effect, at large relative depths, a constant Manning coefficient may produce reliable flow predictions. However, in situations where vegetation is relatively tall (compared to flow depth) and floodplains are wide, a constant Manning resistance coefficient may significantly underestimate vegetation resistance.

Uncertainties of measured flow velocities.

An obvious shortcoming of the current study is the lack of accurate flow measurements in the *entire* water column, and the inability to measure flow velocities of shallow floodplain flows. Because of incomplete data sampling we were forced to make assumptions of the general shape of the velocity field, in order to obtain representative depth-averaged flow velocities. Due to the submergence of the research vessel that was used for data collecting, the top 1.32 m of the water column remained unsampled. In the float tracking method described in Straatsma (2007) the transducer depth and the ADCP blanking distance limit the sampling range, giving an undetectable part of the water column of only 46 cm below the water surface. Therefore, float tracking data would be a valuable supplement to vessel borne measurements. Vessel-borne measurements enable data-collecting along a river's cross-section, while float tracking enables data sampling over a larger part of the water column. In addition, float tracking allows for direct measurement of the streamwise water surface slope.

5.4 Conclusions

In the case studies considered here, the submerged vegetation included predominantly grass species, having average stem heights that are easily an order of magnitude smaller than the flow depths. The vegetative resistance model

proposed in Chapter 4 is consistent with found flow measurements over such vegetation. However, because the flow in the vegetation layer was only of minor importance to the overall flow field, the flow resistance can also be reasonably well described using a constant Manning resistance parameter n. The model predicts increased hydraulic resistance (in terms of Manning's n) for relatively shallow floodplain flows, in accordance with earlier laboratory investigations. However, due to lack of data, the current study could not confirm this trend.

Also, it was shown that topographical variations of the bed level may have a major impact on local flow velocities. In flow models with a resolution that captures these topographical variations, the effect on the flow field follows directly from the boundary conditions. In crude spatially-averaged methods either the equivalent roughness or the cross-sectional flow area should be adjusted to account for such effects.

Acknowledgments

We gratefully thank Aqua Vision for letting us use their data and Anne Wijbenga (HKV Consultants) and Andries Paarlberg (University of Twente) for their valuable comments. We appreciate the help from Ivo Thonon and Chris Roosendaal (both from Utrecht University) who assisted during the measurement campaign in Driel, and the help from Abe Klaas De Jong (HKV Consultants) and Blanca Pérez Lapeña (University of Twente), who assisted in producing the figures.

5.5 Appendix: Assuming a constant water surface slope in unsteady flow conditions

At a fixed location, water level changes due to passing of a flood wave can be represented as:

$$\frac{\mathrm{d}h}{\mathrm{d}t} = \frac{\partial h}{\partial x}\frac{\partial x}{\partial t}, \tag{5.11}$$

where $i_w = \partial h/\partial x$ represents the local water surface slope, and $U_w = \partial x/\partial t$ the propagation speed of the flood wave. Compared to the bed level, the surface slope thus changes as

$$i_w = \frac{1}{U_w}\frac{\mathrm{d}h}{\mathrm{d}t}. \tag{5.12}$$

For the flood event of 1998 we can estimate the rate of change of the water level $\frac{\mathrm{d}h}{\mathrm{d}t}$. Before and after the peak of the flood wave, the water level changes nearly two meters in five days[‡], therefore $\frac{\mathrm{d}h}{\mathrm{d}t} \simeq 5 \cdot 10^{-6}$ m/s. The flow velocity in the cross-section is, on average, about 1.5 m/s (see Figure 5.14). Inserting these values into equation (5.12) yields for a water surface slope (relative to the bed slope) $i_w \simeq 3.3 \cdot 10^{-6}$. The typical bed slope in the considered part of the Dutch Rhine is $i_b \simeq 10^{-4}$. Therefore, in the studied case, water level slope variations due to passing of the flood wave are only a fraction of the bed level

[‡] `www.waterbase.nl`

slope: $i_w \simeq (0.03)i_b$. Hence, it is reasonable to treat water level slopes as a constant when evaluating equivalent hydraulic resistance.

Chapter 6

Practical applicability of vegetation resistance in river flow models

In the previous Chapter it was shown that it is difficult to validate a model for hydraulic resistance of vegetation by investigating field data. This inability is mainly due to lack of accurate flow data collected in the field. To still be able to develop accurate representations of flows in natural rivers, it is important that separate constituents of the overall flow model are reliable. Therefore, in this Chapter, the vegetation resistance methods proposed in Chapters 3 and 4 are compared to a wide range of laboratory data, and also to two other existing vegetation resistance methods. Consequently, an evaluation is made of which method is most accurate, best understood, and which can be used for the widest range of practical application. Also, recommendations are given for further laboratory experiments that may improve practical applicability, or identify unrealistic behavior of existing vegetation resistance models.

6.1 Performance of vegetation resistance methods

6.1.1 Models of hydraulic resistance of vegetation

As mentioned earlier in Chapter 2, several descriptions exist to describe spatially-averaged flow over vegetation; among them are empirical relations and relations that are more physics-based. Here we consider four approaches that have equal input parameters, similar levels of complexity but different theoretical backgrounds. All these methods have in common that they include a drag force component that reflects flow in the resistance layer, and a component attributed to shear flow in the surface layer. The methods that are evaluated are those treated in Chapter 3 (Klopstra et al. 1997) and Chapter 4 (Huthoff et al. 2007), and two methods that have not been considered in detail in this thesis before, i.e. those proposed by Van Velzen et al. (2003) and Baptist et al. (2007).

The method proposed by Van Velzen et al. (2003)

The first additional vegetation resistance method is proposed by Van Velzen et al. (2003), who assumed a flow velocity in the resistance layer that is unaffected by surface layer flow

$$U_r = U_{r0} \qquad \left(= \sqrt{2bgi}\right). \tag{6.1}$$

Flow in the surface layer is described by a logarithmic term, superimposed on the velocity in the resistance layer

$$U_s = U_{r0} + 18\sqrt{(h-k)i}\log\frac{12(h-k)}{k_N}, \tag{6.2}$$

where the roughness height is given by an empirical function, obtained from regression analysis using the data of Meijer (1998b)

$$k_N = 1.6k^{0.7}. \tag{6.3}$$

Taken together, the descriptions for surface layer and resistance layer yield for the total depth of flow

$$U_T = U_{r0} + 18(h-k)^{3/2}\frac{\sqrt{i}}{h}\log\frac{12(h-k)}{k_N}. \tag{6.4}$$

The method proposed by Baptist et al. (2007)

Using a genetic algorithm, Baptist et al. (2007) derived a simple analytical flow description that fits a detailed numerical model. The method enforces rejection of unrealistic dependencies by taking into account the dimensions of relevant parameters. The procedure yielded a depth-averaged flow velocity

$$U_s = U_{r0}\sqrt{\frac{h}{k}} + 2\sqrt{ghi}\ln\frac{h}{k}. \tag{6.5}$$

This outcome is an approximation to the detailed numerical model proposed by Uittenbogaard (2003), which includes vegetation drag in the resistance layer and adopts a k$-\varepsilon$ turbulence model to account for vertical momentum transfer. The result in equation (6.5) resembles that of a two-layer approach, having a contribution due to flow in the resistance layer (the drag-dominated term, including U_{r0}) and in the surface layer (the logarithmic term).

6.1.2 Comparison of vegetation resistance methods to laboratory data

The performance of the selected methods is evaluated by comparison to data from a wide range of laboratory flume experiments that are taken from literature. Table 6.1 gives an overview of the characteristics of the used data (see Baptist 2005 for a more detailed description). The experiments were conducted with various vegetation heights k and various separations between individual vegetation elements s, and included both flexible (f) and rigid (r) vegetation. The separation between vegetation s follows from the surface density m and stem diameter D of the vegetation (i.e. $s = 1/\sqrt{m} - D$). Note the diversity in reported drag coefficients C_D, which in itself is a key issue when describing the hydraulic resistance of flow through vegetation (e.g. Nepf 1999, Järvelä 2004). Furthermore, it is important to note that none of the data included in Table

Table 6.1: Characteristics of flume experiments with submerged vegetation (f: flexible vegetation, r: rigid vegetation).

Reference	Nr. of exps.	D mm	m m^{-2}	s cm	k cm	C_D -	$s/C_D D$ -
Kouwen et al. (1969)	27 (f)	5	5000	1.4	6-10	3	0.9
Ree and Crow (1977)	30 (f)	5	1076-1464	2.6-3	20-30	1	5.2-6.1
Murota et al. (1984)	8 (f)	0.24	4000	1.6	4.8-5.8	2.75	24
Tsujimoto and Kitamura (1990)	8 (r)	1.5	2500	2	4.6	1.46	9.1
Tsujimoto et al. (1993)	12 (f)	0.62	10000	1	6.1-6.5	2	8.1
Ikeda and Kanazawa (1996)	7 (f)	0.24	20000	0.7	4-4.5	1	29.5
López and García (1997)	6 (r)	6.4	42-388	5.1- 15.4	7-17	1.13	7.0-21.3
Meijer (1998a)	7 (f)	5.7	254	6.3	155-164	1.805	6.1
López and García (2001)	12 (r)	6.4	42-384	5.1-15.4	12	1.13	7.1-21.3
Järvelä (2003)	12 (f)	3	512-12000	0.9-4.4	16-30	1	3-14.7

6.1 were previously used to calibrate any of the four investigated vegetation resistance models.

The performance of each of the methods is quantified by comparing predicted depth-averaged velocities with measured values. The relative error is defined as

$$\text{error} = \frac{U_p - U_m}{U_m}, \tag{6.6}$$

where U_p is the predicted and U_m the measured depth-averaged velocity. In Figure 6.1 the performance of the different methods is shown. The graphs also state the corresponding mean error μ and error standard deviations σ.

Figure 6.1 shows that the performance of the different methods is quite similar. All methods yield an error standard deviation σ of around 30%. In relation to the considered experiments, the mean error of Huthoff's method is smallest with 3%, while the other methods yield a mean error of around 10%. Also, the methods by Klopstra and Huthoff appear to become less reliable for relatively sparse vegetation. This may be due to neglect of bed roughness, which becomes important in such cases. Both equations can easily be modified to include bed resistance effects (see Chapter 4). Naturally, such a modification requires additional knowledge of bed roughness characteristics. The methods by Baptist and Van Velzen already perform quite well for sparse vegetation densities, incorporation of bed roughness only introduces larger discrepancies (not shown here).

Based on the model-performance analysis in Figure 6.1, it is not possible to identify one model that is most reliable over the investigated range of vegetation and flow characteristics, nor is it possible to discard any of the methods

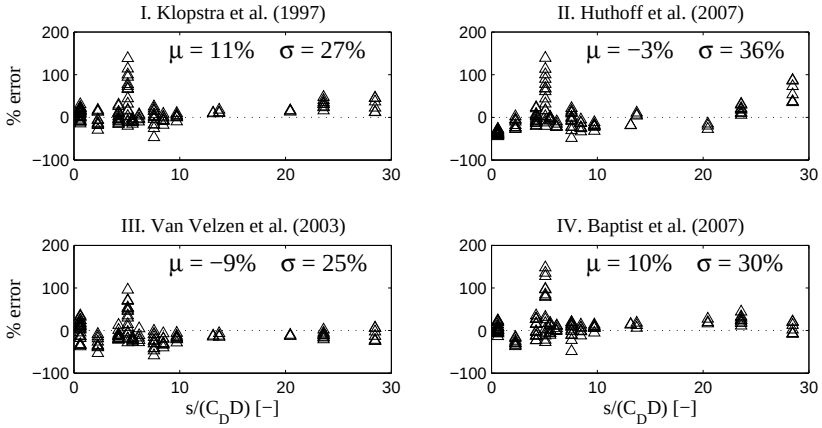

Figure 6.1: Comparison of model performance using equation (6.6) for different methods to describe vegetation resistance. The horizontal axis shows relative separations between individual vegetation elements ($s/C_D D$); from dense (left) to sparse vegetation coverage (right). Also shown are mean error (μ) and error standard deviations (σ) of predicted flow velocities

for further use. Next, fundamental assumptions in the derivation of the different methods are closer examined in relation to turbulence characteristics of turbulent flows.

6.2 Simplified descriptions of turbulent flows affected by vegetation

The four methods considered in section 6.1 all have in common that flow through the vegetation layer is described by a drag force, and that for flow in the surface layer energy transfer due to turbulent mixing is assumed. The latter condition is explicitly followed in the method by Huthoff et al. (2007), who used Kolmogorov's phenomenological theory to estimate the depth-averaged surface layer velocity. In the method by Van Velzen et al. (2003) and Klopstra et al. (1997) fully turbulent (rough) flow is assumed, as this forms the theoretical basis for the logarithmic velocity profile. The model proposed by Baptist et al. (2007) is an approximation to the detailed numerical model by Uittenbogaard (2003), which, in principle, is not restricted to fully turbulent flow (as it also includes viscous effects). However, as viscosity does not appear in Baptist's model, it may be assumed to only represents the fully turbulent state of the model by Uittenbogaard (2003).

Therefore, the four vegetation resistance models are based on similar fundamental assumptions, perform similarly when compared to a wide range of flow experiments, but may produce quite different outcomes for particular flow and vegetation conditions (as evident in Figure 6.1). To understand these differ-

ences, an analysis is made of more subtle assumptions in vegetation resistance methods, in comparison to the characteristics that can be observed in real flows.

6.2.1 Velocity and turbulence profiles

In this section, general characteristics of velocity and turbulence profiles of flow over vegetation are identified and compared to properties of the simplified vegetation resistance methods.

Common properties between flows with rigid cylinders and natural reed

Figure 6.2 shows the velocity and turbulence profiles of two flow experiments from Meijer (1998a) and Meijer (1998b), one referring to flow over rigid cylinders (Figure 6.2a, i.e. left column) and one referring to flow over natural reed (Figure 6.2b, right column). In total 48 experiments were carried out with rigid cylinders and 10 with reed. Even though only results from two experiments are shown, the profiles in Figure 6.2 are representative of the characteristics of the remaining experiments. In both experiments shown, it can be seen that the layer that is occupied by cylinders or reed is characterized by a nearly vertical velocity profile, with only the upper part displaying a vertical shear. Therefore, in the resistance layer hydraulic resistance is dominated by form drag, but may also be significantly affected by shear due to surface layer flow. The overall magnitude of form drag is associated with the spatial extent of the recirculation zone behind an obstructing body, which in the considered cases is (nearly) homogeneous over depth. Flow above the cylinders (or reed) shows a clear vertical shear layer, extending all the way to the water surface, which reflects that flow momentum in the surface layer is transported downwards. Resistance to flow in the surface layer is thus due to an effective roughness of the flow layer below (the resistance layer).

Differences between flow with submerged rigid cylinders and natural reed

Comparing velocity and turbulence profiles of experiments with natural reed and rigid cylinders shows that for similar geometrical vegetation characteristics and similar surface slope i, a nearly equal magnitude of the vertical velocity profile in the resistance layer is found. Geometrical characteristics of the immersed cylinders and reed are stated in the graphs of Figure 6.2. It can be seen that the average diameter (D) of the reed is nearly 30% smaller than the rigid cylinders, but that between both situations the characteristic velocity in the resistance layer is practically the same. Apparently, the drag due to reed is higher than in case of rigid cylinders, which is likely due to the presence of leaves which cause additional blockage area (on average, the reed stems had two leaves, Meijer 1998a).

Looking at the root-mean-square of the turbulent velocity fluctuations (rms(u') and rms(w')), Figure 6.2, shows further differences between flow over rigid cylin-

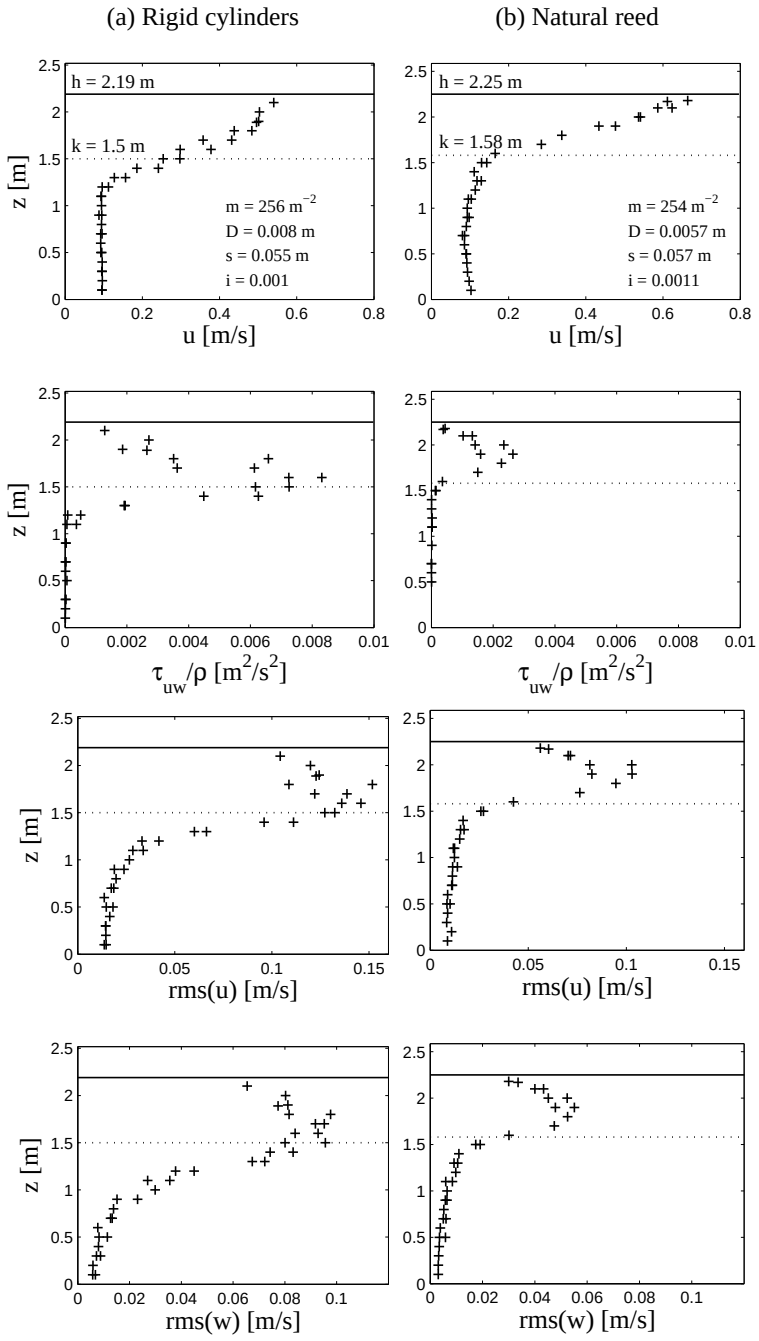

Figure 6.2: Velocity and turbulence profiles for flow over rigid cylinders and natural reed (experiments by Meijer 1998a, Meijer 1998b). The water level 'h' and the (undeflected) average height of the cylinders/reed 'k' are also shown.

ders and reed. In case of rigid cylinders, the turbulent fluctuations are more severe and penetrate further into the resistance layer, even though flow depth h and characteristic velocity U_{r0} are similar. Possibly, the bending of vegetation and the presence of plumes at the top of the vegetation cause a more distinct separation between surface and resistance layer, which prevents the formation of larger turbulent motions. Consequently, flow over natural vegetation experiences a smoother artificial bed, leading to higher flow velocities in the surface layer. In effect, flow in the surface layer appears to be affected by features at the top of the resistance layer.

Qualitative behavior of vegetation resistance methods

Two distinct features of flow over vegetation are identified, (i) drag dominance in the resistance layer and (ii) vertical shear dominance in the surface layer. These assumptions are included in all four of the compared vegetation resistance methods, and are generally valid. However, vertical shear is not entirely restricted to the surface layer, but may penetrate into the resistance layer, thereby accelerating the depth-averaged velocity in the resistance layer. The method by Van Velzen et al. (2003) does not account for this effect, thus underestimating flow in the resistance layer for submerged condition. Likewise, flow in the surface layer is overestimated as the corresponding roughness height is chosen such that the *total* depth-averaged flow velocity corresponds to measured values. Therefore, the roughness height parameterization in the model by Van Velzen et al. (2003) is not strictly related to turbulent length-scales, as it also compensates for important physical shortcomings in the model.

Next, drag in the resistance layer is determined by the blockage area of the vegetation, and may also be affected by leaves. Whether the presence of leaves are included as corrections on a drag coefficient for a pure cylinder, or by correcting the effective blockage area, is irrelevant when trying to differentiate between model descriptions of the resistance layer. Between the four considered model descriptions drag in the resistance layer always appears in the same manner, i.e. as the product '$C_D m D$'.

Flow in the surface layer seems to be affected by features at the top of the resistance layer, independently from the influence of the characteristic velocity U_{r0}. This is an important observation, which is not explicitly represented in all four vegetation resistance models. The models treated in Chapter 3 (Klopstra et al. 1997) and Chapter 4 (Huthoff et al. 2007) both include length-scales that are related to properties present at the top of the resistance layer, namely a dependency on vegetation density. The models by Van Velzen et al. (2003) and Baptist et al. (2007) describe surface layer flow only in terms of vegetation height (and the characteristic velocity U_{r0}).

6.2.2 Turbulent energy spectra

As turbulent length-scales play an important role in each of the four compared vegetation resistance models, energy spectra of turbulent flows are investigated. In Figures 6.3 and 6.4 the turbulence measurements and corresponding energy

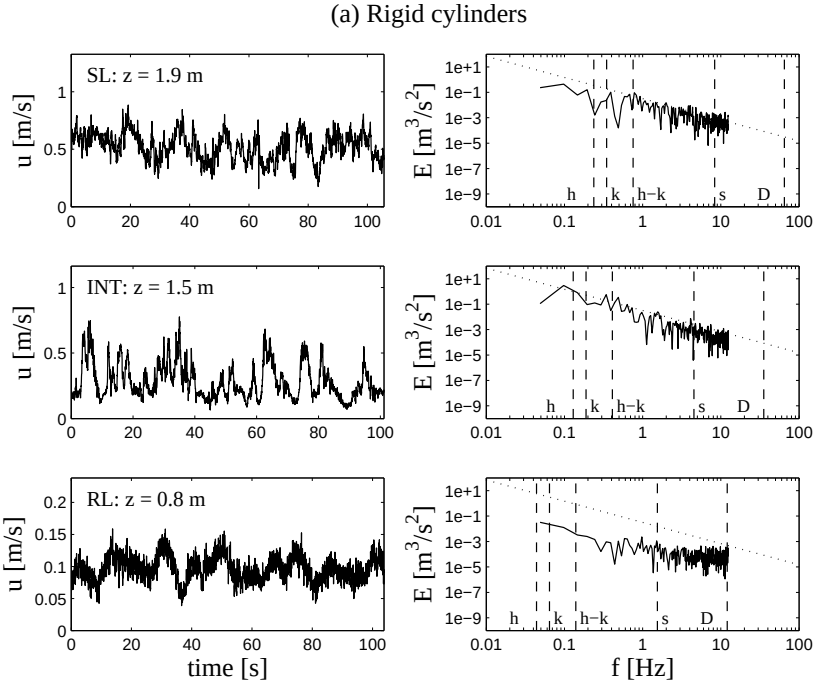

Figure 6.3: Flow velocity time-series and corresponding energy spectra in the surface layer (SL), at the interface between surface and resistance layer (INT) and in the resistance layer (RL) for flow over rigid cylinders (same case as in Figure 6.2a). The dotted line depicts a -5/3 slope associated with the inertial subrange of the turbulent energy cascade.

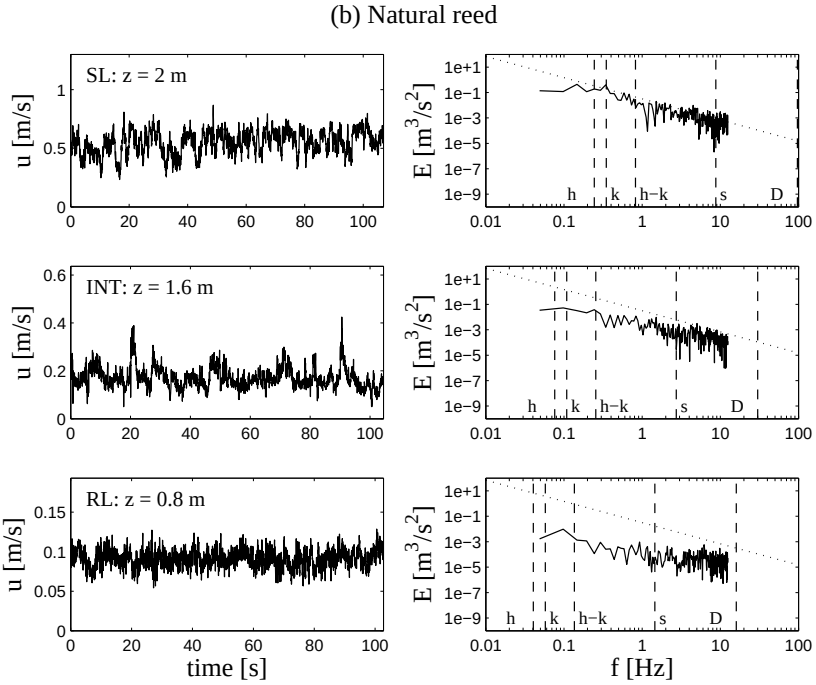

Figure 6.4: Flow velocity time-series and corresponding energy spectra for flow over natural reed (same case as in Figure 6.2b).

spectra are shown for rigid cylinders and natural reed. The spectra are obtained at three different locations in the flow field: (i) in the surface layer, (ii) at the interface between surface layer and resistance layer and (iii) in the resistance layer. In the energy spectra, frequencies associated with particular length-scales are also shown. Assuming Taylor's frozen turbulence hypothesis (Taylor 1938), indicated frequencies (f) in Figures 6.3 and 6.4 are associated with length-scales L according to

$$\mathrm{f} = U(z)/L, \tag{6.7}$$

where $U(z)$ is the mean velocity at depth z and L reflects any of the spatial scales h, k, $h-k$, s or D.

The turbulent energy spectra for flow in the surface layer, and near the top of the vegetation layer, follow Kolmogorov's $-5/3$ scaling for the inertial sub range quite well for both flow over rigid cylinders as flow over reed. We conclude that turbulent energy generated at the largest geometrical scale of the flow (associated with the depth of flow $\sim h-k$, see also Ghisalberti and Nepf 2002) is transferred to smaller scales until, in analogy with Gioia and Bombardelli (2002), a characteristic 'roughness scale' is reached. Experiments by Poggi et al. (2003) have shown that for hydraulically rough flow, a turbulent length-scale can be identified associated with the lower end of the inertial range in the turbulence spectrum. At smaller length-scales, eddies contain less energy, possibly due to an inverse-cascade process triggered by the roughness length (e.g. Jirka 2001).

Unfortunately, the sampling frequency of the experiments shown in Figures 6.3 and 6.4 was not high enough (25 Hz) to identify the lower end of the inertial range. Therefore, the turbulence length-scale that reflects energy dissipation caused by the presence of vegetation (the roughness scale) cannot be identified from the energy spectra. It can only be concluded that the roughness scale is smaller than s, as eddies associated with this length-scale are still well within the inertial range.

6.3 Discussion

Table 6.2 gives an overview of the examined resistance methods, and states some general characteristics of the (theoretical) backgrounds. Comparison with independent laboratory experiments could not decisively identify a method that is, in general, most reliable. However, analysis of turbulence over rigid rods and natural reed indicated some qualitative characteristics of flow over vegetation, such as drag-dependence on foliage or streamlining, the validity of describing surface layer flow with an equivalent roughness height, and the dependency of this roughness height on properties typical to the top of the resistance layer. These insights can be used to develop future experiments that may differentiate realistic from unrealistic behavior between flow models. Below, some suggestions for further experiments are given.

Table 6.2: Performance of different spatially-averaged methods to describe the hydraulic resistance of vegetation (μ is the mean error compared to measured flow velocities in experiments listed in Table 6.1, σ the standard deviation of the mean error).

No.	Method	μ	σ	Comment/Characteristics
I	Klopstra et al. (1997)	11%	27%	Adjusted logarithmic velocity profile, turbulent length scale $\alpha = (0.39)\frac{sh}{2b+(h-k)}$.
II	Huthoff et al. (2007)	-3%	36%	Based on energy considerations of turbulent flow, turbulent length-scale $r \sim D^3/(s+D)^2$.
III	Van Velzen et al. (2003)	-9%	25%	Adjusted logarithmic velocity profile, equivalent roughness height: $k_N = (1.6)k^{0.7}$.
IV	Baptist et al. (2007)	10%	30%	Approximation of detailed flow model that includes energy transport equation.

Determination of species-specific drag coefficients

For flow through vegetation, it is unavoidable to treat the hydraulic impact of vegetation by means of an empirically determined drag force. For idealized objects, where the blockage area and spatial distribution is easily measured, the drag force is proportional to the blockage area per unit volume and a nearly universal drag coefficient. For natural vegetation, the blockage area (per unit volume) may be affected by the flow field due to streamlining effects. Such effects may also be interpreted as modifications to the drag coefficient. It is recommended to perform laboratory experiments for a wide range of vegetation types, and at several flow regimes to determine such species-specific (volumetric) drag parameters. In such experiments flow through *emergent* vegetation should be investigated, to avoid additional shear due to flow in the surface layer. Alternatively, by lack of species-specific drag coefficients, the (undeflected) frontal blockage area per unit volume of a plant species could be used in the drag description, together with a standard drag coefficient for obstructing cylinders.

Vegetation density affecting surface layer flow

For flow over vegetation, all available methods require a description of turbulent energy dissipation as caused by the vegetation layer below. In two of the investigated vegetation resistance models, those proposed by Van Velzen et al. (2003) and Baptist et al. (2007), this energy dissipation is related to the vegetation height and the overall drag that is experienced in the resistance layer (as typified by the drag length b). In the models proposed by Klopstra et al. (1997) and Huthoff et al. (2007), flow in the surface layer is also affected by the specific configurations of vegetation elements, not only by the overall drag length b. In both these models, the separation between vegetation elements s appears in the model-equation for the associated turbulent length-scale (see Table 6.2).

Therefore, to distinguish which qualitative behavior is more realistic, exper-

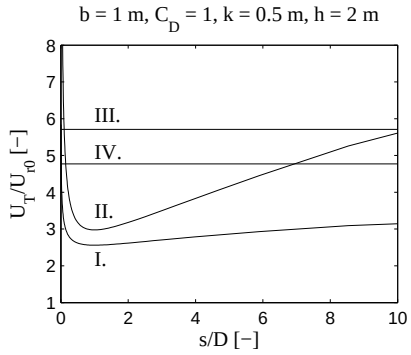

Figure 6.5: Sketch of expected model behavior for proposed experiments where the drag length $b = 1/(C_D m D)$ is kept constant, but the relative spacing between vegetation elements s/D is varied. Roman numerals correspond to resistance models in Table 6.2.

iments could be constructed that focus on the influence of varying vegetation separations s, for conditions where the overall drag length b stays the same. Figure 6.5 illustrates the different model behavior for such an experiment. In this respect, it is interesting to note that detailed flow models, based on the RANS equations and turbulent transport equations (as the model by Uittenbogaard 2003), also show similar qualitative behavior as the models by Van Velzen et al. (2003) and Baptist et al. (2007). Therefore, the proposed experiment may confirm or falsify the qualitative behavior for an even wider range of vegetation resistance models.

Finally, by measuring turbulent fluctuations at a much higher sampling frequency than shown in the current work, the turbulent length scale (associated with the surface-layer roughness-length) can possibly be directly identified from the turbulent energy spectrum. Identification of the roughness length from the turbulence spectrum could strengthen or discard vegetation resistance models. In Poggi et al. (2003) a sampling frequency up to 3000 Hz was achieved using Laser Doppler Anemometry. In terms of the flow characteristics from the energy spectra in Figure 6.3, a similar sampling frequency would be able to identify turbulent eddies of sizes considerably smaller than the diameter of the protruding cylinders or reed stems.

6.4 Conclusions

Four vegetation resistance methods were evaluated on their predictive capability as compared to laboratory flume data. Also, implicit theoretical assumptions and particular qualitative model characteristics were pointed out. All models are based on the assumption of hydraulically rough turbulent flow in the surface layer, and are therefore, in general, restricted to such flow conditions. However, only in the method proposed by Huthoff et al. (2007) this condition

is explicitly followed in the derivation, thus providing insight into the particular model-component that is sensitive to this condition. The other three vegetation resistance models all include model constituents that are less understood.

Comparison to laboratory data could not put additional clear limits to the range of applicability of any of the methods. However, for the vegetation resistance models proposed in Chapters 3 and 4, bed roughness effects seem to be required for relatively sparse vegetation densities ($s/D \gtrapprox 20$). Also, in contrast to remaining vegetation resistance methods, these two models provide more accurate descriptions of flow in the surface layer and in the resistance layer separately. Finally, an experiment is proposed that may be used to discard one or more of the proposed models, based on qualitative model behavior.

Chapter 7

Interacting Divided Channel Method for Compound Channel Flow*

An important process responsible for flow resistance in river flows is the lateral mixing that may occur when flow in the main channel interacts with the slower flow field in the floodplain. In this chapter a new method to calculate flow in such compound channels is proposed: the Interacting Divided Channel Method (IDCM). The proposed method involves a new parameterization of the interface stress between adjacent compartments, typically between the main channel and floodplain of a two-stage channel. This expression is motivated by scaling arguments and allows for a simple analytical solution of the average flow velocities in different compartments. Good agreement is found between the analytical model results and data from literature, referring to eleven laboratory experiments conducted with both symmetric and asymmetric two-stage channels.

7.1 Introduction

Many practical problems in river engineering require accurate flow predictions in compound channels. Such channels consist of different compartments: typically a main channel surrounded by floodplains (two-stage channel, see Figure 7.1). In addition to obtaining stage-discharge relationships, it is in many cases essential to accurately estimate the flow velocities in each compartment. For example, the hydraulic response to flood prevention measures, such as dredging the main channel and lowering or smoothing floodplains, depends on the flow velocities in these compartments. Likewise, local flow conditions determine the erosion and deposition rates of sediment in the main channel and floodplains.

When floodplains are overflown, the difference in flow velocity between the main channel and the floodplain generates mixing patterns and secondary currents. These processes, observed in experimental studies (e.g. Sellin 1964, Van Prooijen 2004), are responsible for the lateral momentum transfer that generally slows down the flow in the main channel, while accelerating the flow in the floodplain. Traditionally, the lateral momentum transfer has been ignored

*This chapter has, in slightly revised form, been submitted for publication as a separate paper: Huthoff, F., P. C. Roos, D. C. M. Augustijn and S. J. M. H. Hulscher (2007). Interacting Divided Channel Method for Compound Channel Flow. *Journal of Hydraulic Engineering*, accepted.

when estimating flow velocities in compound channels. In the so-called Divided Channel Method (DCM), a force balance between gravity and bed friction leads to a cross-sectionally averaged flow velocity for each compartment: U_{mc} in the main channel and U_{fp} in the floodplains (e.g. Chow 1959). Such a compartment-averaged approach has the advantages of requiring little input (geometry, surface slope, bed roughness) and being straightforward to calculate, while recognizing the different properties of the compartments.

DCM produces reasonable overall discharge predictions (Weber and Menéndez 2004) but it systematically overestimates U_{mc} and underestimates U_{fp}, due to neglect of lateral momentum transfer. This shortcoming has inspired many researchers to develop alternative methods, in which three different approaches can be distinguished.

1. Continue to ignore the lateral momentum transfer, while shifting the position and shape of the interfaces (Stephenson and Kolovopoulos 1990, Lambert and Myers 1998, Patra and Kar 2000, Cassels et al. 2001). In effect, these methods treat the cross-sectional area as a tuning parameter to obtain improved velocity estimates.

2. Describe the lateral momentum transfer by introducing an interface stress τ_{int} between adjacent compartments (e.g. Wormleaton et al. 1982, also, see Figure 7.1), often referred to as 'apparent shear stress'. The next step is to parameterize this quantity, often in terms of the velocity difference between main channel and floodplain ($U_{\mathrm{mc}} - U_{\mathrm{fp}}$) and the channel dimensions. In some cases regression analysis is used, leading to purely empirical formulas (Wormleaton et al. 1982, Prinos and Townsend 1984, Wormleaton and Merrett 1990). Based on dimensional analysis and additional theoretical considerations Christodoulou (1992) and Bousmar and Zech (1999) have proposed τ_{int} proportional to $(U_{\mathrm{mc}} - U_{\mathrm{fp}})^2$, where the coefficient of proportionality is determined empirically. The resulting averaged flow velocities are determined from a rather complicated set of analytical equations.

3. Abandon the compartment-averaged approach and resort to a continuum model that resolves the (depth-averaged) flow velocity $U(y)$, as a function of the cross-channel coordinate. Many of these models adopt a Boussinesq approach, where for the associated eddy viscosity different parameterizations have been proposed (Shiono and Knight 1991, Van Prooijen et al. 2005, Castanedo et al. 2005). Solution techniques are relatively cumbersome and, in addition, transverse numerical integration of $U(y)$ is required to obtain stage-discharge relationships.

Despite the availability of methods as cited above, because of its simplicity DCM is still the primary tool used by engineers for modeling stage-discharge relations in compound channels. For example, the treatment of lateral variability in commercial software tools for 1D river modeling as SOBEK, MIKE11 and HEC-RAS are all based on DCM. As a simple alternative, we propose the Interacting Divided Channel Method (IDCM), which includes effects due to lateral

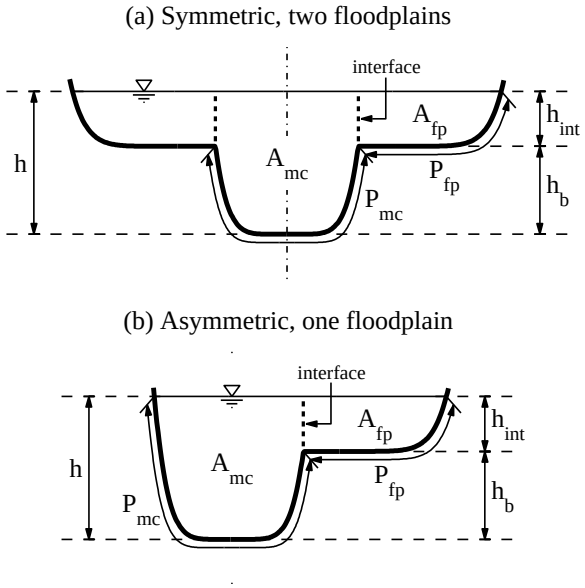

Figure 7.1: Cross-section of a two-stage channel: (a) symmetric with two identical floodplains ($N_{\rm fp} = 2$), (b) asymmetric with one floodplain ($N_{\rm fp} = 1$). The vertical dashed lines show the interfaces between the main channel 'mc' and the floodplain(s) 'fp'. The interface height $h_{\rm int}$ equals the difference between the water depth h and the bankfull depth $h_{\rm b}$.

momentum transfer, yet competes in simplicity with DCM when calculating overall discharges.

7.2 Interacting Divided Channel Method

7.2.1 Model equations for two-stage channel

We consider the channel geometries as depicted in Figure 1, consisting of a main channel with either two identical floodplains ($N_{\rm fp} = 2$) or a single floodplain ($N_{\rm fp} = 1$). The more general situation of a main channel surrounded by two non-identical floodplains is presented in the Appendix.

The total channel discharge Q equals the sum of the discharges in the main channel and the floodplain(s):

$$Q = A_{\rm mc}U_{\rm mc} + N_{\rm fp}A_{\rm fp}U_{\rm fp}. \tag{7.1}$$

Here, $A_{\rm mc}$ is the cross-sectional area (of the main channel 'mc') and $U_{\rm mc}$ the cross-sectionally averaged flow velocity (likewise for the floodplain 'fp').

The flow velocities $U_{\rm mc}$ and $U_{\rm fp}$, assumed steady and longitudinally uniform, follow from the streamwise force balances in both the main channel and the floodplains:

$$\rho g A_{\mathrm{mc}} i = \rho f_{\mathrm{mc}} U_{\mathrm{mc}}^2 P_{\mathrm{mc}} + N_{\mathrm{fp}} \tau_{\mathrm{int}} h_{\mathrm{int}}, \tag{7.2}$$

$$\rho g A_{\mathrm{fp}} i = \rho f_{\mathrm{fp}} U_{\mathrm{fp}}^2 P_{\mathrm{fp}} - \tau_{\mathrm{int}} h_{\mathrm{int}}. \tag{7.3}$$

The left-hand sides of equations (7.2) and (7.3) represent the gravitational force, proportional to the density of water ρ, the gravitational acceleration g, the cross-sectional area A and the streamwise channel slope i. The first term on the righthand side of equation (7.2) represents the shear stress acting along the wetted perimeter P_{mc} of the main channel. Following a classical wall-resistance approach (Chow 1959), this shear stress is modeled proportional to the squared flow velocity U_{mc}^2, with a dimensionless friction coefficient f_{mc}. Accordingly, a friction coefficient f_{fp} for the floodplain appears in equation (7.3). Various formulas exist that express the friction coefficient in terms of roughness properties and geometry (Yen 2002).

Following Sellin (1964), equations (7.2) and (7.3) contain an interface stress τ_{int} associated with the lateral momentum transfer between the main channel and the floodplain(s). This interface stress acts over a height h_{int} (see Figure 1). Moreover, the stress that slows down the main channel flow is exactly the opposite of the stress that accelerates the flow in the floodplain, thus explaining the minus sign in equation (7.3).

Key element of IDCM is a new parameterization of the interface shear stress, where τ_{int} is proportional to $U_{\mathrm{mc}}^2 - U_{\mathrm{fp}}^2$. This dependency is based on physical scaling arguments of turbulent shear in shallow flows, as described below.

7.2.2 Derivation of the interface stress

According to the Reynolds-averaged Navier-Stokes equations, lateral momentum transfer in turbulent flow is due to both turbulent velocity fluctuations and secondary currents. Van Prooijen et al. (2005) demonstrate that lateral momentum transfer in shallow mixing layers of prismatic channels is primarily caused by turbulent velocity fluctuations. The interface stress in equation (7.2) can thus be expressed as

$$\tau_{\mathrm{int}} = \frac{\rho}{h_{\mathrm{int}}} \int_{-h_{\mathrm{int}}}^{0} \overline{u'v'} \, \mathrm{d}z, \tag{7.4}$$

where z is the vertical coordinate and u and v are the streamwise and lateral velocity fluctuations at the (vertical) interface, respectively. The overbar denotes (Reynolds) time-averaging.

Gioia and Bombardelli (2002) argue that turbulent fluctuations are dominated by the largest eddy motions present in the associated flow directions. Such eddy motions emerge due to velocity gradients in the flow field. In mixing layers, the transverse velocity gradient causes coherent eddy structures that affect both streamwise on lateral turbulence intensities. It is widely accepted that in *pure* mixing layers the turbulent velocity fluctuations scale with the transverse difference in flow velocities (e.g. Pope 2000). Consequently, the shear

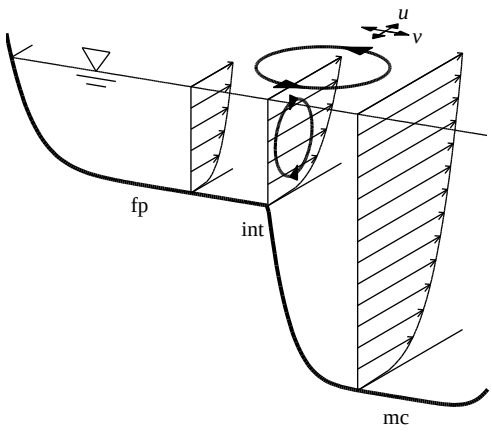

Figure 7.2: Sketch of the eddies that dominate longitudinal and transversal turbulent fluctuations (u' and v', respectively). Also shown are the profiles of streamwise velocities at the interface ('int'), in the floodplain ('fp') and in the main channel ('mc').

stress scales with the squared lateral velocity difference across the mixing layer. However, in a *shallow* mixing layer the flow field has a velocity gradient over depth, as it is influenced by bed resistance. Therefore, in addition to transverse eddy motions, eddy motions in the vertical plane also contribute to turbulent fluctuations (Figure 7.2).

The largest eddies contributing to the fluctuations v in *lateral* direction lie in the horizontal plane (Figure 7.2). Focusing on the mixing layer, these eddies are driven by the largest velocity difference across the interface. Hence, the velocity difference between the main channel and the floodplain controls the lateral velocity fluctuations v:

$$v' \sim U_{\mathrm{mc}} - U_{\mathrm{fp}}. \tag{7.5}$$

Turbulence measurements in shallow mixing layers indicate that turbulence intensities are affected both by the velocity difference across the mixing layer as well as by (the vertical gradient of) the local streamwise velocity (e.g. Carling et al. 2002, Figure 4.10 in Van Prooijen 2004). In particular, the *streamwise* turbulence intensity is strongly affected by the mean streamwise velocity. Therefore, in the streamwise direction, we assume that the largest eddies scale with a typical difference in streamwise velocities (Figure 7.2). Due to the no-slip condition at the channel bed, this velocity difference is of the order of the mean streamwise flow velocity. At the interface between the main channel and the floodplain, its magnitude is estimated as the average of U_{mc} and U_{fp}. This motivates the following scaling expression for u:

$$u' \sim \frac{1}{2}\left(U_{\mathrm{mc}} + U_{\mathrm{fp}}\right). \tag{7.6}$$

Substitution of scaling expressions (7.5) and (7.6) into equation (7.4) yields the stress parameterization

$$\tau_{\text{int}} = \frac{1}{2}\gamma\rho\left(U_{\text{mc}}^2 - U_{\text{fp}}^2\right). \tag{7.7}$$

The dimensionless interface coefficient γ, to be estimated from experiments, absorbs the proportionalities in equations (7.5) and (7.6) as well as the effects of the averaging procedures in equation (7.4).

7.2.3 Analytical solution for two-stage channel

Applying IDCM to the two-stage channel geometries depicted in Figures 7.1a and 7.1b, requires solving equations (7.2), (7.3) and (7.7). This gives

$$U_{\text{mc}}^2 = U_{\text{mc},0}^2 - \frac{\frac{1}{2}\gamma N_{\text{fp}}\epsilon_{\text{mc}}\left(U_{\text{mc},0}^2 - U_{\text{fp},0}^2\right)}{1 + \frac{1}{2}\gamma\left(N_{\text{fp}}\epsilon_{\text{mc}} + \epsilon_{\text{fp}}\right)}, \tag{7.8}$$

$$U_{\text{fp}}^2 = U_{\text{fp},0}^2 + \frac{\frac{1}{2}\gamma\epsilon_{\text{fp}}\left(U_{\text{mc},0}^2 - U_{\text{fp},0}^2\right)}{1 + \frac{1}{2}\gamma\left(N_{\text{fp}}\epsilon_{\text{mc}} + \epsilon_{\text{fp}}\right)}. \tag{7.9}$$

For convenience, we have defined dimensionless parameters $\epsilon_{\text{mc}} = h_{\text{int}}/(f_{\text{mc}}P_{\text{mc}})$ and $\epsilon_{\text{fp}} = h_{\text{int}}/(f_{\text{fp}}P_{\text{fp}})$. The solution is presented in terms of the flow velocities obtained with the traditional DCM, where the interface stress is neglected ($\gamma = 0$, hence subscript '0'):

$$U_{\text{mc},0}^2 = \frac{gR_{\text{mc}}s}{f_{\text{mc}}}, \qquad U_{\text{fp},0}^2 = \frac{gR_{\text{fp}}s}{f_{\text{fp}}}. \tag{7.10}$$

Here, $R_{\text{mc}} = A_{\text{mc}}/P_{\text{mc}}$ and $R_{\text{fp}} = A_{\text{fp}}/P_{\text{fp}}$ are the hydraulic radii of the main channel and the floodplain, respectively. Finally, inserting (7.8) and (7.9) into (7.1) gives the discharge Q.

7.3 Comparison to laboratory data

In this Section, IDCM-results are compared to flume experiments available from literature: KD83 (Knight and Demetriou 1983), AK02 (Atabay and Knight 2002, Seçkin 2004) and SERC-Flood Channel Facility (FCF) data (e.g. Knight and Sellin 1987, Myers and Brennan 1990).

7.3.1 Overview of experiments

We have selected steady uniform flow experiments conducted with straight compound channels that have a fixed bed, a cross-section as depicted in Figure 7.1a or 7.1b and floodplains without large-scale roughness elements[†] (Table 7.1).

[†]When roughness elements take up a considerable part of the water column, classical wall-resistance formulations as adopted in equations (7.2) and (7.3) are no longer adequate. A more detailed approach is then needed, e.g. treating two separate fluid layers: a lower one penetrated by roughness elements and an upper one occupied by fluid only (Huthoff et al. 2007).

Table 7.1: Overview of laboratory experiments and the results from DCM (subscript '0') and IDCM (no subscript).

Exp. (N_{fp})	W_{mc}	S_{mc}	W_{fp}	S_{fp}	h_{b}	i	n	U_{b}	R_0^2	γ	R^2
	[m]	[-]	[m]	[-]	[cm]	[‰]	[s/m$^{\frac{1}{3}}$]	[m/s]	[-]	[-]	[-]
KD83[a]A (2)	0.152	v	0.456	v	7.6	0.966	0.010	0.35	0.86	0.026	0.98
KD83 B (2)	0.152	v	0.304	v	7.6	0.966	0.010	0.35	0.92	0.012	0.97
KD83 C (2)	0.152	v	0.152	v	7.6	0.966	0.010	0.35	0.91	0.008	0.98
FCF[b]s1 (2)	1.50	1	4.10	v	15	1.027	0.010	0.82	0.78	0.046	0.98
FCF s2 (2)	1.50	1	2.25	1	15	1.027	0.010	0.82	0.87	0.029	0.99
FCF s3 (2)	1.50	1	0.75	v	15	1.027	0.010	0.82	0.84	0.017	0.99
FCF s6 (1)	1.50	1	2.25	1	15	1.027	0.010	0.82	0.92	0.031	0.98
FCF s8 (2)	1.50	v	2.25	1	15	1.027	0.010	0.80	0.82	0.039	0.98
FCF s10 (2)	1.50	2	2.25	1	15	1.027	0.010	0.82	0.89	0.025	0.99
AK02a[c] (1)	0.398	v	0.407	v	5	2.024	0.009	0.58	0.93	0.008	0.95
AK02s[c,d](2)	0.398	v	0.407	v	5	2.024	0.009	0.58	0.85	0.013	0.97
Total set	-	-	-	-	-	-	-	-	0.94	0.020	0.98

[a]Knight and Demetriou (1983), [b]SERC-Flood Channel Facility data (e.g. Knight and Sellin 1987, Myers and Brennan 1990), [c]Atabay and Knight (2002), [d]also, see Seçkin (2004).

All experiments have trapezoidal compartment cross-sections, characterized by bottom widths W_{mc} and W_{fp} and bank slopes S_{mc} and S_{fp} (v = vertical bank slope).

The bed roughness has been specified in terms of a Manning roughness coefficient n, obtained from velocity measurements for inbank flows (except KD83 where a reference run without floodplains was carried out; see Figure 7.5d). In each of the experiments, the roughness of the floodplain was identical to that of the main channel, and hence characterized by the same n-value. Combining this empirically obtained value with Manning's formula (Manning 1889), the average flow velocity at bankfull height is calculated according to

$$U_{\mathrm{b}} = \frac{R_{\mathrm{mc,b}}^{2/3} i^{1/2}}{n}. \tag{7.11}$$

Here, $R_{\mathrm{mc,b}}$ is the hydraulic radius of the main channel for bankfull depth $h = h_{\mathrm{b}}$. Note that each of the experiments is in the fully turbulent regime, having a (bankfull) Reynolds number $\mathrm{Re}_{\mathrm{b}} = U_{\mathrm{b}} h_{\mathrm{b}}/\nu$ exceeding 10^4.

For a given water depth h, the geometrical characteristics in Table 7.1 can be readily translated into the parameters required for IDCM: cross-sectional areas A_{mc} and A_{fp}, wetted perimeters P_{mc} and P_{fp}, and friction coefficients $f_{\mathrm{mc}} = gn^2 R_{\mathrm{mc}}^{-1/3}$ and $f_{\mathrm{fp}} = gn^2 R_{\mathrm{fp}}^{-1/3}$.

7.3.2 Results

To demonstrate the influence of lateral momentum transfer in IDCM, we also present predictions from the traditional DCM approach, in which the lateral momentum transfer is neglected. For DCM, the comparison leads to coefficients of determination R_0^2 (Table 7.1). For IDCM, the corresponding coefficients of determination R^2 depend on the value of the interface coefficient γ.

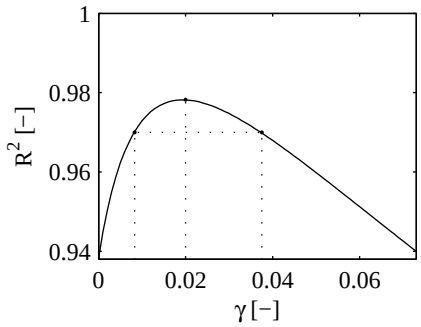

Figure 7.3: Performance of IDCM for the total set of experiments from Table 7.1, as a function of the interface coefficient γ. A maximum value of R^2 is achieved when $\gamma = 0.020$. IDCM reduces to DCM at a value of $\gamma = 0$ (with $R_0^2 = 0.94$).

For each of the eleven experiments, and for the total data set combined, an optimal γ-value is obtained by maximizing R^2 (for total data set, see Figure 7.3). In doing so, the flow velocities have been scaled against the calculated value of the bankfull velocity U_b of the corresponding experiment (Figure 7.4). As shown by Table 7.1, the values of the interface coefficient for the separate experiments are in the range $0.01 - 0.05$, while an overall value of $\gamma = 0.020$ is obtained using the combined data set. For each of the eleven experiments, Figure 7.5 shows compartment-averaged flow velocities at different flow depths. With the individually obtained γ values, or with a general value of $\gamma = 0.020$, the IDCM-results show significantly better agreement with measured values than the DCM-results.

To indicate the sensitivity of IDCM to the values of γ, Figure 7.3 indicates γ-values that correspond to 75% of the maximum increase in R^2 (compared to $R_0^2 = 0.94$). A crude range of uncertainty can thus be attributed to the optimal general value for γ:

$$\gamma = 0.020^{+0.018}_{-0.012}. \tag{7.12}$$

Table 7.2 shows the performance of IDCM as compared to DCM, using a general value of $\gamma = 0.020$ for each of the eleven experiments.

The coefficient of determination does not reflect any systematic overprediction or underprediction of the flow velocities. For each experiment, we therefore also calculate the mean error in the predicted velocities. For the main channel, this error is given by

$$\mu_{mc} = \frac{1}{M} \sum_{j=1}^{M} \frac{U_{mc,j}^{(predicted)} - U_{mc,j}^{(measured)}}{U_b}, \tag{7.13}$$

where M is the number of measured U_{mc}-values and U_b the bankfull flow velocity. Similarly, μ_{fp} is defined as the mean error in the predicted velocities in the floodplain.

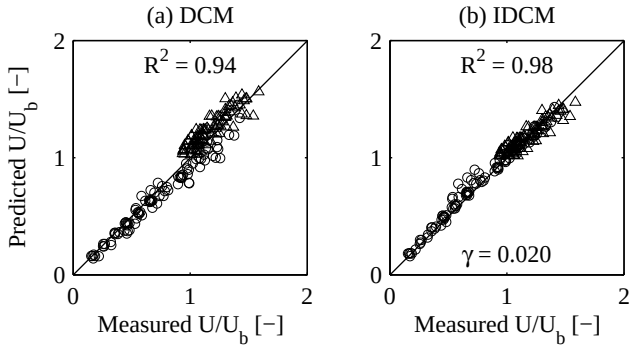

Figure 7.4: Measured versus predicted velocities, from the total data set with all experiments listed in Table 7.1. Predictions from (a) DCM and (b) IDCM with $\gamma = 0.020$. Triangles ($\triangle$) correspond to the main channel, circles ($\circ$) to the floodplain. All velocities have been scaled against the (calculated) bankfull velocity U_b, as given by equation (7.11).

The values of $\mu_{\mathrm{mc},0}$ and $\mu_{\mathrm{fp},0}$ in Table 7.2 show that the traditional DCM systematically overpredicts U_mc, whereas it systematically underpredicts U_fp (see also Figure 7.5). IDCM reduces these systematic errors considerably. The mean errors μ_mc are significantly closer to zero than their DCM-counterparts, errors μ_fp are reduced only marginally. Since flow in the main channel contributes most to the overall discharge, it is important that the main channel velocity is predicted as accurate as possible. The increased *overall* reliability of velocity predictions using IDCM instead of DCM is reflected in the significant increase of R^2 in Table 7.2.

Table 7.2: Performance of IDCM for $\gamma = 0.020$, compared to DCM.

Experiment	DCM			IDCM		
	R^2_0 [-]	$\mu_{\mathrm{mc},0}$ [%]	$\mu_{\mathrm{fp},0}$ [%]	R^2 [-]	μ_mc [%]	μ_fp [%]
Total set	0.94	+7	–6	0.98	+1	+2
KD83 A	0.86	+14	–3	0.98	+2	+1
KD83 B	0.92	+9	–7	0.97	–4	0
KD83 C	0.91	+5	–10	0.95	–9	+2
FCF s1	0.78	+20	–2	0.95	+10	+1
FCF s2	0.87	+16	–5	0.99	+5	+1
FCF s3	0.84	+12	–14	0.99	0	+2
FCF s6	0.92	+11	–4	0.98	+6	+2
FCF s8	0.82	+19	–3	0.96	+8	+3
FCF s10	0.89	+15	–3	0.99	+4	+3
AK02a	0.93	+7	–3	0.93	–1	+8
AK02s	0.85	+10	–9	0.96	–4	+1

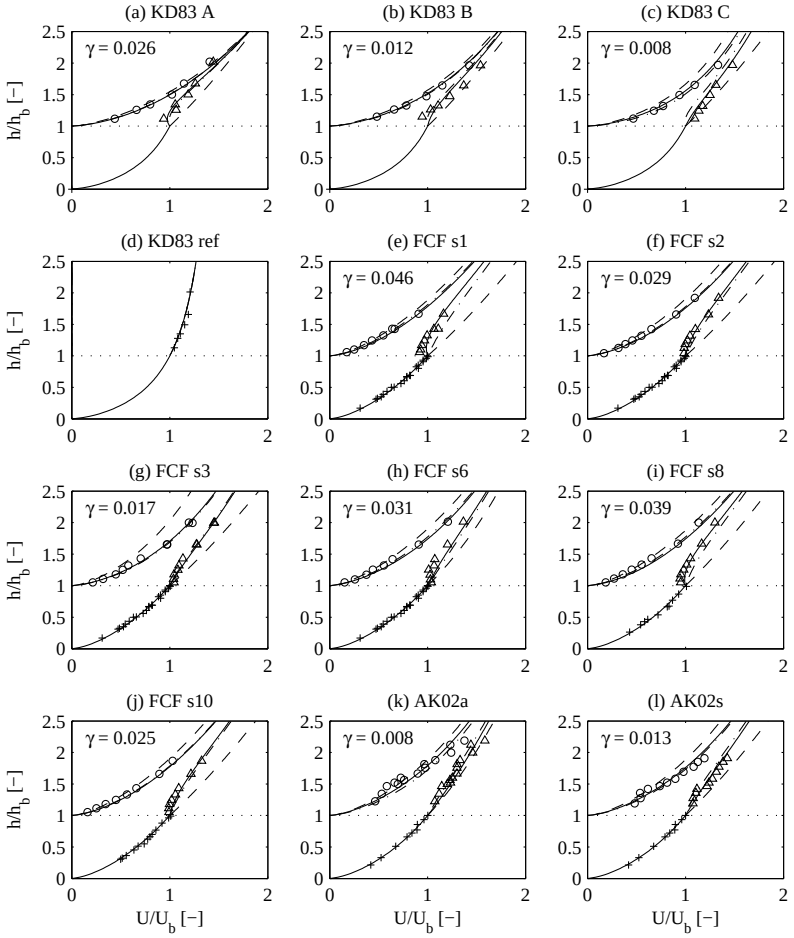

Figure 7.5: Comparison between the IDCM-results (solid lines for the individual γ-value denoted in the plot, dash-dotted for the overall value $\gamma = 0.020$) and the experiments in Table 7.1. For overbank flow, triangles ($\triangle$) correspond to measured velocities in the main channel, circles ($\circ$) to those in the floodplain. For reference, the DCM-results have been denoted with a dashed line. Plus-signs ($+$) indicate the measurements that have been used to estimate n, in most cases from inbank flow except KD83 where n was obtained from a reference run without floodplains: (d) KD83 ref.

7.4 Discussion

The parameterization of the interface stress as given in equation (7.7) involves a dimensionless interface coefficient γ, which can physically be interpreted as a relative drag coefficient. The comparison with measurements produces γ-values in a relatively confined range: $0.01 - 0.05$, with an overall value of 0.020. The derivation of the proposed interface stress parameterization is based on the assumption that bed roughness significantly affects turbulence intensities, and hence, strictly relates to shallow mixing layer flows. If wall-turbulence, originated at the channel bed, has negligible influence on momentum transfer in the transverse mixing zone, then the standard scaling law for shear stress in *pure* mixing layers is more appropriate. In this respect, Bousmar and Zech 1999 proposed the Exchange Discharge Model (EDM), which specifies

$$\tau_{\text{int}} = \Psi \rho \left(U_{\text{mc}} - U_{\text{fp}}\right)^2, \tag{7.14}$$

with Ψ a dimensionless proportionality coefficient for which Proust et al. (2006) give $\Psi \simeq 0.020$. Using equations (7.2) and (7.3), the interface stress τ_{int} can be calculated based on the channel's geometrical dimensions, bed roughness and the measured compartment-averaged flow velocities. In Figure 7.6 these measured interface stresses are compared to the predictions of equation (7.7) and equation (7.14). Neither of the two models produces predictions accurate enough to discard the other. Nevertheless, in situations where the interface stress between adjacent compartments is large, the newly proposed parameterization $\tau_{\text{int}} \sim U_{\text{mc}}^2 - U_{\text{fp}}^2$ behaves similarly to the parameterization for pure mixing layers. Therefore, in flow situations that are strongly affected by interface shear stress, the newly proposed parameterization is expected to perform adequately, even if flows are not shallow. Conversely, in situations where U_{mc} is close to U_{fp}, the interface stress is weak and the parameterization of interface shear is of minor importance.

A practical property of IDCM is that the interface stress parameterization yields a set of model equations that is linear in the squared velocities, leading to an analytical solution. As shown in the Appendix, this property is retained when generalizing IDCM to compound channels with an arbitrary number of compartments. A prerequisite for this generalization is that the interface coefficient γ has either a universal value or an unambiguous dependency on the geometry and roughness of the surrounding compartments. Based on the results from this study, we recommend a constant value of $\gamma = 0.020$.

The way in which the values of γ are obtained inevitably introduces uncertainties: related to the velocity measurements, the compartment-averaged approach and the chosen optimization criterion. We have therefore not attempted to explain the variability in γ in terms of channel geometry and roughness properties. However, an indication that γ may depend on a ratio of length scales is provided by a continuous description of shear stress in a mixing layer. In the Boussinesq approach, the shear stress is modeled using an eddy viscosity chosen equal to λU, with λ a turbulent mixing length (see Castanedo et al. 2005).

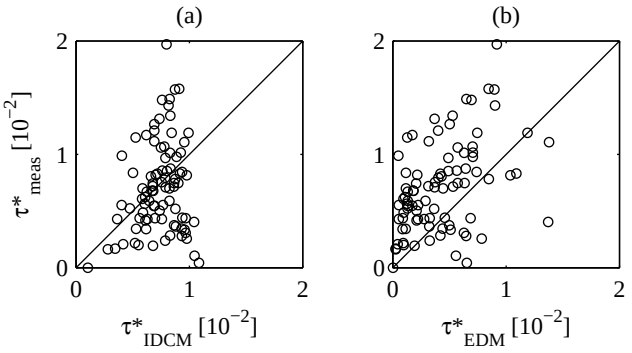

Figure 7.6: Measured interface stresses compared to predictions with (a) the newly proposed interface stress parameterization employed in IDCM and (b) the parameterization in the Exchange Discharge Model (EDM). Shear stresses have been scaled according to $\tau^* = \tau_{\rm int}/(\rho U_{\rm b}^2)$, with bankfull velocity $U_{\rm b}$.

Transverse integration of the turbulent stress term then gives

$$\frac{\tau_{\rm int}}{\rho} = \int_{y_1}^{y_2} \frac{\partial}{\partial y}\left(\lambda U \frac{\partial U}{\partial y}\right) {\rm d}y = \lambda U \frac{\partial U}{\partial y}\bigg|_{y=y_1}^{y=y_2}. \tag{7.15}$$

Letting y_1 and y_2 coincide with the compartment boundaries, $\lambda\frac{\partial U}{\partial y}$ becomes the continuum equivalent of $U_{\rm mc} - U_{\rm fp}$ in equation (7.5), and U the continuum equivalent of $\frac{1}{2}(U_{\rm mc} + U_{\rm fp})$ in equation (7.6). Therefore, the interface coefficient γ reflects the extent to which the turbulent length scale λ differs from the typical lateral distance associated with the velocity gradient. More results, from laboratory or numerical experiments, are required to investigate such dependencies in γ in detail.

7.5 Conclusions

We have proposed a new method to calculate flow in compound channels: the Interacting Divided Channel Method (IDCM). This method has the following features.

1. Lateral momentum transfer is included, based on physical scaling arguments.

2. It leads to simple analytical expressions for the flow velocities in the different compartments.

3. The only free parameter is the dimensionless interface coefficient γ.

4. Comparison with data from various laboratory measurements shows good agreement for γ-values in the range $0.01 - 0.05$. An overall comparison

leads to a general value of $\gamma = 0.020$ and still gives good agreement for the individual data sets.

We conclude that the overall calibration of the proposed interface stress parameterization gives satisfying results for shallow flows in a steady and uniform channel setting. The encouraging results of IDCM illustrate that 1D flow models used in river engineering can be quite easily extended to include effects due to lateral momentum transfer.

Acknowledgements

The authors thank Dr. W. R. C. Myers (University of Ulster, UK) for providing the FCF-data, and Dr. G. Seçkin (Çukurova University, Turkey) for providing the AK02s-data set. Professor D. W. Knight (University of Birmingham, UK) is acknowledged for making available several data sets, including AK02 and FCF, on the website `www.flowdata.bham.ac.uk`, as well.

7.6 Appendix: Generalization of IDCM to arbitrary compound channels

For channel cross-sections consisting of N arbitrary compartments we define the individual properties of each compartment $j = 1, 2, \ldots, N$: cross-sectional area A_j, wetted perimeter P_j, hydraulic radius $R_j = A_j/P_j$ and friction coefficient f_j. Furthermore, the heights of the interfaces with the compartments adjacent to the left and right are denoted with $h_{j-1/2}$ and $h_{j+1/2}$, respectively.

The total channel discharge is now given by

$$Q = \sum_{j=1}^{N} A_j U_j, \tag{7.16}$$

where U_j represents the cross-sectionally averaged flow velocity of compartment j. Completely in analogy with the derivation for a two-stage channel, the velocities follow from momentum balances combining gravity, bed friction and the lateral momentum transfer across the interfaces:

$$U_1^2 + r_1 \left(U_1^2 - U_2^2\right) = U_{1,0}^2, \tag{7.17}$$

$$U_j^2 + \ell_j \left(U_j^2 - U_{j-1}^2\right) + r_j \left(U_j^2 - U_{j+1}^2\right) = U_{j,0}^2, \tag{7.18}$$

$$U_N^2 + \ell_N \left(U_N^2 - U_{N-1}^2\right) = U_{N,0}^2, \tag{7.19}$$

Analogously to equation (7.10), $U_{j,0}^2 = gR_j i/f_j$ represents the squared velocity of compartment j according to the traditional DCM-solution. Furthermore, we define the dimensionless parameters

$$\ell_j = \frac{\gamma h_{j-1/2}}{2 f_j P_j}, \qquad r_j = \frac{\gamma h_{j+1/2}}{2 f_j P_j}. \tag{7.20}$$

Equations (7.17) and (7.19), along with equation (7.18) for $j = 2, \ldots, N-1$ form a set of N coupled equations, linear in the *squared* velocities U_j^2.

Applying the above to a compound channel with a main channel ('2') surrounded by two different floodplains ('1' and '3', so $N = 3$), gives the following solution:

$$\begin{aligned} U_1^2 = \; & \delta^{-1} \left[1+r_2+\ell_3+\ell_2(1+\ell_3)U_{1,0}^2 \right. \\ & \left. +r_1(1+\ell_3)U_{2,0}^2 + r_1 r_2 U_{3,0}^2\right], \qquad (7.21) \\ U_2^2 = \; & \delta^{-1} \left[\ell_2(1+\ell_3)U_{1,0}^2 + (1+r_1)(1+\ell_3)U_{2,0}^2 \right. \\ & \left. +r_2(1+r_1)U_{3,0}^2\right], \qquad (7.22) \\ U_3^2 = \; & \delta^{-1} \left[\ell_2\ell_3 U_{1,0}^2 + \ell_3(1+r_1)U_{2,0}^2 \right. \\ & \left. 1+r_1+\ell_2+r_2(1+r_1)U_{3,0}^2\right], \qquad (7.23) \end{aligned}$$

with $\delta = 1+r_1+\ell_2+r_2+\ell_3+r_1r_2+r_1\ell_3+\ell_2\ell_3$.

Chapter 8

Discussion

In the current work, vegetation resistance methods were compared based on the predictive capability and the general validity of theoretical assumptions. Among these, a new vegetation resistance method is proposed for spatially-averaged river-reach models. The existing methods and the new methodology naturally have some shortcomings, which are discussed below. Also, implications for river-reach modeling and suggestions for further investigations are discussed.

8.1 Simulation of natural floodplain vegetation in river flow models

The vegetation resistance model presented in the current work, Chapter 4, showed very good agreement with a set of laboratory experiments, where vegetation was represented in an idealized form. Relating to this idealized form of homogeneously distributed rigid cylinders, an important aspect is the impact of characteristics of natural vegetation, such as the presence of leaves, side branches and flexibility, which were ignored in development of the proposed vegetation resistance model. In particular, corrections on the drag coefficient related to presence of leaves may provide an important improvement (e.g. Järvelä 2004). Specification of a suitable drag coefficient for a particular vegetation-species has always been a key issue in describing hydraulic resistance of vegetation. This is the case for more detailed models, such as 3D RANS-approaches, Klopstra's method and remains the case for the new method. Properties of the drag coefficient are quite well-understood for rigid cylindrical vegetation elements, but need further specification to also reflect vegetation characteristics as leaf foliage and flexibility. Next, for submerged flow conditions, the required equivalent spacing between vegetation elements is easily determined for idealized (cylindrical) vegetation. However, its value becomes difficult to estimate in case of natural vegetation, where leaves and streamlining effects may be present. Again, detailed flow experiments with natural vegetation need to be carried out to determine the equivalent vegetation spacing. Alternatively, the spacing can be calculated from vegetation density estimates (e.g. Straatsma 2007), but this value would refer to the *static* vegetation spacing, not the equivalent spacing under submerged flow conditions.

Another important aspect related to resistance of natural vegetation is the impact on the overall flow field if the vegetation elements are not distributed

homogeneously. Also, particular configurations need further attention in order to investigate the reliability of the model in limiting situations. For example, what happens if the height of the cylinders is smaller than the spacing between them? Is the spacing between vegetation elements then still the appropriate scaling length? Also, with respect to some other vegetation resistance methods, a decisive experiment would be to vary vegetation configurations in such a way that the overall drag in the resistance layer stays the same. Several models predict that between such cases flow over vegetation also stays the same. Other models, including the newly proposed model in Chapter 4, predict a dependency of surface layer flow on the detailed geometrical characteristics of vegetation in the resistance layer below. The proposed experiment may serve to discard one or more of the existing methods, based on unrealistic qualitative behavior.

8.2 Calibrating river-reach models on resistance parameters

Common practice in river flood forecasting is that hydrodynamic models are calibrated on resistance parameters to fit recorded observations and that these models are extrapolated to more extreme events. As river models can be quite sensitive to hydraulic resistance parameterizations, it is essential that model parameters have realistic values, and that their dependencies are correct. Only then extrapolations to extreme or new situations may be assumed to yield reliable results.

However, studies on calibration procedures of river reach models have shown that several sets of roughness parameters sometimes yield equally accurate agreement with observations (i.e. *equifinality* of model parameters, e.g. Bates 2004 and Pappenberger et al. 2005). Some of these parameters sets may include values that are clearly unrealistic, and can thus be discarded (*parameter abuse*, see the commentary by Hamilton 2007). However, in some cases this may not be as clear. Therefore, restricting the acceptable range of model parameters *a priori* aids in determining which (calibrated) parameter set yields the most realistic representation, and may thus be expected to give the best predictions for new situations. A vegetation resistance model that is constructed from meaningful parameters, for example relating to geometrical dimensions of vegetation, may reduce parameter abuse in large-scale river models.

In the current work, a vegetation resistance method is proposed that has a physical basis, and describes realistic qualitative behavior of flow in presence of vegetation, for both emergent and submerged conditions. Hence, using such a the model as a component in river-reach flow models gives more confidence to the quality of high-discharge predictions, in contrast to flow models that rely on poorly understood calibration coefficients, or are purely based on regression and data-driven techniques.

A parameter in the proposed vegetation resistance model that is not clearly related to geometrical or material vegetation characteristics is the drag coefficient C_D. This parameter thus remains susceptible to parameter abuse, as

the range of realistic values is not well-understood. In case of flow through a field of rigid cylinders, the range of acceptable values is roughly confined to 1-2 (e.g. Baptist 2005, see also values for a single cylinder in Figure 2.3), while for natural vegetation a much larger range is found in literature ($C_D \approx$ 0.1-10, e.g. Wilson and Horritt 2002, James et al. 2004). Therefore, a better understanding of vegetation drag coefficients as related to directly measurable properties is required. For some vegetation types such studies have already been performed (e.g. Fischenich and Dudley 2000, Järvelä 2004), but still a general methodology to estimate a drag coefficient of natural vegetation is lacking.

8.3 Limitations of the Interacting Divided Channel Method

The proposed model to describe lateral momentum transfer in 1D flow models, see Chapter 7, involves an interface shear stress coefficient γ that was determined empirically. So far, a fairly reliable constant value has been determined, but it is likely that γ is in fact flow-dependent. Therefore, a wider range of (laboratory or numerical) experimental data are required to investigate dependencies of parameter γ in greater detail. In particular, if using the proposed method to describe the effect of lateral mixing processes in an arbitrary channel cross-section (section 7.6), the properties of the interface coefficient need further investigation.

Also, the derivation of the method relates to shallow compound channel flows in straight prismatic channels. Any lateral mass transfer due to meandering or narrowing or widening of a channel is thus not represented. One may wonder whether these effects can still be adequately represented in 1D flow models, or whether this marks the transition where more sophisticated models are needed (see also section 8.4).

8.4 The use of simplified flow models

What is the use of simplified flow models, if the exact physical laws are already known, which, in principle, can be accurately modeled? Indeed, modern computing capabilities open the way for more complex flow systems to be modeled with detailed numerical simulation techniques. However, these techniques are extremely costly, not only in development effort but also in required computation time and memory space. In cases where a description of the overall kinematics of a complex system is desired, and if it is not of primary importance to know small-scale flow patterns, a bulk flow description may offer a useful alternative. Also, simplified idealized models based on theoretical assertions often add significantly to the understanding of the system. Such insights can aid in interpreting results from detailed flow simulation. On the other hand, situations where phenomenological or simplified models fail, point out fields of investigation where detailed simulations should focus on. Simplified flow models thus do not compete with modern more detailed techniques, but may supplement them and point out new research area's.

In the current work, it was shown that scaling considerations of the bulk flow field for flow over vegetation could be used to avoid complications associated with describing details of turbulent flow. An important condition that allowed a bulk treatment of flow over vegetation, is that length-scales responsible for most momentum loss are of a different order of magnitude than dimensions of the flow domain (i.e. the flow depth). This separation of scales allowed general treatment of small-scale flow patterns because they are not influenced by large-scale geometrical dimensions.

The success of using scaling considerations of turbulent flow over vegetation has also been the motivation for considering an additional widely studied issue related to floodplain flows: flow in compound channels. Referring to the simplified model to describe lateral momentum transfer in a compound channel, the bulk flow approach was possible because turbulent shear could be estimated based on interacting flow velocities, and that no geometrical dimensions had to be explicitly accounted for. Therefore, again, dominant mixing processes are treated separately from forcing mechanisms at large geometrical scales.

Possibly, similar methodologies can be applied to other types of flow processes, as long as the dominant mixing processes are not significantly affected by large-scale geometrical scales. For example, another potential application could be found in turbulent flows over or through a porous medium. In contrast, flows over dunes on river beds are more difficult to treat this way, as dune dimensions are of the same order of magnitude as the flow depth. Turbulent eddies generated by the presence of dunes thus interfere with forcing mechanisms at scales of the entire flow domain. Other situations where internal mixing processes are associated with geometrical variations in the flow domain, include mass transfer in narrowing or widening channels (e.g. Bousmar and Zech 1999, Proust et al. 2006), or resistance effects caused by channel meandering (e.g. Ervine et al. 1993). For these type of processes more detailed modeling techniques seem necessary.

8.5 Flood prevention: where to go next?

Before the hydrodynamics of a river-reach can be modeled, the following properties have to be known: (i) how much water is flowing in the (river) system, (ii) what are the topographical characteristics and (iii) which surface (or material) characteristics are present in the flow domain. Next, by understanding the physical impacts that these properties may have on each other, the entire dynamics of the river system can be modeled: water levels and flood extent at a certain discharge, flow velocities affecting erosion and deposition, which in turn affect the topography, and so on.

The current work was restricted to describing the hydraulic effect of present vegetation, given a certain water discharge. The work is thus not concerned with predicting discharge levels as based on rain intensities, nor expected future discharge rates associated with climate change. However, understanding the *amount* of water that a river system could face in the future is probably the most important but also the least understood component in flood prevention

studies. Naturally, physics of the present situation is more accessible to quantitative investigation than future climate scenarios. In analogy to the saying that a chain is as weak as its weakest link, flood studies can use hypothetical flood scenarios to identify locations most threatened by floods. Such studies demand that physics of the system is accurately represented. In this respect, physical processes that still require better understanding are the impact of inhomogeneous surface characteristics on the flow field, including natural variability within vegetated covers or varying surface roughness properties, but also localized impacts of isolated large objects. Another process still not adequately represented in river flow models, is the dynamic hydraulic resistance of a river bed, if dunes develop during non-steady flood conditions. Now that the hydraulic resistance in floodplains can be quite adequately represented in river flow models, the dynamics of main channel roughness are easier to isolate, such that in overbank flows the hydraulic conditions in the main channel can be more accurately investigated.

Chapter 9

Conclusions & recommendations

In the Introduction, Chapter 1, the objective of this work was stated as:

> To develop a model of hydraulic resistance of vegetation for river management purposes that is able to describe the hydraulic response for a wide range of vegetation types and flow conditions, allows for incorporation in river-reach flow models and requires input data that can be measured in the field.

Towards this end, five research questions were formulated, which are answered below.

9.1 Answers to research questions

Q1: How can vegetation effects be included in flow models, and which methods are suitable at river-reach scales?

The fundamental laws for fluid flows, the Navier-Stokes equations, have long been known, and these can in principle be used for modeling river flows. The impact of geometrical boundaries and obstructing elements (such as vegetation) naturally enters these flow models through specification of the boundary conditions. However, such flow descriptions require extremely detailed calculation procedures and correspondingly detailed boundary conditions, which for river-reach scales is a practical impossibility. Alternatively, cruder flow models need to be used that require parameterizations of important mixing patterns in the flow field, which also reflect the impact of obstructing vegetation.

Relating to flow with emergent vegetation, various studies have shown that an effective drag force approach describes the impact of obstructing vegetation in a flow layer adequately, allowing a large-scale treatment of vegetation resistance. Vegetation is characterized by an effective blockage parameter, which is representative of the spatially-averaged enhanced turbulent mixing (and hence, the flow resistance) caused by the vegetation.

For flow *over* vegetation it is more difficult to describe the impact on the overall flow field by means of a physically meaningful vegetation parameter. This difficulty is largely due to the poor understanding of a dominant mixing length or equivalent roughness-length than can be attributed to specific vegetation properties. Detailed turbulence transport equations appear to be the most

generally applicable methods to describe flow over vegetation. Unfortunately, these methods require numerical computation techniques, which would imply extremely large computation times if applied at river-reach scales.

In conclusion, at least two components are required to describe flow over vegetation in river-reach models: (i) a drag description, that describes flow in the vegetation layer (reflecting effective vegetation blockage area) and (ii) a parameterization that describes the equivalent resistance in the surface layer (a turbulence transport model, a mixing length or an equivalent roughness length). A practical complication is that both components may still be flow-dependent. Also, the distinction between both flow layers may be ambiguous in case of natural vegetation (due to flexibility and inhomogeneous vegetation heights).

Q2: Focussing on ease of application and reliability, among existing methods, what is potentially the most generally applicable method to describe vegetation in river-reach models?

As stated in the objective of this thesis, a *generally applicable method* to describe vegetation resistance should have the properties (i) that it is able to describe the hydraulic response for a wide range of vegetation types and flow conditions, (ii) that it allows incorporation in river-reach flow models and (iii) that it requires input data that can be measured in the field. As 2D and 1D flow models are still the primary tools used in hydraulic studies for river engineering purposes, spatially-averaged vegetation resistance methods would be most suitable. Also, as concluded in response to Q1, the model should combine a drag force description with a parameterization of flow over vegetation, such that hydraulic resistance of both submerged and emergent vegetation conditions may be represented. Finally, in order to warrant a wide range of applicability of such a method, it is preferably based on fundamental principles of fluid flows, such that all model dependencies are well-understood.

Among previously existing vegetation resistance methods, the one proposed by Klopstra et al. (1997) was identified as being the most promising towards a qualification of being such a *generally applicable method*. The method is based on fundamental flow principles, describes flow in-between and above the vegetation separately, depends on measurable (idealized) vegetation characteristics and allows incorporation in spatially-averaged flow models.

Q3: What are limitations of this method and can these be solved?

The method proposed by Klopstra et al. (1997) still has some shortcomings. While the method is mostly specified in terms of measurable vegetation characteristics, the associated turbulence model requires specification of a turbulent length-scale, which appears to be difficult in terms of readily measurable quantities. Reasonable correlations with some of the geometrical properties of the vegetation were found, but a clear relation is still lacking. Also, in combination with the adopted turbulence description, the model performs best when assuming a complete-slip bed boundary condition. This result is inconsistent

with one of the best established empirical results of wall-bounded flow: no-slip at all solid boundaries. Furthermore, in order to achieve an analytic description for the depth-averaged flow velocity, approximations are required to the vertical velocity profile. These approximations are reasonable as long as the vegetation is not very short and spacing between individual vegetation elements is not far between. Finally, an empirical drag coefficient is required to represent turbulent energy losses associated with the blockage area of the vegetation.

It seems impossible to solve the mentioned issues related to the turbulence model adopted in the method proposed by Klopstra et al. (1997), and to still yield an analytical description that can be easily incorporated in river-reach flow models. Therefore, a new approach is attempted that aims at directly describing the bulk properties of the flow field, without going into the detail of depth-variations of the flow velocity.

Q4: In floodplain flows, is it possible to describe the overall flow field in a physically sound way, without explicitly describing detailed flow processes?

Even though the method by Klopstra et al. (1997) included some inconsistencies and poorly understood parameters, its accurate prediction of particular flow situations already suggested the potential for describing flow affected by vegetation without going into the detail of small-scale turbulence patterns. The new method proposed in Chapter 4 took the simplification of the flow field even further, by only looking at the bulk (overall) flow behavior. Based on scaling considerations of the turbulent mixing patterns and energetics of the flow field, a simple flow resistance model was derived that yielded accurate predictions of large-scale flow conditions (i.e. the depth-averaged flow velocity).

Reflecting again on Q3, naturally, there are practical limitations to the newly proposed vegetation resistance model. In particular, two required input parameters are difficult to measure in the field: (i) the drag coefficient and (ii) the equivalent spacing between vegetation elements. These shortcomings are related to the fact that the model describes hydraulic resistance of *idealized* vegetation, and that the influences of foliage, flexibility and inhomogeneous vegetation properties are not explicitly included. However, because all components in the proposed resistance model have a clear physical meaning, the model provides a reliable basis for more elaborated (natural) vegetation resistance models. Therefore, provided that the drag coefficient and the equivalent spacing between vegetation elements is known for particular vegetation types, the newly proposed method best matches the conditions for being a generally applicable vegetation resistance method (Q2).

Motivated by the successful turbulence scaling technique in Chapter 4, another mathematically simple bulk flow method related to floodplain flows is proposed in Chapter 7. The proposed Interacting Divided Channel Method (IDCM) describes the compartment-averaged flow velocity in a compound channel, including the effect of lateral mixing. Comparison with laboratory data revealed that

this method gives an accurate representation of large-scale flow conditions in straight compound channels, using a constant empirical proportionality coefficient in the lateral shear parameterization. Further investigations are necessary to understand properties of the included empirical coefficient.

Q5: How does the method perform in full-scale vegetated waterway settings?

The newly developed vegetation resistance method in Chapter 4 was evaluated using flow measurements collected in two vegetated waterways in the Netherlands: a Green River and a grass-covered floodplain along the river Rhine. It was shown that model predictions are consistent with the measured hydraulic conditions and the known characteristics of present vegetation. However, additional influences on the flow field, such as large-scale topographical variations, were sometimes large, making it difficult to isolate the effect of vegetation resistance. Also, flow measurements could not be determined accurately enough to really validate the model. In conclusion, model predictions seemed promising.

Finally, has the objective been achieved?

A new method to describe vegetation resistance is proposed that has a sound theoretical foundation, making it applicable to describe the response to wide range of flow conditions (turbulent flow with emergent and submerged vegetation) and vegetation types (requiring associated drag-coefficients). Also, the method allows for incorporation in river-reach models because of its mathematically simple form, and is dependent on measurable quantities (idealized geometrical vegetation characteristics). The method is based on scaling considerations of the turbulent mixing patterns and energetics of the flow field, was shown to correspond well with results from laboratory flow experiments and gave promising results in a full-scale field setting. A shortcoming of the proposed method is that the required input parameters may be difficult to determine for natural vegetation characterized by side-branches and leaves. To include these effects, further research should be carried out to investigate the necessary corrections on model parameters that now reflect idealized vegetation characteristics.

9.2 Achievements

In the current thesis, two methods related to floodplain flows are proposed that may increase the reliability of spatially-averaged river flow models: (i) a model of the depth-averaged velocity to represent vegetation resistance (relevant for 1D or 2D river models) and (ii) a method that accounts for lateral momentum transfer in compound channels (for 1D river models). Both methods are mathematically simple, which would also appeal to engineers who desire tools for quick evaluation purposes.

9.3 Recommendations

Associated with the proposed methods for floodplain flows in this thesis, some shortcomings were identified. Follow-up studies are proposed to solve these issues:

- More detailed laboratory experiments are required that investigate flow over cylindrical vegetation elements in particular situations: (i) relatively low vegetation with large spacings in-between individual vegetation elements, (ii) experiments that focus on flow in the surface layer while depth-averaged flow in-between the vegetation elements is kept constant, despite different geometrical vegetation configurations and (iii) effects of inhomogeneous spatial distributions of vegetation elements.
- The drag coefficient in vegetation resistance models requires better understanding. More detailed laboratory flow experiments need to be carried out that investigate the impact of leaf foliage, side-branching and flexibility.
- The properties of the interface shear stress coefficient in the proposed interacting divided channel method need to be better understood. In particular, application to straight channels with arbitrary cross-section geometries requires further investigation.

Bibliography

Akilli, H. and D. Rockwell (2002). Vortex formation from a cylinder in shallow water. *Physics of Fluids 14*(9), 2957–2967.

Armanini, A., M. Righetti, and P. Grisenti (2005). Direct measurement of vegetation resistance in prototype scale. *Journal of Hydraulic Research 43*(5), 481–487.

Atabay, S. and D. Knight (2002). The influence of floodplain width on the stage-discharge relationship for compound channels. In *River Flow 2002*, Volume 1, pp. 197–204. Balkema.

Baptist, M. J. (2005, April). *Modelling Floodplain Biogeomorphology*. Ph. D. thesis, Delft University of Technology.

Baptist, M. J., V. Babovic, J. Rodriguez Uthurburu, M. Keijzer, R. E. Uittenbogaard, A. Mynett, and A. Verwey (2007). On inducing equations for vegetation resistance. *Journal of Hydraulic Research 45*(4).

Barenblatt, G. I. (2003). *Scaling*. Cambridge Texts in Applied Mathematics. Cambridge University Press.

Bates, P. D. (2004). Remote sensing and flood inundation modelling. *Hydrological Processes 18*(13), 2593–2597.

Bentham, T. and R. Britter (2003). Spatially averaged flow within obstacle arrays. *Atmospheric Environment 37*, 2037–2043.

Bentz, D. P. and N. S. Martys (1995). Hydraulic radius and transport in reconstructed model three-dimensional porous media. *Transport in Porous Media 17*(3), 221–238.

Bousmar, D. and Y. Zech (1999). Momentum transfer for practical flow computation in compound channels. *Journal of Hydraulic Engineering 125*(7), 696–706.

Breugem, W. P. (2004). *The influence of wall permeability on laminar and turbulent flows: theory and simulations*. Ph. D. thesis, Delft University of Technology.

Brookes, C. J., J. M. Hooke, and J. Mant (2000). Modelling vegetation interactions with channel flow in river valleys of the Mediterranean region. *Catena 40*, 93–118.

Busch, N., W. Fröhlich, R. Lammersen, R. Oppermann, and G. Steinebach (1999). Strömungs- und Durchflussmodellierung in der Bundesanstallt für

Gewässerkunde. In *Mathematische Modelle in der Gewässerkunde: Stand und Perspektiven*, BfG Mitteilungen Nr. 19, pp. 70–82. Bundesanstalt fü Gewässerkunde.

Carling, P. A., C. Zhixian, M. J. Holland, D. A. Ervine, and K. Babaeyan-Koopaei (2002). Turbulent flow across a natural compound channel. *Water Resources Research 38*(12), 1270.

Casas, A., G. Benito, V. R. Thorndycraft, and M. Rico (2006). The topographic data source of digital terrain models as a key element in the accuracy of hydraulic flood modelling. *Earth Surface Processes and Landforms 31*(4), 444–456.

Cassels, J. B. C., M. F. Lambert, and W. R. C. Myers (2001). Discharge prediction in straight mobile bed compound channels. *Water & Marine Engineering 148*(3), 177–188.

Castanedo, S., R. Medina, and F. J. Mendez (2005). Models for the turbulent diffusion terms of shallow water equations. *Journal of Hydraulic Engineering 131*(3), 217–223.

Chen, D. and G. H. Jirka (1995). Experimental study of plane turbulent wakes in a shallow water layer. *Fluid Dynamics Research 16*, 11–41.

Choi, S. U. and H. Kang (2004). Reynolds stress modeling of vegetated open-channel flows. *Journal of Hydraulic Research 42*(1), 3–11.

Choi, S. U. and H. Kang (2006). Numerical investigations of mean flow and turbuelnce structures of partly-vegetated open-channel flows using the Reynolds stress model. *Journal of Hydraulic Research 44*(2), 203–217.

Chow, V. T. (1959). *Open-channel Hydraulics* (International edition 1973 ed.). McGraw-Hill.

Christodoulou, G. C. (1992). Apparent shear stress in smooth compound channels. *Water Resources Management 6*, 235–247.

Cook, H. L. and F. B. Campbell (1939). Characteristics of some meadow strip vegetation. *Agricultural engineering 20*(9), 345–348.

Copeland, R. R. (2000). Determination of flow resistance coefficients due to shrubs and woody vegetation. Technical report, U.S. Army Engineer Research and Development Center, Vicksburg, MS, USA.

Cui, J. and V. S. Neary (2002). Large eddy simulation (LES) of fully developed flow through vegetation. In *Hydroinformatics 2002: Proceedings of the Fifth International Conference on Hydroinformatics*, Cardiff, UK, pp. 39–44.

Darby, S. (1999). Effect of riparian vegetation on flow resistance and flood potential. *Journal of Hydraulic Engineering 125*(5), 443–454.

Darrigol, O. (2005). *Worlds of Flow: a history of hydrodynamics from the Bernouillis to Prandtl*. Oxford University Press.

De Doncker, L., P. Troch, R. Verhoeven, K. Bal, and P. Meire (2006). Influence of aquatic plants on the flow resistance and the hydraulic capacity of vegetated rivers. In Ferreira, Alves, Leal, and Cardoso (Eds.), *River Flow 2006*, Volume 1, pp. 593–602.

De Vriend, H. J. (2006). Flood management research needs. In J. Van Alphen, E. Van Beek, and M. Taal (Eds.), *Floods, from Defence to Management*, Third International Symposium on Flood Defence, pp. 49–61.

Defina, A. and A. C. Bixio (2005). Mean flow and turbulence in vegetated open channel flow. *Water Resources Research 41*(W07006), doi:10.1029/2004WR003475.

Douben, N. and R. M. W. Ratnayake (2006). Characteristic data on river floods and floodings; facts and figures. In J. Van Alphen, E. Van Beek, and M. Taal (Eds.), *Floods, from Defence to Management*, Third International Symposium on Flood Defence, pp. 19–35.

Duel, H., M. J. Baptist, and W. J. Penning (2001). Cyclic floodplain rejuvenation: A new strategy based on floodplain measures for both flood risk management and enhancement of the biodiversity of the river rhine. IRMA SPONGE report 7.

DVWK (1991). Hydraulische Berechnung von Fliessgewässern. Merkblätter zur Wasserwirtschaft 220, DVWK (Deutsche Vereinigung für Wasserwirtschaft und Kulturbau).

Eij, J. M. (2004). Verwerking van ADCP stromingsmetingen rond de Pannerdensche Kop tijdens hoogwater in november 1998. Technical Report AV DOC 040211, Aqua Vision, Utrecht, the Netherlands.

Erduran, K. S. and V. Kutija (2003). Quasi-three-dimensional numerical model for flow through flexible, rigid, submerged and non-submerged vegetation. *Journal of Hydroinformatics 5*(3), 189–202.

Ervine, D. A., B. B. Willetts, S. R. H. J, and M. Lorena (1993). Factors affecting conveyance in meandering compound flows. *Journal of Hydraulic Engineering 119*(12), 1383–1399.

Fathi-Maghadam, M. and N. Kouwen (1997). Nonrigid, nonsubmerged, vegetative roughness on floodplains. *Journal of Hydraulic Engineering 123*(1), 51–57.

Fischenich, C. (2000, May). Resistance due to vegetation. Ecosytem Management & Restoration Research Program SR 07, U.S. Army Corps of Engineers.

Fischenich, C. and S. Dudley (2000, February). Determining drag coefficients and area for vegetation. Ecosytem Management & Restoration Research Program SR 08, U.S. Army Corps of Engineers.

Fisher, K. R. (1995, March). The impact of temporal and spatial variations in vegetation in rivers. Technical Report SR 393, HR Wallingford, Wallingford, England.

Fisher, K. R. (2001, May). Handbook for assesment of hydraulic performance of environmental channels. Technical Report SR 490, HR Wallingford.

Freeman, G. E., W. J. Rahmeyer, and R. R. Copeland (2000). Determination of resistance due to shrubs and woody vegetation. Technical report, U.S. Army Engineer Research and Development Center, Vicksburg, MS.

García Díaz, R. (2005). Analysis of Manning coefficient for small-depth flows on vegetated beds. *Hydrological Processes 19*, 3221–3233.

Ge, L. and F. Sotiropoulos (2005). 3D unsteady rans modeling of complex hydraulic engineering flows. I: Numerical model. *Journal of Hydraulic Engineering 131*(9), 800–808.

Gendelman, M. M. (1981). Passage of floods over river floodplains. *Power Technology and Engineering 15*(11), 692–697.

Ghisalberti, M. and H. Nepf (2002). Mixing layers and coherent structures in vegetated aquatic flow. *Journal of Geophysical Research 107*(C2), 1–11.

Ghisalberti, M. and H. Nepf (2004). The limited growth of vegetated shear-layers. *Water Resources Research 40*, W07502.

Gioia, G. and F. A. Bombardelli (2002). Scaling and similarity in rough channel flows. *Physical Review Letters 88*(1), 14501–14504.

Green, J. C. (2005). Comparison of blockage factors in modelling the resistance of channels containing submerged macrophytes. *River Research and Applications 21*, 671–686.

Green, J. C. (2006). Effect of macrophyte spatial variability on channel resistance. *Advances in Water Resources 29*, 426–438.

Green, J. E. P. and J. E. Garton (1983). Vegetation lined channel design procedures. *Transactions of the American Society of Agricultural Engineers 26*(2), 437–439.

Gullbrand, J. and F. K. Chow (2003). The effect of numerical errors and turbulence models in large-eddy simulations of channel flow, with and without explicit filtering. *Journal of Fluid Mechanics 495*, 323–341.

Hamilton, S. (2007). Just say NO to equifinality. *Hydrological Processes 21*, 1979–1980.

Heddleson, C. F., D. L. Brown, and R. T. Cliffe (1957). Summary of drag coefficients of various shaped cylinders. Technical Publication APEX-299, General Electric Co., Atomic Products Division, Aircraft Nuclear Propulsion Department, Cincinnati, OH, USA.

Helmiö, T. (2002). Unsteady 1D flow model of compound channel with vegetated floodplains. *Journal of Hydrology 268*, 89–99.

Helmiö, T. (2004). Flow resistance due to lateral momentum transfer in partially vegetated rivers. *Water Resources Research 40*(5), W05206.

Hoerner, S. F. (1965). *Fluid-dynamic drag*. 148 Busteed Drive, Midland Park, NJ, USA: Published by author.

Hoffmann, M. R. and F. M. van der Meer (2002). A simple space-time averaged porous media model for flow in densely vegetated channels. In W. G. S.M. Hassanizadeh, R.J. Schotting and G. Pinder (Eds.), *Developments in Water Science : Computational methods in water resources*, pp. 1661–1668. Elsevier Science.

Horritt, M. S. and P. D. Bates (2002). Evaluation of 1D and 2D numerical models for predicting river flood inundation. *Journal of Hydrology 268*(1), 87–99.

Huthoff, F. and D. C. M. Augustijn (2004). Sensitivity analysis of floodplain roughness in 1D flow. In Liong, Phoon, and Babovic (Eds.), *6th International Conference on HydroInformatics, Singapore*. World Scientific Publishing Company.

Huthoff, F. and D. C. M. Augustijn (2006). Hydraulic resistance of vegetation: Predictions of average flow velocities based on a rigid-cylinders analogy. Civil Engineering & Management report 2006R-001/WEM-003 (ISSN 1568-4652), University of Twente.

Huthoff, F., D. C. M. Augustijn, and S. J. M. H. Hulscher (2007). Analytical solution of the depth-averaged flow velocity in case of submerged rigid cylindrical vegetation. *Water Resources Research 43*(W06413), doi:10.1029/2006WR005625.

Huthoff, F. and J. Stijnen (2005). Efficiency of emergency retention areas along the river Rhine: Monte Carlo simulations of a 1D flow model. In *International Symposium on Stochastic Hydraulics ISSH 2005, 23 and 24 May 2005, Nijmegen, The Netherlands*.

Ikeda, S. and M. Kanazawa (1996). Three-dimensional organized vortices above flexible water plants. *Journal of Hydraulic Engineering 122*(11), 634–640.

Jackson, D. and B. Launder (2007). Osborne Reynolds and the publication of his papers on turbulent flow. *Annual review of Fluid Mechanics 39*, 19–35.

James, C. S., L. Birkhead, A. A. Jordanova, and J. J. O'Sullivan (2004). Flow resistance of emergent vegetation. *Journal of Hydraulic Research 42*(4), 390–398.

Järvelä, J. (2002). Flow resistance of flexible and stiff vegetation: a flume study with natural plants. *Journal of Hydrology 269*, 44–54.

Järvelä, J. (2003). Influence of vegetation on flow structure in floodplains and wetlands. In A. Sanchez-Arcilla and A. Bateman (Eds.), *Proceedings of the 3rd Symposium on River, Coastal and Estuarine Morphodynamics (RCEM 2003)*, Madrid, pp. 845–856. IAHR.

Järvelä, J. (2004). Determination of flow resistance caused by non-submerged woody vegetation. *Journal of River Basin Management 2*(1), 61–70.

Jia, Y., S. Scott, Y. Xu, S. Huang, and S. S. Y. Wang (2005). Three-dimensional numerical simulation and analysis of flows around a sub-

merged weir in a channel bendway. *Journal of Hydraulic Engineering 131*(8), 682–693.

Jirka, G. H. (2001). Large scale flow structures and mixing processes in shallow flows. *Journal of Hydraulic Research 39*(6), 567–573.

Julien, P. Y., G. J. Klaassen, W. B. M. Ten Brinke, and A. W. E. Wilbers (2002). Case study: bed resistance of Rhine river during 1998 flood. *Journal of Hydraulic Engineering 128*(12), 1042–1050.

Kaiser, W. (1984, September). Fliesswiderstandsverhalten in Gerinnen mit Ufergebüsch. Wasserbau-Mitteilungen Heft 23, TH Darmstadt.

Keulegan, G. H. (1938). Laws of turbulent flow in open channels. *Journal of Research of the National Bureau of Standards 21*(Research paper 1151).

Khublaryan, M. G., A. P. Frolov, and V. N. Zyryanov (2004). Modeling water flow in the presence of higher vegetation. *Water Resources 31*(6), 668–674. (Translated from Vodnye Resursy, Vol. 31, No. 6, 2004).

Klopstra, D., H. J. Barneveld, J. M. van Noortwijk, and E. H. van Velzen (1997). Analytical model for hydraulic roughness of submerged vegetation. In *Managing Water: Coping with scarcity and abundance*, San Fransisco, pp. 775–780. Proceedings of the 27th IAHR Congress.

Knight, D. W. and J. D. Demetriou (1983). Flood plain and main channel flow interaction. *Journal of Hydraulic Engineering 109*(8), 1073–1092.

Knight, D. W. and R. H. J. Sellin (1987). The SERC flood channel facility. *J. Inst. Water Env. Management 1*, 198–204.

Kolmogorov, A. N. (1941, July 8, 1991,Translation.). The local structure of turbulence in incompressible viscous fluid for very large reynolds numbers (translated 1991). *Proceedings of the Royal Society (London), Series A - Mathematical and Physical Sciences 434*(1890), 9–13.

Kouwen, N. and M. Fathi-Moghadam (2000). Friction factors for coniferous trees along rivers. *Journal of Hydraulic Engineering 126*(10), 732–740.

Kouwen, N., T. Unny, and H. M. Hill (1969). Flow retardance in vegetated channels. *Journal of Irrigation and Drainage Division 95*(IR2), 329–342.

Kouwen, N. and T. E. Unny (1973, May). Flexible roughness in open channels. *Journal of the Hydraulics Division HY5*.

Kraichnan, R. H. (1967). Inertial ranges in two-dimensional turbulence. *Physics of Fluids 10*(7), 1417–1423.

Kutija, V. and H. T. M. Hong (1996). A numerical model for addressing the additional resistance to flow introduced by flexible vegetation. *Journal of Hydraulic Research 34*(1), 99–114.

Lambert, M. F. and W. R. C. Myers (1998). Estimating the discharge capacity in compound channels. In *Proc. Inst. Civ. Eng.*, Volume 130 of *Water, Maritime and Energy*, pp. 84–94.

Lauga, E., M. P. Brenner, and H. A. Stone (2005). Microfluids: the no-slip boundary condition. In *Handbook of Experimental Fluid Dynamics*, Volume chapter 5, New York. Springer.

Lee, J. K., L. C. Roig, H. L. Jenter, and H. M. Visser (2004). Drag coefficients for modeling flow through emergent vegetation in the Florida Everglades. *Ecological Engineering 22*, 237–248.

Lightbody, A. F. and H. M. Nepf (2006). Prediction of velocity profiles and longitudinal dispersion in emergent salt marsh vegetation. *Limnology and Oceanography 51*(1), 218–228.

López, F. and M. H. García (1997). Open channel flow through simulated vegetation; turbulence modelling and sediment transport. Hydrosystems laboratory WRP-CP-10, University of Illinois.

López, F. and M. H. García (2001). Mean flow and turbulence structure of open channel flow through non-emergent vegetation. *Journal of Hydraulic Engineering 127*(5), 392–402.

Lumley, J. L. (1992). Some comments on turbulence. *Physics of Fluids A 4*(2), 203–211.

L'vov, V. and I. Procaccia (1997). Hydrodynamic turbulence: a 19th century problem with a challenge for the 21st century. In O. Boratav, A. Eden, and A. Erzan (Eds.), *Turbulence modeling and vortex dynamics: Proceedings of a Workshop Held at Istanbul, Turkey, 2 - 6 September 1996*. Springer.

Manning, R. (1889). On the flow of water in open channels and pipes. *Transactions of the Institution of Civil Engineers of Ireland 20*, 161–207.

Meijer, D. G. (1998a). Modelproeven overstroomd riet. Technical Report PR177, HKV Consultants, Lelystad, the Netherlands.

Meijer, D. G. (1998b). Modelproeven overstroomde vegetatie. Technical Report PR121, HKV Consultants, Lelystad, the Netherlands.

Meijer, D. G. and E. H. van Velzen (1998). Prototype-scale flume experiments on hydraulic roughness of submerged vegetation. Technical report, HKV Consultants, Lelystad, The Netherlands.

Meneveau, C. and J. Katz (2000). Scale invariance and turbulence models for Large-Eddy Simulation. *Annual review of Fluid Mechanics 32*, 1–32.

Moin, P. and K. Mahesh (1998). Direct Numerical Simulation: A tool in turbulence research. *Annual review of Fluid Mechanics 30*, 539–578.

Muhar, S., S. Schmutz, and M. Jungwirth (1995). River restoration concepts - goals and perspectives. *Hydrobiologia 303*(1-3), 183–194.

Mujumdar, P. P. (2001). Flood wave propagation - the Saint Venant equations. In *Resonance*, Volume 6(5), pp. 66–73. Indian Academy of Sciences.

Murota, A., T. Fukuhara, and M. Sato (1984). Turbulence structure in vegetated open channel flow. *Journal of Hydroscience and Hydraulic engineering 2*(1), 47–61.

MX.Systems (2005). *User guide WAQUA* (Version 10.41 ed.). Rijswijk, the Netherlands: MX.Systems / Ministry of Transport, Public works and Water Management.

Myers, W. R. C. and E. K. Brennan (1990). Flow resistance in compound channels. *Journal of Hydraulic Research 28*, 141–155.

Nadaoka, K. and H. Yagi (1998). Shallow-water turbulence modeling and horizontal Large-Eddy computation of river flow. *Journal of Hydraulic Engineering 124*(5), 493–500.

Naden, P., P. Rameshwaran, O. Mountford, and C. Robertson (2006). The influence of macrophyte growth, typical of eutropic conditions, on river flow velocities and turbulence production. *Hydrological Processes 20*, 3915–3938.

Neary, V. S. (2003). Numerical solution of fully-developed flow with vegetative resistance. *Journal of Engineering Mechanics 129*(5), 558–563.

Nepf, H. M. (1999). Drag, turbulence, and diffusion in flow trough emergent vegetation. *Water Resources Research 35*(2), 479–489.

Nezu, I. (2005). Open-channel flow turbulence and its research prospects in the 21st century. *Journal of Hydraulic Engineering 131*(4), 229–246.

Nezu, I. and K. Onitsuka (2001). Turbulent structures in partly vegetated open-channel flows with LDA and PIV measurements. *Journal of Hydraulic Research 39*(6), 629–642.

Nicholas, A. P. and C. A. Mitchell (2003). Numerical simulation of overbank processes in topographically complex floodplain environments. *Hydrological Processes 17*, 727–746.

Nikora, V., D. Goring, I. McEwan, and G. Griffiths (2001). Spatially averaged open-channel flow over rough bed. *Journal of Hydraulic Engineering 127*(2), 123–133.

Nikora, V., A. N. Sukhodolov, and P. M. Rowinski (1997). Statistical sand wave dynamics in one-directional water flows. *Journal of Fluid Mechanics 351*, 17–39.

Nikuradse, J. (1932). Gesetzmässigkeiten der turbulenten Strömung in glatten Rohren. *Forschung auf dem Gebiete des Ingenieurswesen Heft 356*.

Nikuradse, J. (1933). Strömungsgesetze in rauhen Rohren. *Forschungsheft VDI Verlag Berlin B*(362).

Ninni, V., R. Camussi, and G. Guj (1999). Statistical study of anisotropic anomalous behavior of a cylinder wake. *Experiments in Fluids 26*, 161–168.

Noordam, D. and F. Huthoff (2006). Hydraulic resistance in flow models. Civil Engineering & Management Research Report 2006W-003/WEM-007, University of Twente, Enschede, the Netherlands.

Oberez, A. T. (2001). Turbulence modelling of hydraulic roughness of submerged vegetation. Master thesis, International Institute for Infrastructural, Hydraulic, and Environmental Engineering (IHE), Delft, the Netherlands.

Pappenberger, F., K. Beven, M. Horritt, and S. Blazkova (2005). Uncertainty in the calibration of effective roughness parameters in HEC-RAS using inundation and downstream level observations. *Journal of Hydrology 302*(1-4), 46–69.

Pasche, E. and G. Rouvé (1985). Overbank flow with vegetatively roughened flood plains. *Journal of Hydraulic Engineering 111*(9), 1262–1278.

Patra, K. C. and S. K. Kar (2000). Flow interaction on meandering river with floodplains. *Journal of Hydraulic Engineering 126*(8), 593–604.

Petryk, S. and G. Bosmajian (1975). Analysis of flow trough vegetation. *Journal of the Hydraulics Division 101*(HY7), 871–884.

Phillips, O. M. (1991). The Kolmogorov spectrum and its oceanic cousins: a review. *Proceedings of the Royal Society of London. Series A, Mathematical and Physical Sciences 434*(1890), 125–138.

Piomelli, U. and E. Balaras (2002). Wall-layer models for Large-Eddy Simulations. *Annual review of Fluid Mechanics 34*, 349–374.

Pluimakers, W. H. M. A. and H. F. M. W. van Rijswick (2003). *Teksten waterwetgeving* (ISBN 90 1209 770 3, NUR 823 ed.). Sdu uitgevers.

Poggi, D., A. Porporato, and L. Ridolfi (2003). Analysis of the small scale structure of turbulence on smooth and rough walls. *Physics of Fluids 15*(1), 35–46.

Poggi, D., A. Porporato, L. Ridolfi, J. D. Albertson, and G. G. Katul (2004). The effect of vegetation density on canopy sub-layer turbulence. *Boundary Layer Meteorology 111*, 565–587.

Pope, S. B. (2000). *Turbulent Flows* (third ed.). Cambridge University press.

Pouquet, A., U. Frisch, and J. P. Chollet (1983). Turbulence with a spectral gap. *Physics of Fluids 26*(4), 877–879.

Prinos, P. and R. D. Townsend (1984). Comparison of methods for predicting discharge in compound open channels. *Advances in Water Resources 7*, 180–187.

Proust, S., D. Bousmar, N. Rivière, A. Paquier, and Y. Zech (2006). A methodology for computing non-uniform flows in compound channels. In *River Flow 2006*, Volume 1, pp. 405–414. Balkema.

Raupach, M. R. (1992). Drag and drag partition on rough surfaces. *Boundary-Layer Meteorology 60*, 375–395.

Raupach, M. R., P. A. Coppin, and B. J. Legg (1986). Experiments on scalar dispersion within a model plant canopy. part 1: The turbulence structure. *Boundary-Layer Meteorology 35*, 21–52.

Raupach, M. R., J. J. Finnigan, and Y. Brunet (1996). Coherent eddies and turbulence in vegetation canopies: the mixing-layer analogy. *Boundary-Layer Meteorology 78*, 351–382.

Raupach, M. R. and R. H. Shaw (1982). Averaging procedures for flow within vegetation canopies. *Boundary Layer Meteorology 22*, 79–90.

Ree, W. O. and F. R. Crow (1977). Friction factors for vegetated waterways of small slope. Technical Report Publication S-151, U.S. Department of Agriculture, Agricultural Research Service.

Rodi, W. (1980). Turbulence models and their application in hydraulics. Presented by the IAHR-section on fundamentals of division II: experimental and mathematical fluid dynamics, Delft, the Netherlands.

Rodi, W. (1995). Impact of Reynolds-average modelling in hydraulics. In *Proceedings of the Royal Society, Mathematical and Physical Sciences, Osborne Reynolds Centenary Volume*, Volume 451, pp. 141–164.

Schlichting, H. and K. Gersten (2000). *Boundary Layer Theory* (8th ed.). New York: Springer.

Seçkin, G. (2004). A comparison of one-dimensional methods for estimating discharge capacity of straight compound channels. *Canadian Journal of Civil Engineering 31*, 619–631.

Sellin, R. H. J. (1964). A laboratory investigation into the interaction between the flow in the channel of a river and that over its flood plain. *La Houille Blanche 20*(7), 793–801.

Shi, Z. and J. M. R. Hughes (2002). Laboratory flume studies of microflow environments of aquatic plants. *Hydrological Processes 16*, 3279–3289.

Shimizu, Y. and T. Tsujimoto (1994). Numerical analysis of turbulent open-channel flow over vegetation layer using a $k-\varepsilon$ turbulence model. *Journal of Hydroscience and Hydraulic Engineering 11*(2), 57–67.

Shiono, K. and D. W. Knight (1991). Turbulent open-channel flows with variable depth across the channel. *Journal of Fluid Mechanics 222*, 617–646.

Silberman, E., R. W. Carter, H. A. Einstein, J. Hinds, and R. W. Powell (1963). Friction factors in open channels: Progress report by the Task Force on Friction Factors in Open Channels of the Committee on Hydromechanics of the Hydraulics Division. *Journal of the Hydraulics Division 89*(HY2), 97–143.

Silva, W., F. Klijn, and J. P. M. Dijkman (2001). Room for the Rhine branches in the Netherlands; what research has thaught us. Technical Report 2001.031, RIZA, Netherlands.

Singh, S. P. and S. Mittal (2005). Flow past a cylinder: shear layer instability and drag crisis. *International Journal for Numerical Methods in Fluids 47*, 75–98.

Smart, G. M., M. J. Duncan, and J. M. Walsh (2002). Relatively rough flow resistance equations. *Journal of Hydraulic Engineering 128*(6), 568–578.

Spalart, P. R., W.-H. Jou, M. Stretlets, and S. R. Allmaras (1997). Comments on the feasibility of LES for wings and on the hybrid RANS/LES approach. In *Advances in DNS/LES, Proceedings of the First AFOSR International Conference on DNS/LES*.

Stelling, G. S. and A. Verwey (2005). Numerical flood simulation. In M. G. Anderson and J. J. McDonnell (Eds.), *Encyclopedia of Hydrological Sciences*, Volume 1, Chapter 16. John Wiley & Sons Publishers.

Stephan, U. and D. Gutknecht (2002). Hydraulic resistance of submerged flexible vegetation. *Journal of Hydrology 269*, 27–43.

Stephenson, D. and P. Kolovopoulos (1990). Effects of momentum transfer in compound channels. *Journal of Hydraulic Engineering 116*(12), 1512–1522.

Stewartson, K. (1981). d'Alembert's paradox. *SIAM Review (Society for Industrial and Applied Mathematics) 23*(3), 308–343.

Stoesser, T. and W. Rodi (2004). LES of bar and rod roughened channel flow. In *Advances in Hydro-Science and -Engineering, International Conference on Hydroscience and Engineering (ICHE 2004)*, Volume VI, Brisbane, Australia.

Stone, B. M. and H. T. Shen (2002). Hydraulic resistance of flow in channels with cylindrical roughness. *Journal of Hydraulic Engineering 128*(5), 500–506.

Straatsma, M. (2007). *Hydrodynamic roughness of floodplain vegetation - Airborne parameterization and field validation*. Ph. D. thesis, Utrecht University, the Netherlands.

Strickler, A. (1923). Beitrage zur Frage der Geschwindigkeitsformel und der Rauhigkeitszahlen für Ströme, Kanäle und geschlossene Leitungen. Mitteilungen des Amtes für Wasserwirtschaft 16, Eidg. Department des Innern, Bern, Switserland.

Sukhodolova, T., A. Sukhodolov, and C. Engelhardt (2004). A study of turbulent flow structure in a partly vegetated river reach. In Greco, Carravetta, and D. Morte (Eds.), *River Flow 2004*, Volume 1, pp. 469–478.

Sumner, D., J. L. Heseltine, and O. J. P. Dansereau (2004). Wake structure of a finite circular cylinder of small aspect ratio. *Experiments in Fluids 37*(5), 720–730.

Tayefi, V., S. N. Lane, R. J. Hardy, and D. Yu (2007). A comparison of one- and two-dimensional approaches to modelling flood inundation over complex upland floodplains. *Hydrological Processes*, in press.

Taylor, G. I. (1938). The spectrum of turbulence. *Proceedings of the Royal Society of London. Series A, Mathematical and Physical Sciences 164*(919), 476–490.

Tollner, E. W., B. J. Barfield, and J. C. Hayes (1982). Sedimentology of erect vegetal filters. *Journal of the Hydraulics Division 108*(HY12), 1518–1531.

Townsend, A. A. (1949). Momentum and energy diffusion in the turbulent wake of a cylinder. *Proceedings of the Royal Society of London. Series A, Mathematical and Physical Sciences 197*(1048), 124–140.

Townsend, A. A. (1976). *The Structure of Turbulent Shear Flow* (2nd ed.). Cambridge University press.

Truesdell, C. (1953). Notes on the history of the general equations of hydrodynamics. *The American Mathematical Monthly 60*(7), 445–458.

Tsujimoto, T. and T. Kitamura (1990). Velocity profile of flow in vegetated bed channels. KHL progressive report 1, Kanazawa University.

Tsujimoto, T., T. Kitamura, Y. Fujii, and H. Nakagawa (1996). Hydraulic resistance of flow with flexible vegetation in open channel. *Journal of Hydroscience and Hydraulic Engineering 14*(1), 47–56.

Tsujimoto, T., T. Kitamura, and T. Okada (1991). Turbulent structure of flow over rigid vegetation-covered bed in open channels. KHL progressive report 2, Kanazawa University.

Tsujimoto, T., T. Okada, and K. Kontani (1993). Turbulent structure of open channel flow over flexible vegetation. KHL progressive report 4, Kanazawa University.

Uijttewaal, W. S. J., V. Weitbrecht, C. F. Graf von Carmer, and G. H. Jirka (2001). Experiments on shallow flow turbulence. In *Proceedings of the 2001 International Symposium on Environmental Hydraulics*.

Uittenbogaard, R. (2003, february). Modelling turbulence in vegetated aquatic flows. In *Riparian Forest Vegetated Channels*, Trento, Italy.

US Soil Conservation Service (1954). Handbook of channel design for soil and water conservation. Technical Report SCS-TP61.

Van Lohuizen, K. (2003). *Aderen*. Amsterdam: Mets & Schildt. in Dutch.

Van Prooijen, B. (2004). *Shallow Mixing Layers*. Ph. D. thesis, Delft University of Technology.

Van Prooijen, B. C., J. A. Battjes, and W. S. J. Uijttewaal (2005). Momentum exchange in straight uniform compound channel flow. *Journal of Hydraulic Engineering 131*(3), 175–183.

Van Velzen, E. H., P. Jesse, P. Cornelissen, and H. Coops (2003). Stromingsweerstand vegetatie in uiterwaarden. Handboek report 2003.028, RIZA, Arnhem, The Netherlands.

Van Vuren, S., H. J. De Vriend, S. Ouwerkerk, and M. Kok (2005). Stochastic modelling of the impact of flood protection measures along the river Waal in the Netherlands. *Natural Hazards 36*, 81–102.

Velasco, D., A. Bateman, and V. De Medina (2005). A new integrated hydro-mechanical model applied to flexibel vegetation in river beds. In Parker and Garcia (Eds.), *River, Coastal and Estuarine Morphodynamics: RCEM 2005*, pp. 217–227.

Vincent, A. and M. Meneguzzi (1991). The spatial structure and statistical properties of homogeneous turbulence. *Journal of Fluid Mechanics 225*, 1–20.

Vionet, C. A., P. A. Tassi, and J. P. Martin-Vide (2004). Estimates of flow resistance and eddy viscosity coefficients for 2D modelling on vegetated floodplains. *Hydrological Processes 18*, 2907–2926.

Von Kármán, T. (1930). Mechanische Ähnlichkeit und Turbulenz. Nachrichten der Akademie der Wissenschaften, Math-Phys. Klasse 58, Universität Göttingen.

Wang, C. and P. Wang (2007). Hydraulic resistance characteristics of riparian reed zone in river. *Journal of Hydrologic Engineering 12*(3), 267–272.

Wasantha Lal, A. M. (1995). Calibration of riverbed roughness. *Journal of Hydraulic Engineering 121*(9), 664–671.

Weber, J. F. and A. N. Menéndez (2004). Performance of lateral velocity distribution models for compound channel sections. In *River Flow 2004*, Volume 1, pp. 449–457. Balkema.

Werlé, H. and M. Gallon (1972). Contrôle d'écoulements par jet transversal. *L'Aéronautique et l'Astronautique 34*, 21–33.

Werner, M. G. F. and M. F. Lambert (2007). Comparison of modelling approaches used in practical flood extent modelling. *Journal of Hydraulic Research 45*(2), 202–215.

Wheater, H. S. (2002). Progress in and prospects for fluvial flood modelling. *Philosophical Transactions of the Royal Society of London, Series A - Mathematical and Physical Sciences 360*, 1409–1431.

Wijbenga, J. H. A., M. T. Duits, and J. M. van Noortwijk (1998). Parameter optimisation for two-dimensional flow modelling. In *Proceedings of the Third International Conference on Hydroinformatics*, Copenhagen, Denmark, pp. 1037–1042. Rotterdam: Balkema.

Wilbers, A. W. E. (2004). *The development and hydraulic roughness of subaqueous dunes*. Ph. D. thesis, University of Utrecht.

Willems, P., J. Berlamont, R. van looveren, M. Sas, and C. Bogliotti (2000, July). Practical comparison of the modelling systems mike11 and isis for river flood modelling by the quasi two-dimensional approach. In *HydroInformatics 2000*, Iowa.

Willi, H. P. (2006). Meeting the challenge of flood protection. *EAWAG News - Aquatic Research 61*, 9–11.

Williams, J. J. R. and K. M. Singh (2004). Structure of the turbulent flow over a rough bed. In *Advances in Hydro-Science and -Engineering, International Conference on Hydroscience and Engineering (ICHE 2004)*, Volume VI.

Williamson, C. H. K. (1996). Vortex dynamics in the cylinder wake. *Annual review of Fluid Mechanics 28*, 477–539.

Wilson, C. A. M. E. and M. S. Horritt (2002). Measuring the flow resistance of submerged grass. *Hydrological Processes 16*, 2589–2598.

Wilson, C. A. M. E., T. Stoesser, P. D. Bates, and A. Batemann-Pinzen (2003). Open channel flow through different forms of submerged flexible vegetation. *Journal of Hydraulic Engineering 129*, 847–853.

WL|Delft Hydraulics (1993). *User guide SOBEK* (version 2.52 ed.). Delft, the Netherlands.

WL|Delft Hydraulics (2005). *Technical Documentation WAQUA* (Version 1.2 ed.). Delft, the Netherlands.

Wormleaton, P. R., J. Allen, and P. Hadjipanos (1982). Discharge assessment in compound channel flow. *Journal of the Hydraulics Division 108*(9), 975–993.

Wormleaton, P. R. and D. J. Merrett (1990). An improved method of calculation for steady uniform flow in prismatic main channel/floodplain sections. *Journal of Hydraulic Research 28*(2), 157–174.

Wu, F.-C., H. W. Shen, and C. Y-J (1999). Variation of roughness coefficients for unsubmerged and submerged vegetation. *Journal of Hydraulic Engineering 125*(9), 934–942.

Yen, B. C. (2002). Open channel flow resistance. *Journal of Hydraulic Engineering 128*(1), 20–39.

Zocchi, G., P. Tabeling, J. Maurer, and H. Willaime (1994). Measurement of the scaling of the dissipation at high Reynolds numbers. *Physical Review E 50*(5), 3693 – 3700.

Notation

The following symbols are used in this thesis:

Roman

a	Blockage area
A	Cross-sectional area of compartment
b	Drag length
C_D	Drag coefficient
d	Pipe diameter
D	Diameter of cylindrical resistance elements
E	Energy spectrum (energy/wave number)
f	Friction coefficient (bed resistance)
f	Frequency
F	Force per unit area
F	Force per unit volume
g	Gravitational acceleration
h	Water depth
h_{int}	Height of the interface between main channel and floodplain
$h_{j\pm1/2}$	Height of interface to the left ('–') and right ('+') of compartment j
h_s	Artificial roughness height
i	Streamwise channel slope (inclination)
k	Height of resistance elements
k_w	Wave number
k_S	Strickler's equivalent roughness height
k_N	Nikuradse's equivalent roughness height
K	Coefficient of proportionality
K	Kinetic energy
L	Characteristic length scale of flow domain
L_f	Formation length
l	Characteristic length scale in analytical velocity profile
ℓ	Turbulent scaling length for flow over vegetation
ℓ_j	Parameter in generalization of IDCM to arbitrary compound channels

m	Bed surface density of resistance elements
M	Number of overbank flow depths for which velocities have been measured in one experiment
N	Total number of compartments
N_{fp}	Number of floodplains
n	Manning roughness coefficient
p	Pressure
P	Wetted perimeter of compartment
Q	Total channel discharge
R	Hydraulic radius
R^2	Coefficient of determination
Re	Reynolds number
r	Spacing hydraulic radius of resistance layer
r_j	Parameter in generalization of IDCM to arbitrary compound channels
s	Separation between individual resistance elements
S	Water level slope
t	Time coordinate
u'	Turbulent velocity fluctuations in streamwise direction
u_*	Friction velocity
U	Compartment-averaged streamwise flow velocity
U_b	Cross-sectionally averaged streamwise flow velocity for bankfull depth
u_r	Characteristic eddy-velocity near top of resistance elements
U_r	Depth-averaged flow velocity in the resistance layer
U_{r0}	Depth-averaged flow velocity in the resistance layer for emergent resistance elements
U_s	Depth-averaged flow velocity in the surface layer
U_T	Depth-averaged flow velocity over entire (Total) flow depth
U_w	Wave propagation speed
v'	Turbulent velocity fluctuations in lateral direction
w'	Turbulent velocity fluctuations in vertical direction
W	Bottom width of compartment
x	Streamwise coordinate
y	Lateral coordinate
z	Vertical coordinate

Greek

α	Characteristic length scale in turbulence model for free shear flow
β	Transition exponent
γ_i	Any geometrical length-scale

γ	Dimensionless interface coefficient
δ	Parameter in solution for compound channel with two different floodplains
ϵ	Parameters in solution for two-stage channel
ε	Energy dissipation rate
η	Similarity exponent
η_κ	Kolmogorov's spatial micro scale
κ	Von Kármán's constant
λ	Turbulent mixing length
μ	Mean error in predicted velocities
ν	Molecular kinematic viscosity
ρ	Density of water
σ	Standard deviation
τ	Shear stress
τ_{int}	Interface stress between main channel and floodplain
τ_κ	Kolmogorov's temporal micro scale
Φ	Correction factor for incomplete sampling

Subscripts

b	Corresponding to bankfull flow conditions
D	Drag
j	Compartment j
k	Top of resistance layer
fp	Floodplain
mc	Main channel
r	Resistance layer
s	Surface layer
T	Total flow depth
$,0$	Reference case with $\gamma = 0$ (equivalent to DCM)

Abbreviations

3D, 2D, etc.	3-Dimensional, etc.
ADCP	Acoustic Doppler Current Profiler
ADV	Acoustic Doppler Velocimeter
DCM	Divided Channel Method
DES	Detached-eddy simulation
DNS	Direct numerical simulation
fp	Floodplain
IDCM	Interacting Divided Channel Method
LES	Large eddy simulation
mc	Main channel
RANS	Reynolds-averaged Navier-Stokes
rms	Root-mean-square

List of publications

1. Huthoff, F. and D. C. M. Augustijn (2004). Sensitivity analysis of floodplain roughness in 1D flow. In: 6th International Conference on HydroInformatics, Singapore , Liong, Phoon, and Babovic (eds.). World Scientific Publishing Company.

2. Huthoff, F. (2005). Channel Roughness in 1D Steady Uniform Flow: Manning or Chézy? In: NCR days 2004: Research for managing rivers: Present and future issues. Makaske, Wolfert and van Os (eds.), NCR publication 26-2005, p. 98.

3. Huthoff, F. and J. W. Stijnen (2005). Efficiency of emergency retention areas along the river Rhine: Monte Carlo simulations of a 1D flow model. In: International Symposium on Stochastic Hydraulics, Nijmegen, the Netherlands, van Gelder (eds.).

4. Huthoff, F. and D. C. M. Augustijn (2006). Hydraulic resistance of vegetation: predictions of average flow velocities based on a rigid-cylinders analogy, University of Twente, CE&M research report 2006R-001/WEM-003.

5. Huthoff, F. and D. C. M. Augustijn (2006). Evaluation of an analytical model for hydraulic resistance of submerged vegetation, Geophysical Research Abstracts, Vol. 8, 02711.

6. Huthoff, F., D. C. M. Augustijn, and S. J. M. H. Hulscher (2006). Depth-averaged flow in presence of submerged cylindrical elements, Proceedings of River Flow 2006 - Third International Conference on Fluvial Hydraulics, Lisbon, Portugal, 575-582.

7. Huthoff, F., D. C. M. Augustijn, J. H. A. Wijbenga and S. J. M. H. Hulscher (2006). Hydraulic resistance of submerged cylindrical elements: A two-layer scaling approach. In: NCR days 2005: Research on River Dynamics from geological to operational time scales. Weerts, Ritsema and van Os (eds.), NCR publication 29-2006, p. 63.

8. Noordam, D. and F. Huthoff (2006). Hydraulic resistance in flow models, University of Twente, CE&M research report 2006W-003/WEM-007.

9. Huthoff, F., D. C. M. Augustijn, and S. J. M. H. Hulscher (2006). Hydraulic Resistance of Vegetation in River flow Applications, Proceedings

of the International Conference of Hydroscience and Engineering (ICHE 2006), Philadelphia, PA, USA.

10. Huthoff, F., D. C. M. Augustijn and S. J. M. H. Hulscher (2007). Analytical solution of the depth-averaged flow velocity in case of submerged rigid cylindrical vegetation. *Water Resources Research* 43(W06413), doi: 10.1029/2006WR005625.

11. Huthoff, F., P. C. Roos, D. C. M. Augustijn and S. J. M. H. Hulscher (2007). Interacting Divided Channel Method for Compound Channel Flow. Accepted by *Journal of Hydraulic Engineering*.

12. Huthoff, F., M. Straatsma, D. C. M. Augustijn and S. J. M. H. Hulscher (2007). Evaluation of a simple hydraulic resistance model using flow measurements collected in vegetated waterways. Submitted to *Hydrological Processes*.

13. Huthoff, F., P. C. Roos, D. C. M. Augustijn and S. J. M. H. Hulscher (2007). A new method to account for large-scale mixing processes in spatially-averaged flow models. The Fifth International Symposium on Environmental Hydraulics, Tempe, AZ, USA.

14. Veldman, W., D. C. M. Augustijn, F. Huthoff and M. Visser (2007). Effect of vegetation growth in drainage canals on water management. The Fifth International Symposium on Environmental Hydraulics, Tempe, AZ, USA.

About the author

Fredrik Huthoff was born in Bremen, Germany, on 29 March 1974. He grew up in Oegstgeest, the Netherlands, where he received primary education at 'OBS De Springplank' and secondary education at the 'Rijnlands Lyceum'. In the year 1990-1991 he participated in a student exchange programm of the American Institute For Foreign Study (AIFS), enrolling him for one year at the Canon-McMillan High School in Canonsburg, Pennsylvania (U.S.A.). Upon return to the Netherlands he entered the 'International Baccalaureate' programm at the Rijnlands Lyceum, from where he received his diploma in 1993.

Later in the same year, Fredrik started studying physics at the University of Amsterdam. In 1997/98 the study was interrupted for a year of working experience and travels in South America. Continuation of the study resulted in a specialization in Astronomy. Towards receiving the Master's degree in Astronomy in January 2001, Fredrik conducted research projects on stellar evolution at the Amsterdam Astronomical Institute 'Anton Pannekoek' and, as part of the BIS student-exchange programm, a project on cosmology at the School of Physics at the University of New South Wales in Sydney, Australia.

After graduation from university, Fredrik worked for a year as software developer at Net.Footworks in Haarlem, before starting in 2002 as consultant river management at HKV Consultants in Lelystad. In cooperation with HKV Consultants, Fredrik conducted a Ph.D. research at the Department of Water Engineering and Management (Faculty of Engineering Technology) at the University of Twente, Enschede, from August 2003 to August 2007. Following the Ph.D. defense in October 2007, Fredrik continues to work as consultant at HKV, and as assistant professor at the University of Twente.